Theme lecture: Characterising the pre-failure deformation properties of geomaterials

Exposé sur le thème: Caractérisation des propriétés de déformation avant rupture des géomatériaux

F.Tatsuoka – *Department of Civil Engineering, University of Tokyo, Japan*
R.J.Jardine – *Department of Civil Engineering, Imperial College of Science, Technology and Medicine, UK*
D. Lo Presti – *Dipartimento di Ingegneria Strutturale, Politecnico di Torino, Italy*
H. Di Benedetto – *Département Génie Civil et Bâtiment, Ecole Nationale des Travaux Publics de l'Etat, France*
T. Kodaka – *Institute of Industrial Science, University of Tokyo, Japan*

ABSTRACT: Recent developments in the characterisation of geomaterial prefailure deformation properties are reviewed, focusing on the data required to predict ground deformations and structural displacements at working loads. Descriptions are given of the deformation characteristics developed at very small to intermediate strains, of a variety of geomaterials, in testing using modern laboratory and field techniques. The relationships between static and dynamic experiments, between laboratory and field techniques, and between testing and field full-scale behaviour are discussed. Important features that are highlighted include: kinematic yielding, effects of recent stress-time history, anisotropy, structuration and destructuration, non-linearity by strain and pressure and effects of cyclic loading. Careful distinctions are made between elastic, plastic and viscous properties.

RESUME: Les développements récents traitant de la caractérisation des propriétés avant rupture des géomatériaux sont décrits, en insistant sur les données requises afin de prédire les déformations du sol et les déplacements des structures sous charges. Les caractéristiques de drivers géomatériaux sont développées, dans le domaine des petites déformations et déformations intermédiaires, à patir de résultats obtenus à l'aide de techniques récentes d'investigation en laboratoire et in-situ. Les relations entre les expériences statiques et dynamiques, les techniques de laboratoire et in situ, et les comportements lors d'essais sur modèle et en vrai grandeur, sont discutés. Les points importants qui sont soulignés incluent: l'écrouissage cinématique, les effets de l'histoire récente de contrainte, l'anisotropie, la structuration et la destructuration, et la non linéarité créée par la déformation, la pression et les effets de chargements cycliques. Une distinction précise est faite entre les propriétés élastiques, plastiques et visqueuses.

1 INTRODUCTION

As Geotechnical Engineering has developed, soil property characterisation has grown into a large area of study and it is now impossible to cover the full spread of activity in a single review. Instead, the Authors call attention to a general list of key conferences (**Table 1.1**), and in the remainder of the paper, concentrate solely on pre-failure deformation behaviour, a subject which has developed rapidly over the past 15 years and has been a central feature of the Authors' own research. Key reports by others include: Burland (1989); Jamiolkowski et al. (1991); Atkinson and Sällfors (1991); Mair (1992); Hight and Higgins (1995); and Biarez and Hicher (1994) and three books describing the Greco II project in France (Les Géomatériaux 1995; Mécanique des géomatériaux 1995 and Les Géomatériaux 1996; see the end of REFERENCES). The principal developments can be summarized as:

1. A much better ability to predict ground movements at working loads;
2. A shift from the use of conventional laboratory and field tests towards relatively sophisticated laboratory and field loading tests and field geophysics;
3. Moving from a relatively simple picture of geomaterial behaviour towards a more realistic one considering many relevant factors; and
4. The development of a more unified view which inter-links static and dynamic behaviour and laboratory and field testing.

The main impetus for the recent development was the consensus in the late 1970's that the stiffness evaluated by conventional laboratory and field tests, which were conventionally considered as linear elastic properties, were usually far too low to explain many field full-scale behaviour, particularly with hard soils and soft rocks (e.g., Jardine et al. 1985, 1991; Burland 1989; Tatsuoka and Shibuya 1992; Jardine 1995; Tatsuoka and Kohata 1995; Tatsuoka et al. 1995c: Hight and Higgins 1995). The main reasons for the discrepancy have been identified as:

a. With the exception of deformable materials such as soft clays or loose sands, the ground strains developed by construction are generally less than about $5x10^{-3}$, as

Table 1.1 Main topics of recent international conferences on testing and characterisation of ground properties.

Special topic	Title and Date of IS, SIP or Conference
Site characterisation	'Advances in Site Investigation Practice' , ICE, London; 1995
Sample disturbance	'Offshore site investigations and foundation behaviour', London; 1992 IS-Hokkaido; 1994
In-situ testing	First IS on Penetration testing, Orlando; 1988 Third IS on Pressuremeter, Oxford; 1990
Geophysical methods	New Delhi ICSMFE, Special Volume prepared by TC-10, 'Geophysical characterisation of sites' ; 1994
Soil pre-failure behaviour	Florence ECSMFE; 1991 Bangkok ARCSMFE; 1991 IS-Hokkaido; 1994 Geotechnique SIP 'Pre-failure deformation behaviour'; 1997
Yielding and failure	'Advanced triaxial testing of soil and rock' ASTM STP; 1988 Geotechnique SIP 'Bothkennar clay' ; 1992 'Hard soils-soft rocks' , Athens; 1993
Cyclic loading, liquefaction, dynamics and earthquake geotechnics	10th WCEE, Madrid; 1992 'Dynamic Geotechnical Testing II' ASTM STP; 1994 'Geotechnical Earthquake Engineering and Dynamics' , IS-Tokyo '95; 1995 ASCE, St Louis 1995 11th WCEE, Acapulco; 1996
Rate effects	'Measuring and modelling time dependent soil behaviour', ASCE, Washington; 1996
Consolidation and permeability	Geo-coast '91; Yokohama; 1991 IS-Hiroshima '95; 1995
Regional and 'special soils'	'Geomechanics in tropical soils' , Singapore; 1988 'Engineering for calcareous sediments' , Perth; 1988
Unsaturated soils	'Un-sat 95', Paris, 1995
Environmental Geotechnics	'Environmental geotechnics' , Edmonton; 1994 'Geoenvironment 2000' , ASCE, New Orleans; 1995 IS-Osaka '96; 1996
Use of advanced methods for practical predictions	Florence ECSMFE; 1991 Wroth Memorial Symposium, Oxford; 1992 IS-Hokkaido '94; 1994 Settlement, Austin; 1994 Geotechnique SIP 'Pre-failure deformation behaviour'; 1997

IS: International Symposium; SIP: Symposium in Print

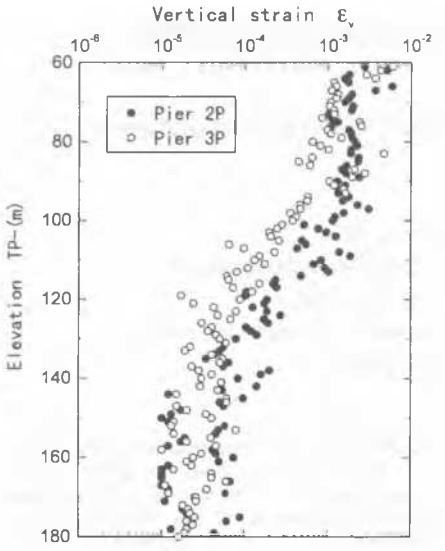

Fig. 1.1 Centre-line vertical strains in the gravel and sedimentary softrock below the piers for the world's longest suspension bridge: Akashi Kaikyo Bridge. The average contact pressure and foundation diameters are 5.3 kgf/cm^2 and 80 m for Pier 2P; 4.8 kgf/cm^2 and 78 m for Pier 3P, respectively (Takeuchi et al. 1997).

Table 1.2 Factors determining ground and structure movements (Hight and Higgins 1995).

● Site conditions - topography - geology - stratigraphy/soil profile - groundwater - site development history - in situ stresses - details of adjacent structures
● Soil or rock behaviour - stress-strain properties - yield and strength characteristics - permeability and its variation with void ratio or stress level
● Construction details - form, scale and method of construction - geometry and boundary conditions - sequence and timing of events - stiffness of temporary and permanent supports - nature and pattern of imposed loading (maintained, dynamic, cyclic)

illustrated in **Fig. 1.1**, falling below the levels at which stiffnesses could be defined reliably in conventional laboratory or field tests; and

b. Geomaterial stiffness is often highly non-linear over the 'practical' range of strain.

It has also become clear that field pre-failure deformation behaviour is affected by the particular structure (or fabric) of each geomaterial and by each site's stress-time history. In most cases, a simple geomaterial model which involves only a density parameter and consistency indexes (such as plasticity index for cohesive soils and relative density for cohesionless soils) and a simple stress history parameter such as OCR will not be sufficiently representative. The shortcomings of stress-strain models developed based on laboratory test results of reconstituted specimens have been appreciated. Realistic prediction of ground deformations and structural displacements are only possible when relatively sophisticated laboratory stress-strain tests using high quality undisturbed samples and/or careful field tests are performed.

The great value of such predictions is that they help to:

1. Ensure that excessive foundation displacements do not lead to expensive super-structure design changes for building or large bridges;
2. Ensure high serviceability levels for the completed structures;
3. Avoid damage to associated structures due to ground movements (examples include low and high-rise buildings supported by a single raft foundation, and the effects of excavations on nearby masonry buildings, piles or tunnels); and
4. Predict the stresses acting on structural elements (rafts, retaining walls, tunnels, offshore structures etc).

Table 1.3 Factors influencing the stress-strain behaviour of geomaterials (Hight and Higgins 1995).

A	Composition: ● grading, mineralogy, grain shape, texture Fabrics: ● particle packing (including density), layering, discontinuities (joints, fissures, open cracks) Chemical alteration and diagenesis: ● bonding, fusing, recrystallisation
B	Current stress state: ● mean effective stress level, p', stress difference, principal stress direction, α Current strain state: ● time at current stress state Stress history: ● formative (large strain) consolidation stress history, OCR ● recent (small strain) stress history (reloading, cyclic events, sampling disturbance) ● time since previous stress changes, ageing
C	Stress path (or strain path) imposed by construction and subsequent loading: ● Δq, Δp, Δu, Δα, Δb Rate of stress (or strain) change: ● viscous effects ● degree of pore pressure dissipation ● inertia effects on stress reversals Drainage conditions: ● drainage path lengths, pore pressure gradients, permeability, rates of stress (or strain) change

Table 1.2 lists the full set of factors that control ground movements. In this paper, we discuss only geomaterial stress-strain behaviour, concentrating mainly on relatively stiff structured clays, sands and gravels and sedimentary softrocks. Particular emphasis is placed on:

1. Deformation characteristics from very small to intermediate strains, and their non-linearity due to strain (shear or volumetric) and pressure;
2. Some of the important influential factors summarized in **Table 1.3**; and
3. Models for interpreting field data and extrapolating future ground movements.

We will also discuss recent advances and trends in laboratory and field testing and the relationships between laboratory and in-situ tests and full-scale behaviour. While we will focus on the poorly understood topic of deformation characteristics at very small strains, we do not over-emphasize its importance. The properties at strains exceeding the elastic strain limit control ground movements in most design cases.

In soft ground conditions, local failure and pore-pressure dissipation affect even the short-term ground movements developed by excavations, tunnels and surface loading activities (Jardine 1995). Although these phenomena are also affected by non-linear stiffness at small strains, they will not be discussed in this short report. Other important issues that will not be touched upon include; peak strength; post-peak strain-softening associated with shear banding; unsaturated soils; and (visco-) elasto-plastic numerical analysis.

2 ELASTICITY AND YIELDING

Elasticity: Under fully drained conditions, **elastic** and **plastic** deformations are time-independent. Time-dependency is considered as **viscous** behaviour; inertia effects are not

considered as soil properties. Plastic and viscous deformations are irreversible for most closed stress cycles, exhibiting energy dissipation. For a linear elastic material, we have:

$$[\varepsilon^e_{ij}] = [C_{ijkl}^e] \cdot [\sigma_{kl}] \quad (2.1)$$

where $[\varepsilon^e_{ij}]$ and $[\sigma_{kl}]$ are strain and stress tensors and $[C_{ijkl}^e]$ is the **stress state-independent** elastic compliance matrix. A **hyper**-elastic medium has a potential elastic energy function ϕ defined as;

$$\varepsilon^e_{ij} = \partial \phi / \partial \sigma_{ij} \quad (2.2)$$

There is no energy dissipation for any closed stress cycle, which results in a symmetric matrix $[C_{ijkl}^e]$, whether or not the matrix has coupling terms.

For a **hypo**-elastic medium, Eq. 2.1 is not valid, but only a strain increment tensor $[d\varepsilon^e_{ij}]$ can be related linearly to a stress increment tensor $[d\sigma_{kl}]$ as:

$$[d\varepsilon^e_{ij}] = [(C_1)_{ijkl}^e] \cdot [d\sigma_{kl}] \quad (2.3)$$

The compliance matrix $[(C_1)_{ijkl}^e]$ is independent of the stress increment path $[d\sigma_{kl}]$, but it could depend on the stress state. The very small strain deformation properties of most geomaterials could be modelled only by hypo-elasticity, but the experimental evidence is scarce. This independence was checked through special hollow cylindrical tests on Hostun sand (**Fig. 2.1**). At three stress states, **0** and **1-triaxial** and **1-torsional,** three types of very small unload/reload cycles were applied, which are; **A)** triaxial compression, changing σ_v' at constant σ_h' and τ_{vh}; **T)** pure torsional shear, changing τ_{vh} at constant σ_v' and σ_h', and **A+T)** a combined test changing proportionally both τ_{vh} and σ_v' at a constant σ_h'. The sum of the very small strain increments obtained from tests **A** and **T** are essentially the same as those obtained from tests **A+T**, indicating that the relationship given in Eq. 2.3 is valid.

In many previous studies of the elastic properties of geomaterials (e.g., Boyce 1980; Graham and Houlsby 1983; Muir-Wood 1990; Tatsuoka and Kohata 1995), $[(C_1)_{ijkl}^e]$ was assumed to be symmetrical in the same way as $[C_{ijkl}^e]$. Note that the elastic strains $\Delta\varepsilon^e_{ij}$ that are obtained by integrating $d\varepsilon^e_{ij}$ of Eq. 2.3 having a symmetric $[(C_1)_{ijkl}^e]$ for a finite stress change $\Delta\sigma_{ij}$ may noticeably depend on the intermediate stress path due to a specific stress state-dependency of $[(C_1)_{ijkl}^e]$ (Hoque and Tatsuoka 1998). In that case, $[C_{ijkl}^e]$ obtained from integrated strains $\Delta\varepsilon^e_{ij}$ and stress changes $\Delta\sigma_{ij}$ may not be symmetric.

Linear stress-strain relationships often indicate elastic behaviour, but not always. For example, the drained triaxial compression (TC) test on a very dense gravel reported in **Fig. 2.2** showed an initially linear stress-strain relationship until the axial strain ε_v reached about 0.001 %. A second apparently linear phase was then exhibited, followed by an increase in the tangent stiffness over the range ε_v= 0.1 to 0.2 %. However the plastic straining developed over the intermediate strain range can be seen by comparing the primary loading curve with those measured in small unload/reload test stages. The peculiar shape of the primary stress-strain curve can be attributed to the fact that the drained Young's modulus $(E_v)_d = \Delta q/\Delta\varepsilon_v$ defined at an axial strain amplitude $\Delta\varepsilon_v = 10^{-5}$ in each small unload/reload cycle increases as the axial stress σ_v' increases (Fig. 2.2e), and this behaviour is reflected in the tangent Young's modulus E_{tan} of the primary loading relation (Fig. 2.2d) (see **Fig. 2.3** for the definitions of Young's modulus). In such cases, quasi-elastic behaviour is difficult to identify only from the linearity or non-linearity of the primary loading curve. Similar apparently linear behaviour was observed at large strains in drained TC tests on sedimentary soft sandstone (Tatsuoka and Kohata 1995; Kohata et al. 1997) and in drained TC stress path probing tests on Bothkennar clay (Smith et al. 1992).

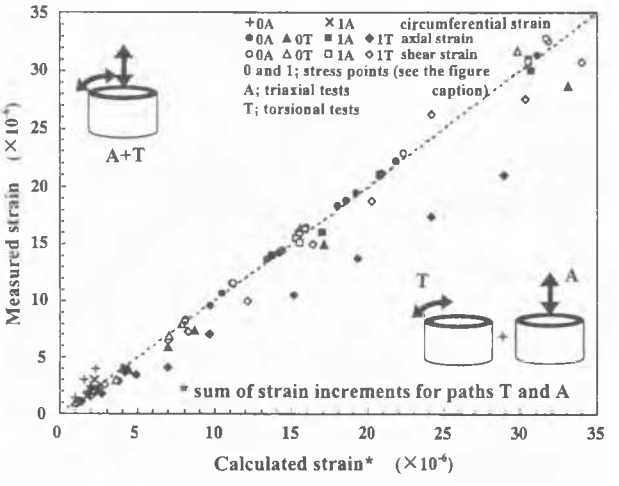

Fig. 2.1 Relationship between measured circumferential, axial and shear strain increments for combined stress path **A+T** and the sum of strain increments for path **A** and those for path **T** for loose air-pluviated Hostun sand (e= 0.75 - 0.77); Point **0** (σ_h'/σ_v' = 0.5; σ_h' = 70 or 80 kPa and τ_{vh}= 0), Point **1**-triaixal (σ_v' = 220 kPa, σ_h' = 70 kPa and τ_{vh}= 0) and Point **1**-torsional (σ_v' = 140 kPa, σ_h' = 70 kPa and τ_{vh}= 20 kPa); see Fig. 3.6b for the apparatus (Cazacliu 1996; Di Benedetto et al. 1997).

Yielding: The strength and yielding characteristics of geomaterials at relatively large strains are described within a classical visco-elasto-plastic theory by defining a yield locus. Historically, the behaviour within this locus has been considered to be either rigid, linear elastic or non-linear elastic. The shortcoming of such simplifications are now widely appreciated. Following Mroz (1967), multiple kinematic yield surfaces have been proposed by several workers to describe better the elasto-plastic behaviour seen inside the larger scale yield envelope. The simplified scheme summarized in **Fig. 2.4** was proposed on the basis of laboratory tests on clays by Jardine (1985, 1992b). Stress changes that remain within the large scale yield locus Y_3 develop only small to moderate strains, while tangent stiffnesses change abruptly when a probing stress path reaches the Y_3 locus. The Y_3 yield surface remains comparatively immobile and is only affected by relatively large strain events. When plotted in (p_e') normalized stress space, the envelope represents the current bounding surface. The more extensive State Boundary Surface (SBS) lies outside this current surface.

The current effective stress point is surrounded by two distinct sub-yield surfaces (Y_1 and Y_2). When the stress point reaches the initial Y_1 and Y_2 boundaries, the surface is engaged and dragged with the stress point: they are kinematic. If the soil is allowed to age at a fixed effective stress point, the surfaces may grow in size and move away from the stress point through creep processes and, possibly, bond formation. Under most circumstances, natural soils experience very slow in-situ creep strain rates. If we wish to characterise their behaviour when loaded from such an initial 'equilibrium' condition, it is convenient to define the initial stress and strain increment origins from the in-situ effective stress point. The Y_1 surface then represents the limits to the region over which the response is predominantly linearly elastic, even though some of the formal requirements of elasticity, such as complete strain rate independence, may not be satisfied. Therefore, in this report, the term "quasi-elastic" will be used for the behaviour within the Y_1 boundary. A sharp change in stress path direction may cause the stress point to re-enter the elastic region.

It is thought that a significant number of particle contacts start to experience local yielding due to normal stress concentrations when the Y_1 boundary is engaged, leading to some energy being lost when cyclic loading is performed. But any plastic strains that are developed are relatively small. For undrained clays, load-unload cycles (performed at the same loading rates, with

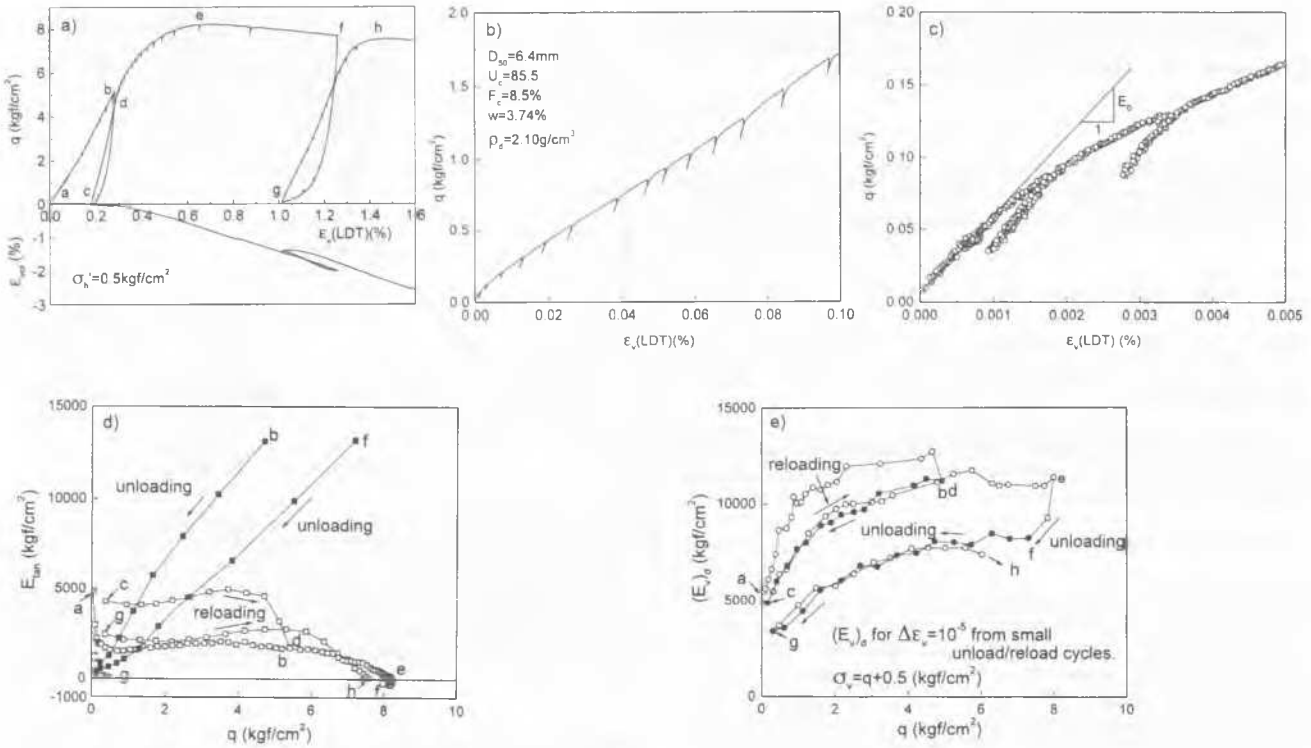

Fig. 2.2 Stress-strain relationships from a CD TC test on a large specimen (60 cm h x 30 cm d) of a very dense well graded Chiba gravel of crushed sandstone; a) overall relationships up to ε_v= 1.6%, b) $\varepsilon_v \leqq 0.1$ % and c) $\varepsilon_v \leqq 0.005$ %, d) E_{tan}-q relationship and e) $(E_v)_d$-q relationship (Jiang and Kohata 1997).

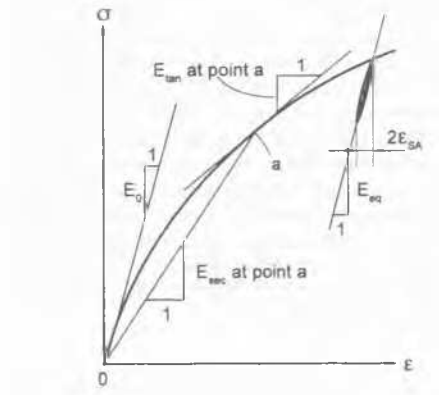

Note: 1) $E_{eq}=E_v$ when $\varepsilon=\varepsilon_v$, or E_h when $\varepsilon=\varepsilon_h$, and when $\varepsilon \leqq 10^{-5}$.
2) $E_v(E_h)=E_0$ when $E_v(E_h)$ is measured near the initial consolidation stress state (i.e., when $\sigma=0$ in this case)
3) $E_{sec}=E_{tan}=E_0$ when "ε at point a" $\leqq 10^{-5}$.
4) G_0, G_{eq}, G_{sec} and G_{tan} for τ and γ relationships are defined in the same way.

Fig. 2.3 Definitions for Young's moduli.

identical peak and through pause periods) appear to form closed loops, even for the first cycle (Jardine 1992b, 1995). Significant plastic straining is delayed until the stress point engages the Y_2 yield surface, at which stage a significant number of contacts points probably start to fail in shear, leading to interparticle slippage. The plastic strains experienced at this point may also be expressed by a marked shift in the directions of the strain increment vector.

A further feature of the Y_2 envelope is that it defines the threshold at which drained or undrained cyclic loading starts to affect the soil significantly. Sharp increases are seen in: the ratio of plastic to elastic strains; the creep rates observed when

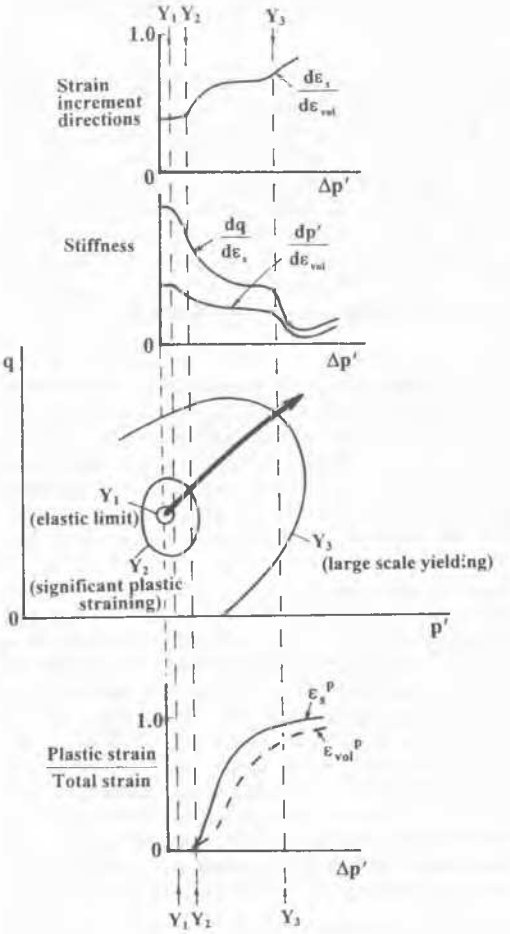

Fig. 2.4 Scheme of multiple yield surfaces (Jardine 1985, 1992b)

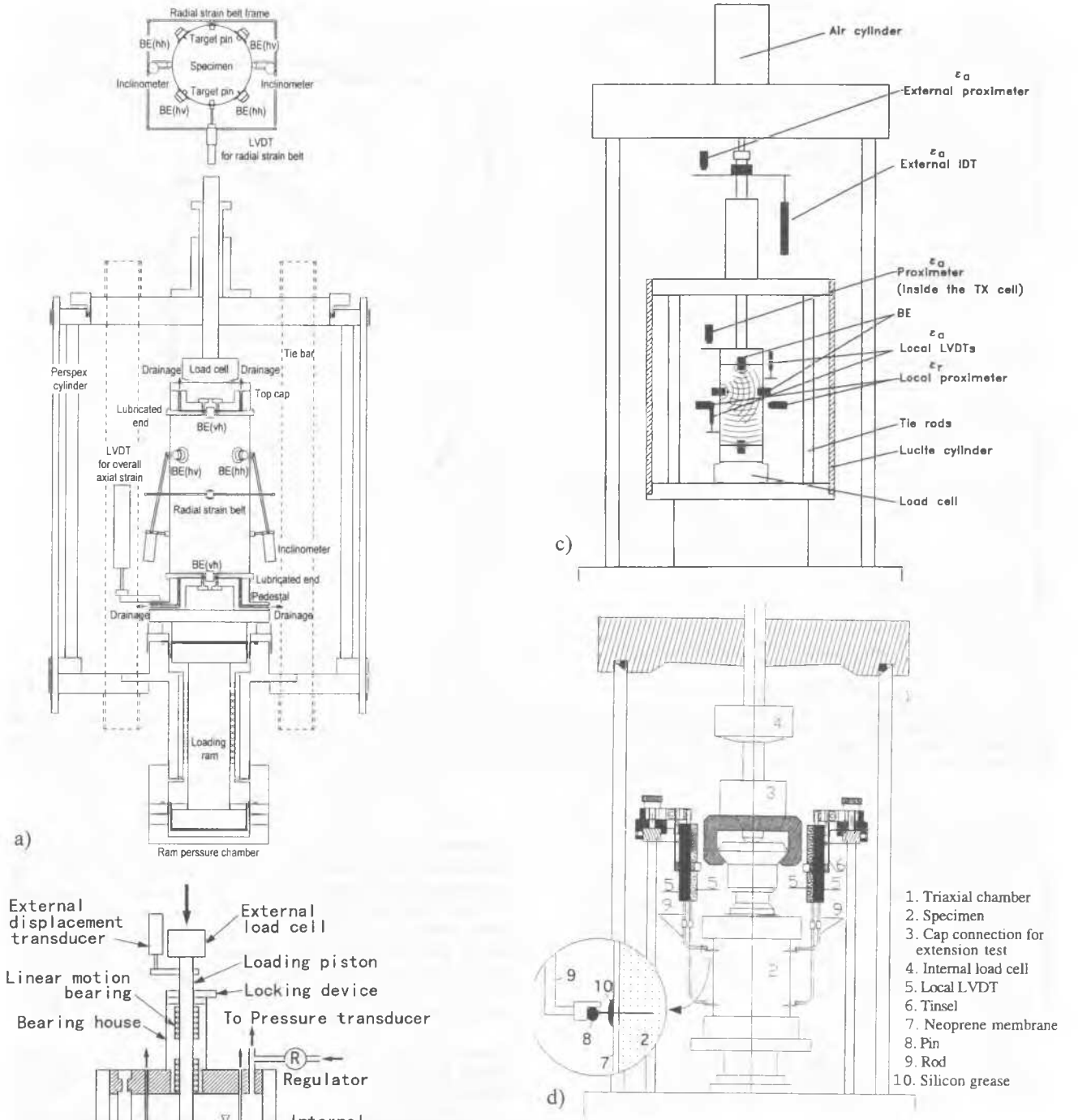

Fig. 3.1 Triaxial test systems developed at; a) Imperial College (IC; Kuwano 1997), b) Univ. of Tokyo (UT; Tatsuoka et al. 1994a), c) Politecnico di Torino (PT; Lo Presti et al. 1994), and d) Ecole Nationale des Travaux Publics de l'Etat (ENTPE; Di Benedetto et al. 1996).

the stresses are held constant; the energy dissipated in load cycles (and the hysteretic damping ratio); the rate of pore pressure development in undrained cyclic tests (Dobry et al. 1982). The strains developed by a stress path which progresses towards the Y_3 locus become increasingly plastic and time-dependent in their nature. As before, a sharp change in stress path direction leads to re-entry into the Y_1 and Y_2 regions.

3 SOME RECENT ADVANCES IN LABORATORY TESTING METHODS

Significant advances have been made recently in the triaxial testing method, which now allow sensitive and accurate stress

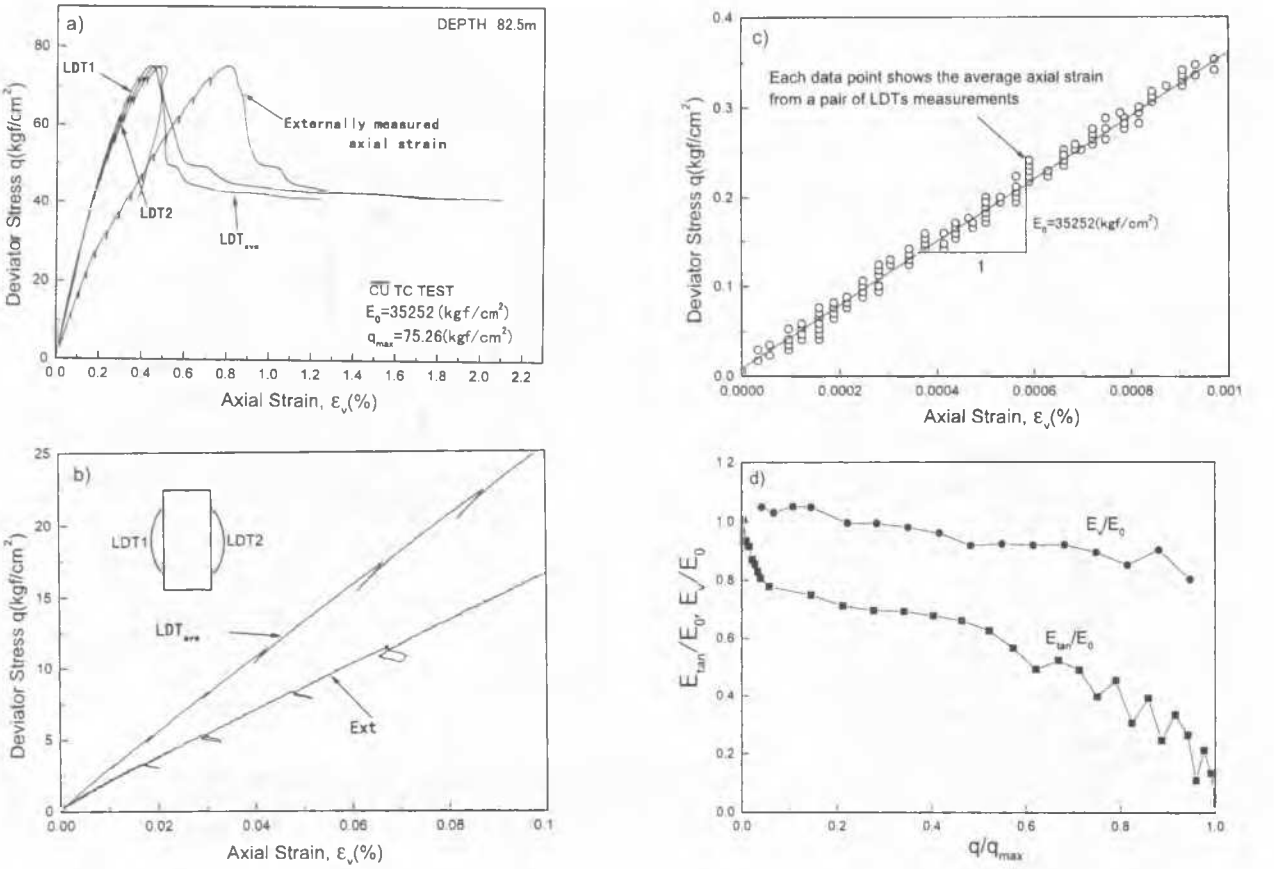

Fig. 3.2 CU triaxial compression (TC) test results for Sagamihara sedimentary soft mudstone (age approximately 1.5M years) tested using the system shown in Fig. 3.1b. The i2.5 cm H x 5 cm D sample was obtained by hand-operated direct coring at a depth of 82.5 m and reconsolidated isotropically to the field effective overburden pressure σ_{v0}'. The q and ε_v relationships are shown for a) $\varepsilon_v \leqq 2.2$ %, b) $\varepsilon_v \leqq 0.1$ % and c) $\varepsilon_v \leqq 0.001$ %. Part d) shows the E_{tan} and E_v - q/q_{max} relationship (Matsushita et al. 1997).

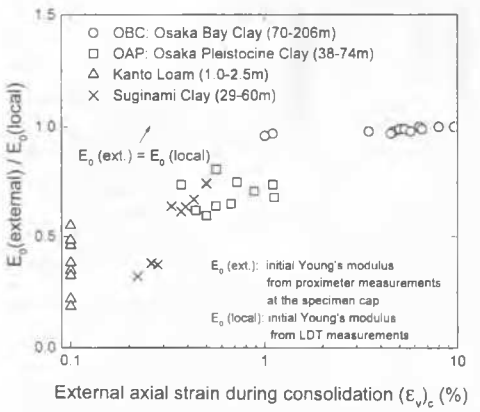

Fig. 3.3 Effects of bedding error on the initial Young's modulus E_0 in CUTC tests on undisturbed clays as a function of externally measured axial strain during reconsolidation (Tatsuoka and Kohata 1995).

and strain measurements to be made from strains less than 10^{-5} up to peak, or ultimate failure conditions, using a single specimen. In the systems presented in **Fig. 3.1,** an inner load cell is used; the IC and PT systems can measure locally both axial and lateral strains, while the IC system can also measure pore water pressure locally. The UT system can control axial displacements to less than 0.001 mm with practically no backlash when reversing the axial loading direction, as shown in **Fig. 3.2**. This allows elasto-plasticity to be examined at any arbitrary load level (see also Fig. 2.2). In this test, the top and bottom ends of the specimen were trimmed very carefully and capped with gypsum, and axial strains were measured with a pair of local gauges, LDTs (local deformation transducers; Goto et al. 1991). However, the large effects of bedding error and system compliance on measured axial strains can be seen. **Fig. 3.3** summarizes the ratios of the initial Young's moduli E_0 calculated at strains less than 10^{-5} from the locally and externally measured axial strains, plotted against externally measured axial strains during reconsolidation $(\varepsilon_v)_c$, obtained from CU TC tests on undisturbed clays reconsolidated isotropically or anisotropically to the respective field stress state. Strains $(\varepsilon_v)_c$ exceeding 1 % were required to eliminate the bedding errors.

Research reported by Tatsuoka and Shibuya (1992), Lo Presti (1995), Scholey et al. (1995), Cuccovillo and Coop (1996) and others shows that:

1. A strain resolution less than 10^{-5} is necessary to evaluate the quasi-elastic properties (see Figs. 2.2 and 3.2);
2. It is preferable that the pre-failure deformation characteristics and the large strain (failure) behaviour are evaluated from single tests on single specimens.
3. It is important to consider cost, easiness of handling, versatility for different specimen dimensions, and the ability to vary strain rates and apply cyclic loads (sometimes relatively fast cyclic loads) when designing equipment.
4. The transducers must have good long-term stability, particularly when submerged.

For the purpose **2** above, a) either a single very-sensitive but high-capacity load cell (as in the system shown in Fig. 3.1b) or a pair of very sensitive and high-capacity loads cells, and b) either a single very sensitive but high-capacity strain gauge or a pair of very sensitive and high-capacity strain gauges should be used. In the UT system, LDTs can measure strains up to about 2 %, while the measurable axial strain is up to 20 % in the IC system.

It is not possible to vary the σ_1 direction continuously in triaxial tests and several types of **torsional shear apparatuses** have been

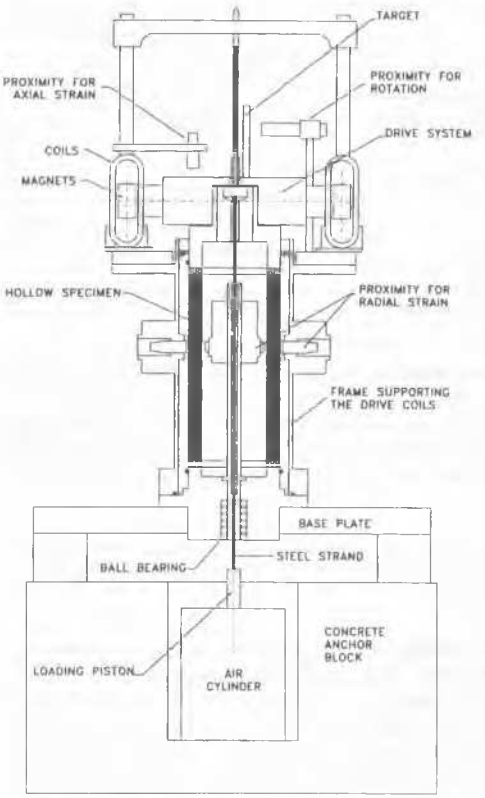

Fig. 3.4 RC-static torsional shear apparatus developed at Politecnico di Torino (Lo Presti et al. 1993).

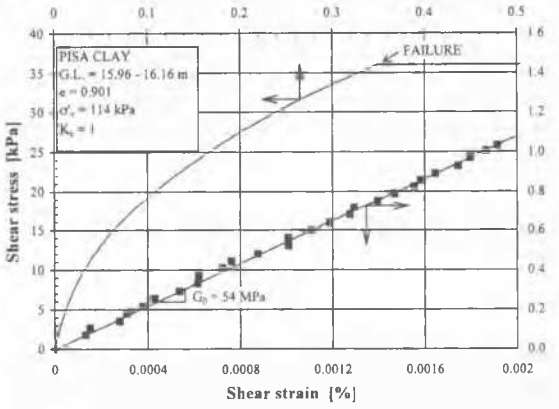

Fig. 3.5 Undrained stress-strain relationships at small and large strains from a torsional shear test on Pisa Clay (Lo Presti et al. 1996).

developed to obtain the entire pre-failure deformation characteristics over a wide torsional shear strain range by improving shear stress and strain measurements (e.g., Teachavorasinskun et al. 1991; Lo Presti et al. 1993; Kim and Stokoe 1994; Di Benedetto et al. 1997; Porovic and Jardine 1994; Shibuya et al. 1995a; Zdravkovic and Jardine 1997; d'Onofrio et al. 1997). **Fig. 3.4** shows a typical apparatus and **Fig. 3.5** shows a result from a typical test on Pisa Clay reconsolidated to the estimated in-situ stress conditions, performed by stress control at a shear strain rate from 0.004 to 0.008 %/min.

The large Hollow Cylinder Apparatus (HCA) developed at Imperial College (**Fig. 3.6a**) can control the three principal stresses and vary the σ_1 direction. Another HCA developed at ENTPE (**Fig. 3.6b**) can perform cyclic loading tests for strain amplitudes smaller than 10^{-5} in various forms (see Fig. 2.1), while it can measure various body wave velocities.

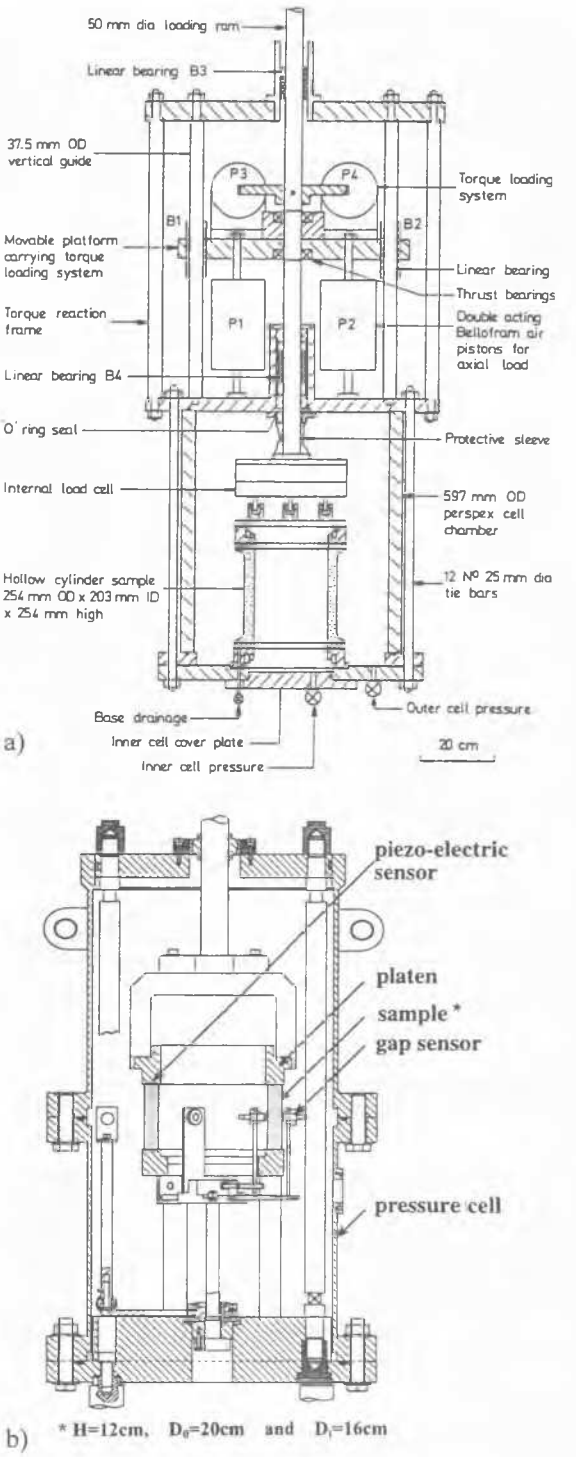

Fig. 3.6 Hollow cylinder apparatuses developed at; a) Imperial College (Hight et al. 1983, note: local strain sensors not shown), and b) ENTPE (Di Benedetto et al. 1997).

Among the several techniques for **wave propagation measurements**, the ultra-sonic wave technique is best established for hard rock cores. For intact cores of hard rock without open cracks, the elastic stiffnesses deduced from body wave velocities are similar to those obtained from equivalent slow static tests (see Figs. 5.3 and 5.4 of Tatsuoka and Shibuya 1992), as should be the case with any truly elastic homogeneous medium, provided the perturbing stress or strain paths are the same. The advantages of wave propagation measurements over static tests are that the tests are non-destructive, relatively compact and fast to perform. However, before the results are used for design purposes, the

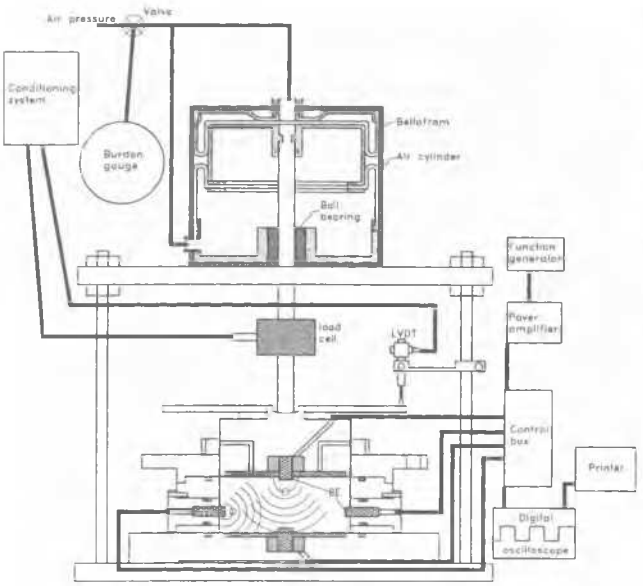

Fig. 3.7 Oedometer apparatus installing a BE test system (Jamiolkowski et al. 1995).

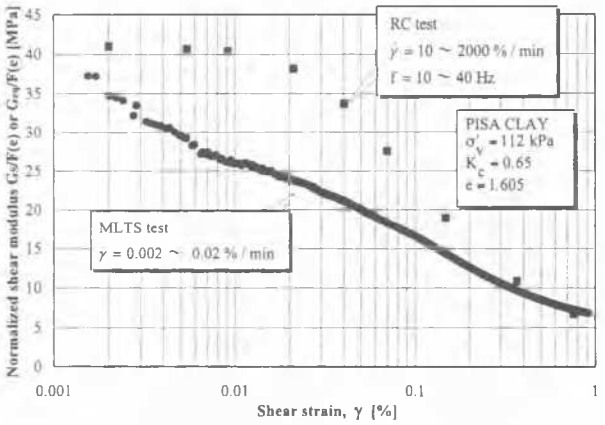

Fig. 3.8 Typical results from a ML torsional test followed by a RC test on Pisa clay; see Fig. 3.4 for the apparatus (Lo Presti et al. 1995).

effects of the following factors on the measured "stiffness" should be confirmed; 1) the ratio of the body wave length to the size of any discontinuity (particle size for granular materials, thin layering in soil and micro and macro cracks, joints and faults in rocks); and 2) strain rate or loading frequency. The effects of local heterogeneity are poorly understood, and they could cause the elastic stiffnesses obtained from body wave velocities to be larger than the average values from static tests, as discussed in **7.1**.

The Bender Element (BE) method (Schulthesis 1981; Dyvik and Madshus 1985) has been applied widely in recent years in triaxial, torsional shear and oedometer systems to evaluate elastic shear stiffness and its change during static loading and/or with time, see Figs. 3.1a, c, 3.6b and **3.7**. The exact definition of the precise travel distance can be problematic with short oedometer or simple shear specimens, but not for most triaxial test specimens (Brignoli et al. 1996). Another potential problem is the accurate determination of the travel time (Viggiani and Atkinson 1995a), which could be overcome by using waves reflected between the top and bottom of the samples (Riemer et al. 1996). To accurately evaluate damping values from BE tests is still very difficult. Applying the methodologies of seismology, Riemer et al. (1996) evaluated damping values of sand from the distance attenuation properties of reflecting waves. Other issues include; 1) whether the BE can be used with softrocks; 2) techniques for measuring across a specimen diameter (Figs. 3.1a,

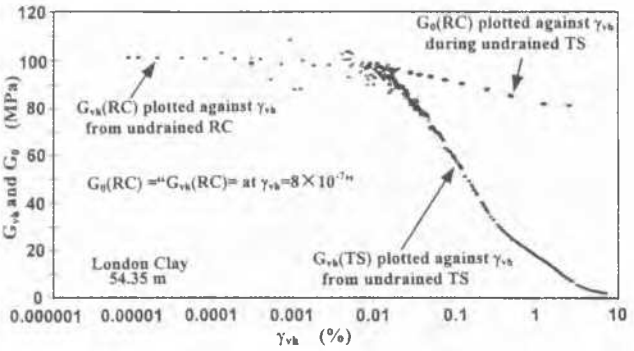

Fig. 3.9 Shear modulus G_{vh}(RC) from a torsional RC test (f ≅ 160 Hz), and $(G_{vh})_{sec}$ from a ML torsional shear test ($\dot{\gamma}$ = approx. 3×10^{-3} %/min) and $G_0(RC)(\gamma_{vh}= 8\times10^{-4})$ from RC tests performed during the MLTS test plotted against γ_{vh} during the MLTS test; undrained saturated undisturbed London clay (Porovic 1995; Hight et al. 1997).

c); and 3) the use of piezoelectric shear plates, which, unlike bender elements, do not penetrate into the specimen (Brignoli et al. 1996).

The Resonant-Column (RC) test has been used primarily to evaluate stiffness for a strain range from less than 10^{-5} to about 10^{-3}. In the RC tests, an average stiffness for the entire specimen is measured, unlike the wave velocity measurements. Stress and strain uniformity is best with hollow cylindrical samples. However, it is difficult to control the loading rate and the number of cycles imposed, and a constitutive model (usually a visco-elastic one) for soil has to be assumed. Recently, several workers have performed both RC and static cyclic torsional tests on single specimens (Rampello and Silvestri 1993; Kim and Stokoe 1994, 1995; Lo Presti et al. 1995; Lo Presti 1995; Porovic and Jardine 1994). **Fig. 3.8** shows the shear moduli G, plotted against the static shear strain at which the respective TS and RC G values were defined, obtained from typical RC-static torsional shear tests using a single specimen. **Fig. 3.9** shows similar results from HCA tests on undisturbed London clay.

4 BEHAVIOUR IN THE QUASI-ELASTIC LINEAR (Y_1) ZONE

4.1 General

For stiff geomaterials having relatively large Y_1 and Y_2 zones, the quasi-elastic properties are important as bench marks both for their engineering characterisation and the construction of a general framework of pre-peak deformation characteristics. However, the importance of the elastic properties may not be obvious for less stiff geomaterials, and there has been controversy, concerning: 1) whether can an essentially quasi-elastic stiffness be defined confidently in laboratory stress-strain tests ?; and 2) if it can be defined, what are the most influential factors ?

4.2 Viscous effects at very small strains

A number of researchers have compared initial values of shear modulus G_0 and Young's modulus E_0 developed at strains less than about 10^{-5} from static tests (monotonic loading ML and cyclic loading CL) with those from dynamic tests (e.g., RC and BE tests). For clean sands, a good agreement has been generally obtained albeit over a limited range of strain rate (**Figs. 4.1** and **4.2**). A broadly similar agreement was also obtained among G_0 values from torsional RC, TC and BE tests on saturated reconstituted Ham River sand (Porovic and Jardine 1994), although care is need when making such comparisons to account

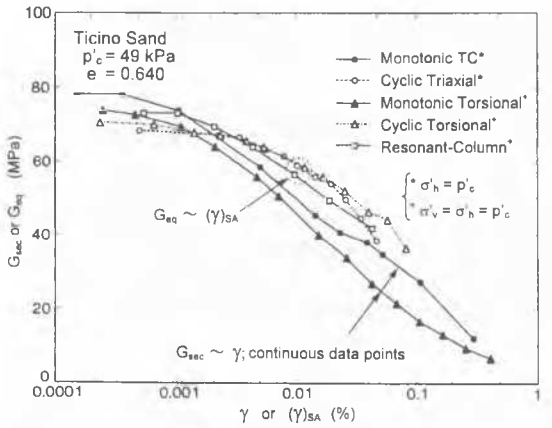

Fig. 4.1 Shear moduli of isotropically consolidated Ticino sand from static and dynamic tests (Tatsuoka et al. 1995).

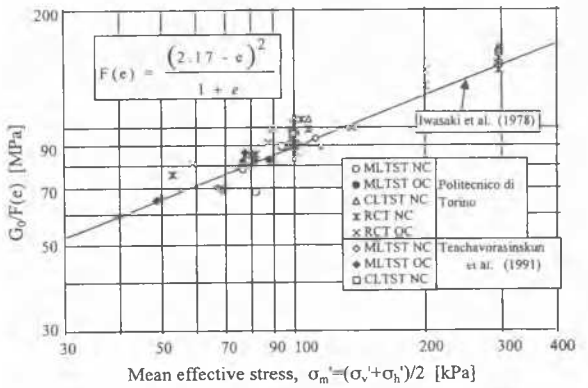

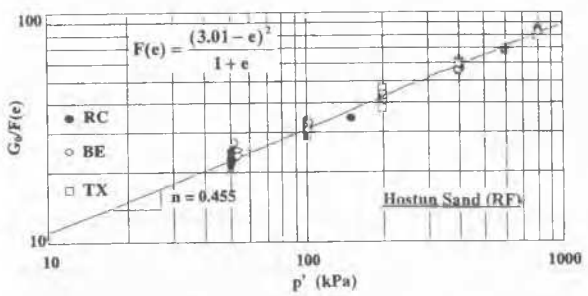

Fig. 4.2 G_0 values from static and dynamic tests at isotropic stress states; a) Toyoura sand (Jamiolkowski et al. 1994) and b) Hostun sand (Hameury 1995) (TX; cyclic triaxial tests, ML and CLTST; monotonic and cyclic torsional shear tests, RCT; torsional RC tests and BE; Bender Element tests measuring $(V_s)_{vh}$).

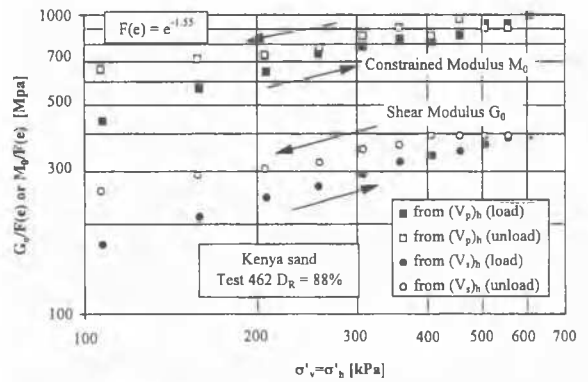

Fig. 4.3 G_0 from wave velocities of air-pluviated fine uniform carbonate Kenya sand (D_{50}= 0.145mm, U_C= 1.64) at isotropic stress states in a large calibration chamber (Fioravante et al. 1997).

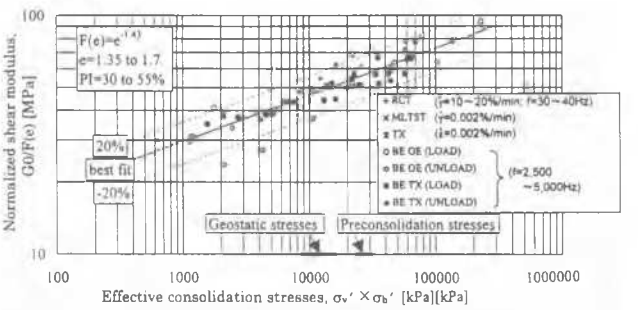

Fig. 4.4 G_0 values of undisturbed Pisa clay under NC and OC conditions from static and dynamic tests (after Lo Presti et al. 1995).

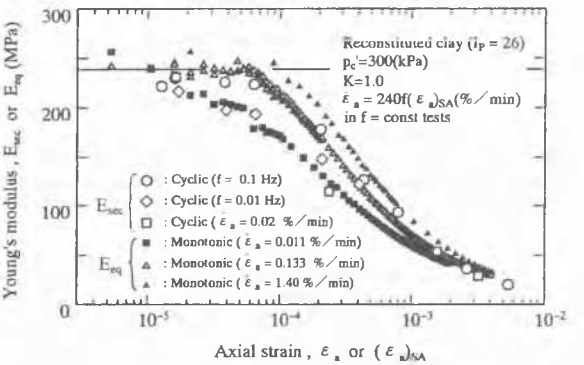

Fig. 4.5 Young's moduli from ML and CL triaxial tests on undrained saturated reconstituted NSF clay (w_p = 29 %; PI=26) (Shibuya et al. 1996).

for possible stiffness anisotropy. For clean silica or quartzitic sands, the effects on initial stiffness of stress history including over-consolidation and cyclic pre-straining have been found insignificant provided the results are normalized for void ratio by dividing by the function F(e), as shown in Fig. 4.2a and by Teachavorasinskun et al. (1994), Tatsuoka et al. (1995b) and Lo Presti et al. (1995). For carbonate and crushable sands, on the other hand, the effects of over-consolidation are more significant (**Fig. 4.3**), and G_0 is a function of $F(e) \cdot OCR^{0.24}$.

G_0 values from static and dynamic tests which follow similar stress paths also appear to be similar for the soft Quaternary Pleistocene marine Pisa clay (**Fig. 4.4**) and for undisturbed London clay (Fig. 3.9). **Fig. 4.5** shows that for a reconstituted soft clay, E_0 values at very small strains are similar between ML and CL static tests at different strain rates. Hardin and Black (1968) suggested that for clays, G_0 depends on p′, void ratio and OCR. With undisturbed Pisa clay, however, the effects on G_0 of over-consolidation are not noticeable after normalisation by F(e) (see Fig. 4.4). Similar results were obtained for Augusta clay (Lo Presti et al. 1997) and soft Holocene clay (Shibuya et al. 1995b, 1996, 1997). Viggiani and Atkinson (1995) argued that the G_0 values of undisturbed and reconstituted clays can be represented as functions of only OCR and p′, following a more complex 'Critical State' normalisation procedure: more research will be required to obtain a general conclusion.

Strain rate effects have also been considered. **Fig. 4.6** summarizes the dependency of E_0 (defined at $\varepsilon_v = 10^{-5}$) on the peak-to-peak average strain rate seen in cyclic unconfined or triaxial shear tests on a variety of geomaterials, in ML TC tests on Kaolin, and in wave propagation tests on concrete and mortar. Except for the rock samples, all the data are from either undrained tests on saturated specimens or fully drained tests on wet or air-dried specimens. The following may be noted:

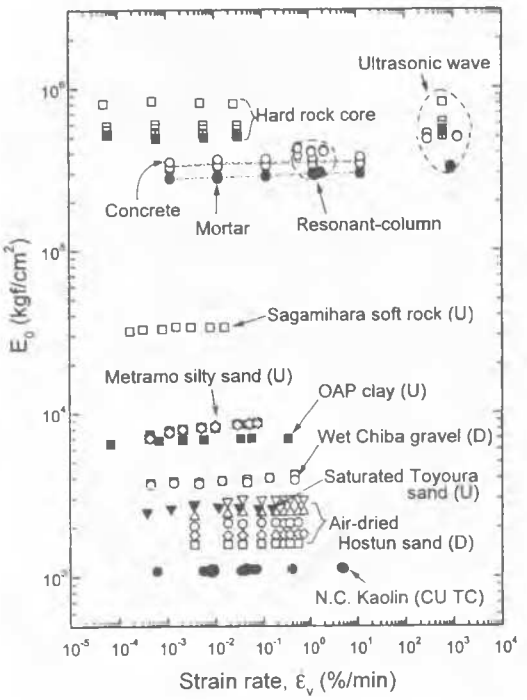

Fig. 4.6 Summary of the dependency of E_0 on strain rate from 1) cyclic triaxial tests (U; undrained and D; drained) on Sagamihara soft mudstone, OAP clay and gravel (Di Benedetto and Tatsuoka 1997), air-pluviated Toyoura sand (e= 0.658 and $\sigma_v' = \sigma_h' = 1.0$ kgf/cm^2; Amaya 1997), air-pluviated Hostun sand (e= 0.72 and $\sigma_v' = 0.8 \sim 2.5$ kgf/cm^2 and $\sigma_h' = 0.8$ kgf/cm^2; Hoque 1996) and compacted Metramo silty granite sand ($\sigma_c' = 4.0$ kgf/cm^2; Santucci de Magistris and Hamaya 1996), 2) CU TC tests on NC Kaoline ($p_c' = 3.0$ kgf/cm^2, Kc=0.6~1.0) (Tatsuoka et al. 1994b), and 3) unconfined cyclic tests and ultrasonic tests on rocks, concrete and mortar (Sato et al. 1997a, b).

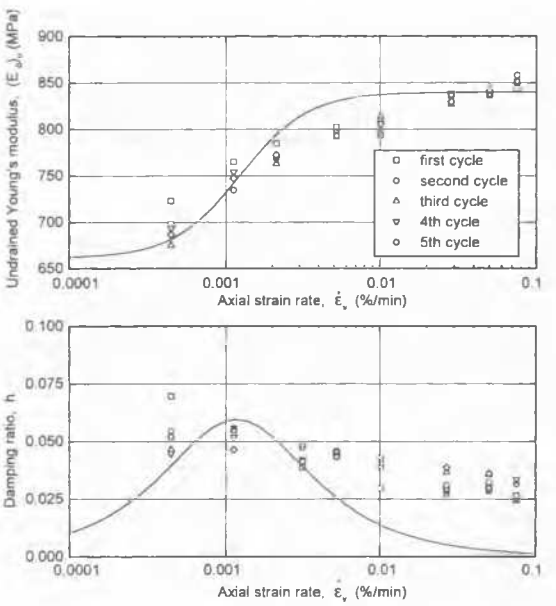

Fig. 4.7 $(E_0)_u$ and damping **h** of Metramo silty sand and best fitting curves for the SAB model (fitted by Di Benedetto).

1. For cohesionless soils, hard rocks, concrete and mortar, the dependency appears small.
2. For silty sand, soft and stiff clay and sedimentary soft mudstone, the dependency is marginally greater (see **Fig. 4.7** for Metramo sand).
3. Generally, the rate of increase in E_0 per log cycle of strain rate is greater at slow strain rates.

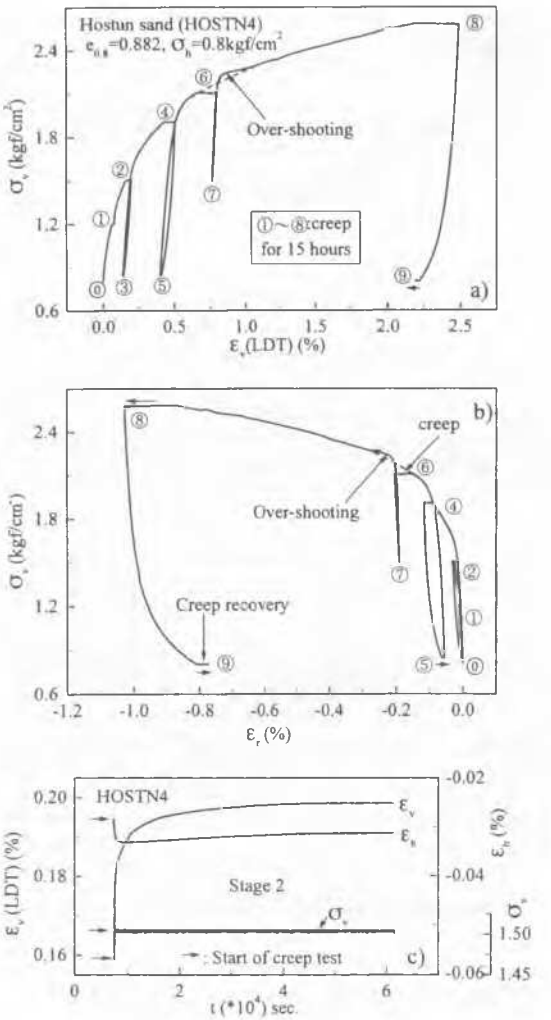

Fig. 4.8 Creep behaviour of air-dried loose Hostun sand from a TC test (loading rate: q= 0.125 kgf/cm^2/min except for creep stages); a) and b) overall q- ε_v- ε_h relationships, and c) time histories of σ_v', ε_v and ε_h at Stage 2 (Hoque 1996).

Kim and Stokoe (1995) reported results from torsional cyclic shear and RC tests on single specimen of cohesionless and cohesive soils, showing that the dependency of G_0 on strain rate increases with PI. However, this trend may be compensated for, or overwhelmed, in clays subjected to an extremely slow strain rate by the effects of structuration over time (Leroueil et al. 1996). In Fig. 4.6, some difference seen between the static and wave propagation tests for concrete would be due largely to heterogeneity in the specimens, as discussed later.

Creep also influences the small-strain response of geomaterials. As seen from **Figs. 4.8, 4.9** and **4.10**, even sands and gravels exhibit noticeable creep deformation, as reported by Murayama et al. (1984) and Di Benedetto and Tatsuoka (1997) and confirmed by field observations (e.g., Burland and Burbridge 1985). Similar data for sedimentary softrock are shown in **Fig. 4.11**.

These results suggest that even at very small strain rates, viscosity cannot be ignored, as discussed by Tatsuoka and Shibuya (1992), who also proposed that an upper bound for the E_0 or G_0 value may exist at some large strain rate, which forms an elastic limiting line for the initial stress-strain relationships in the Y_1 zone (**Fig. 4.12**).

In Fig. 4.6, Metramo sand showed the steepest strain rate dependency of the undrained Young's modulus $(E_0)_u$. Fig. 4.7 shows the details along with some predictions made by Di Benedetto with the use of a three-component SAB model,

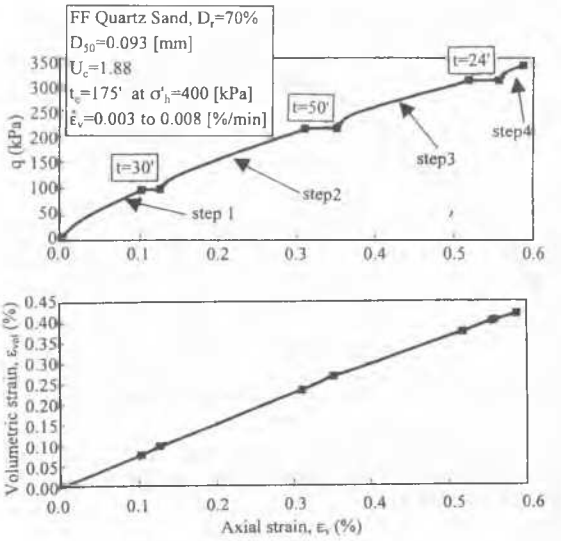

Fig. 4.9 Creep behaviour of saturated dense fine quartz sand (87 % sand and 13 % silt) from a TC test; a) q and ε_v relationship and b) ε_{vol} and ε_v relationship (Fioravante 1996).

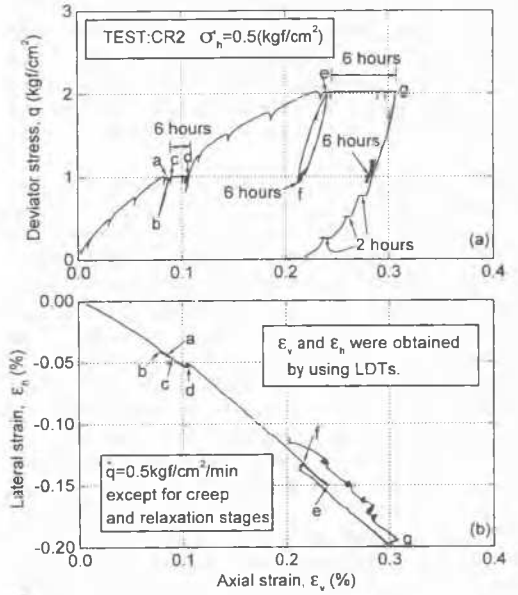

Fig. 4.10 Drained TC test on dense well-graded Chiba gravel with creep and relaxation tests at several stress levels during TC loading and unloading, using a rectangular prism specimen (57cm high × 23 cm × 23 cm) (Uchimura 1996a).

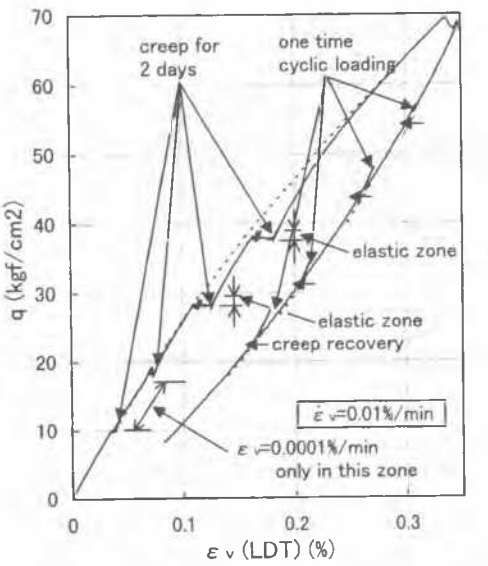

Fig. 4.11 Drained TC test on ≅ 1.5 million years old sedimentary soft mudstone from Sagamihara ($\dot{\varepsilon}_v$ = 0.01 %/min and 0.0001 %/min; σ_h' = 784 kPa) with creep at several stages (Matsumoto et al. 1997).

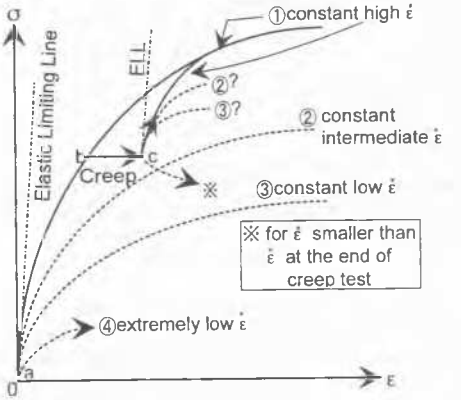

Fig. 4.12 Illustration of elastic limit line and effects of strain rate on stress-strain relationships.

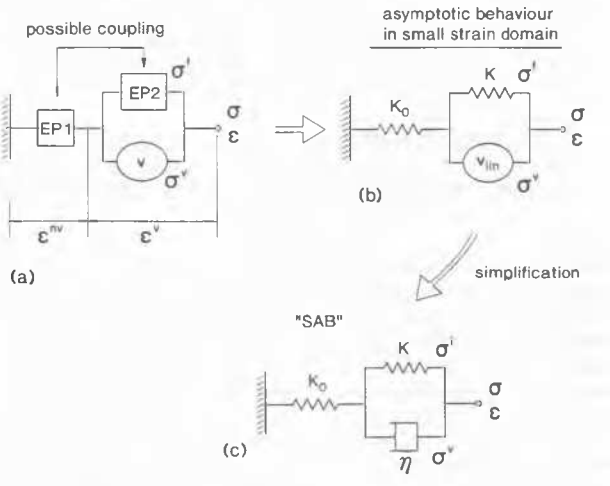

Fig. 4.13 Three-component rheology models (Di Benedetto and Tatsuoka 1997).

described in **Fig. 4.13**. This is the simplest version of a more generalized rheological model consisting of two elasto-plastic components and a non-linear viscous component (Di Benedetto et al. 1991). According to the SAB model, the values of E_0 or G_0 and damping ratio **h** for harmonic cyclic loading are functions of the loading frequency **f**, rather than strain rate, and upper and lower bounds of stiffness exist at very large and very small **f** values, where **h** becomes zero. A maximum in **h** is predicted when the logarithmic rate of stiffness change with **f** is greatest. The model explains the general trend of the data of the silty sand (and others), but some discrepancy can be noted in the detailed response, particular for **h**.

4.3 Size and shape of Y_1 and Y_2 zones

The following three factors have an important influence on the size and shape of Y_1 and Y_2 zones;

A. Recent stress and time history before arriving at the current stress state;
B. Structuration due to ageing and cementation occurring at the current stress state; and
C. Loading rate and path of perturbing stresses or strains.

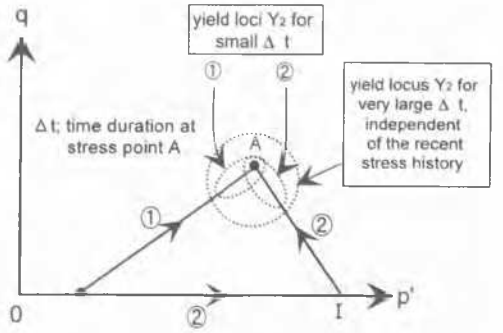

Fig. 4.14 Development of Y_1 and Y_2 zones by different recent stress-time histories.

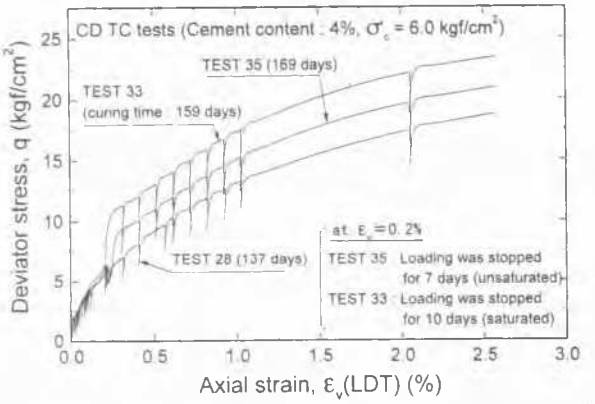

Fig. 4.15 Three CD TC tests on cement-mixed sand at $\dot{\varepsilon}_v$ = 0.03 %/min with and without ageing at the intermediate loading stage; sand (D_{50}= 0.5 mm, U_c= 3.0, and the initial ρ_d= 1.33 g/cm^3) (Sugo et al. 1997).

The factor **A** is sub-divided into; A1) a positive factor, which expands the Y_1 and Y_2 zones, as discussed immediately below, and A2) a negative factor, in which damage (or destructuration) develops through straining, as discussed in **4.6**. Although the effects of the factors A1) and B) cannot be separated completely from each other, we note (**Fig. 4.14**):

1. When the ageing period experienced at the current stress state is short, the effects of recent stress history become more important. The shapes and positions of the Y_1 and Y_2 zones are such that the regions of linear and relatively stiff behaviour extend as the relative angle between the recent effective stress path trajectory and the direction of the perturbing path decreases (e.g., Atkinson et al. 1990, Jardine et al. 1991); and
2. After prolonged ageing, the configuration of the Y_1 and Y_2 zones may be less dependent on the previous stress history. Geomaterials which have been aged for very long time in the field have well defined Y_1 and Y_2 zones.

The development and re-positioning of Y_1 and Y_2 zones by ageing can be seen in Figs. 4.8 to 4.11. **Fig. 4.15** shows results from three TC tests on a cement-mixed sand which had been cured for extended periods under the atmospheric pressure at a constant water content (i.e., w_{opt}= 12.5 %). While control unconfined compression tests showed little difference in stiffness and strength between samples cured for 137 and 169 days, triaxial tests involving ageing under applied loads showed major differences. Two specimens, 28 and 33, were saturated after curing and then isotropically consolidated to σ_c' = 6 kgf/cm^2, and then loaded in drained triaxial compression (TC). Specimen 28 was brought to failure. After developing a rather smaller axial strain of about 0.2 %, specimen 33 was re-cured in the triaxial cell for ten days without relaxing ε_v. The loading test was then re-started, showing very stiff behaviour: the Y_1 and Y_2 zones had extended, due probably to cementation at the new particle

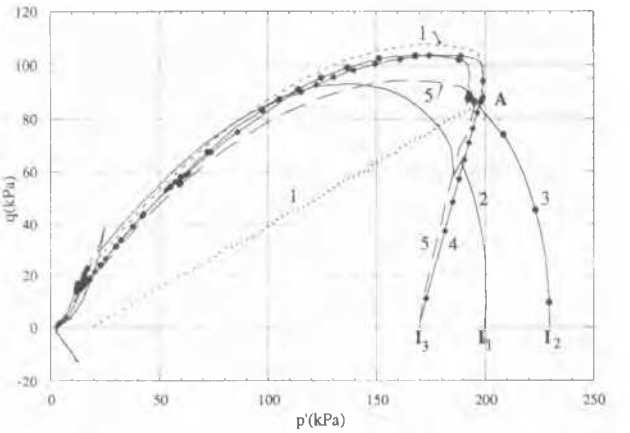

Fig. 4.16 Undrained TC behaviour of five very loose Hostun sand specimens having different stress-time histories; see Fig. 3.1d for the apparatus (Di Benedetto et al. 1997).

contacts developed during the initial loading phase. The third specimen 35 was tested in the similar same way as specimen 33, but without saturation before consolidation. This resulted into smaller Y_1 and Y_2 zones, perhaps due to the re-hydration of the cement being hampered by the smaller amount of pore water. These test results indicate that in the field, the Y_1 and Y_2 zones may develop on a geological or construction time scale through both ageing associated with both creep and cementation.

An initially stiff response upon the restart of loading after (re-) consolidation along such an anisotropic stress path as ① in Fig. 4.14 has been observed by many researchers (e.g., Ampadu and Tatsuoka 1989). The results shown in Figs. 4.8 through 4.11 suggest, however, that such behaviour may not be totally due to the anisotropic (re-)consolidation stress path itself, but may also be associated with creep deformations developed at the recent and current anisotropic effective stress states. This speculation is supported by the test results shown in **Fig. 4.16**. Specimen **1** was anisotropically consolidated at $\dot{\varepsilon}_v$= 0.02 %/min directly to stress state **A** and not aged before undrained TC loading ($\dot{\varepsilon}_v$ = 0.21 %/min), while specimens **2** and **3** were first isotropically consolidated ($\dot{\varepsilon}_v$ = 0.22 %/min) to effective stress states $\mathbf{I_1}$ and $\mathbf{I_2}$, followed by undrained TC loading ($\dot{\varepsilon}_v$= 0.015 %/min). Undrained TC shearing of specimen **3** was interrupted by drained creep at stress state **A** until the axial and volumetric creep strains reached 0.043 % and less than 0.001 %, respectively, after 45 minutes. The stress path behaviour of specimen **3** upon the restart of loading ($\dot{\varepsilon}_v$ = 0.015 %/min) is nearly the same as that of specimen **1**, while specimen **2**, which was sheared undrained to the ultimate state without interruption, showed quite different behaviour. Specimen **4** was brought by slow drained TC ($\dot{\varepsilon}_v$ = 0.033 %/min) from an isotropic stress state I_3 to stress point **A**, where axial and volumetric creep strains of 0.09 % and 0.07 % were allowed to develop over 50 minutes, followed by undrained TC. Specimen **5** was taken to effective stress point **A** through fast drained TC ($\dot{\varepsilon}_v$=0.25%/min), followed by undrained TC without any creep ageing at **A**, and failed to follow the same effective stress paths or show the same stiffness response as specimens **1**, **3** or **4**. The development of Y_1 and Y_2 zones at point A is due to an abrupt increase in strain rate (Specimen **1**) or drained ageing (Specimens **3** and **4**). Both phenomena are basically the same from a rheological point of view.

Similar features are shown for reconstituted Kaolin in **Fig. 4.17**: an undrained TC test was performed from an isotropic stress state (from point **a** to point **b**) with drained creep for 30 days at an intermediate stage (moving from point **b** to point **c**). On resuming undrained TC loading, large Y_1 and Y_2 zones developed (from point **c** to point **d**) and the stress-strain curves show sharply discontinuous trends. The stress-strain relationship and effective stress path prior to the drained creep

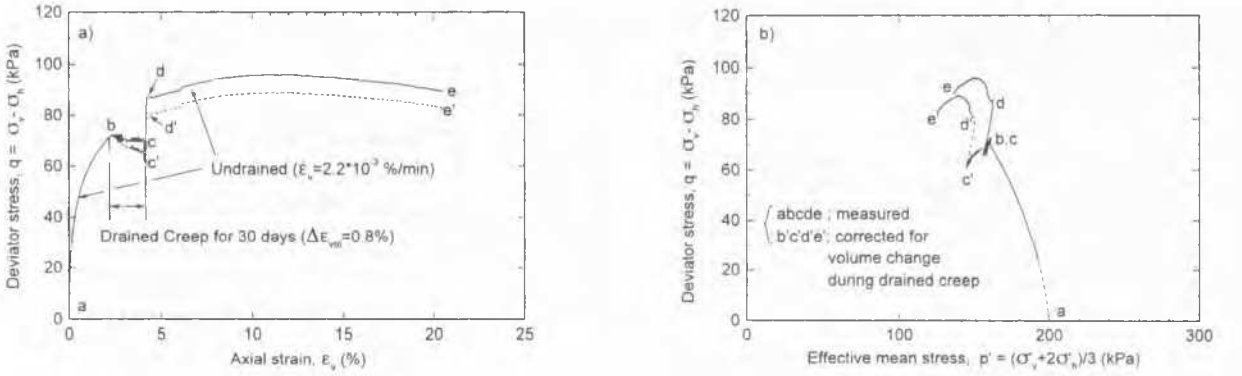

Fig. 4.17 Undrained TC behaviour of N.C. kaolin (w_p=41.6%, PI= 38; w= 61.1 % at p′ =200 kPa and q=0) (Momoya 1997).

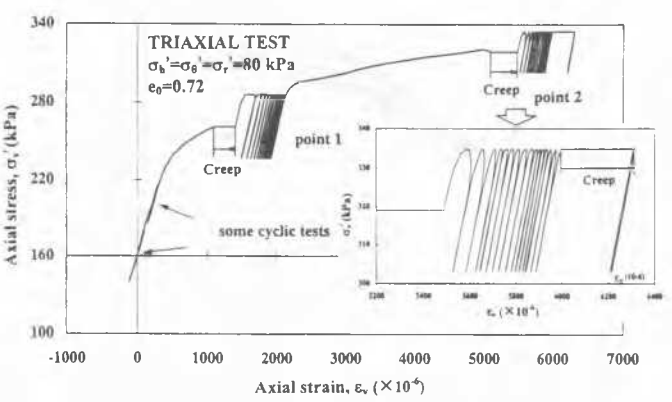

Fig. 4.18 σ_v' and ε_v relationships from a drained TC test on loose Hostun sand (e= 0.72) with small cyclic loading and creep deformation at intermediate loading stages (Cazacliu 1996; Di Benedetto et al. 1996).

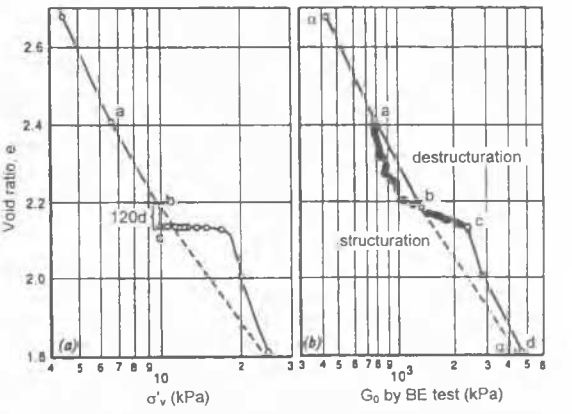

Fig. 4.20 Stiff and over-shooting behaviour of clay after extended creep deformation and destructuration during primary consolidation in an oedometer test (Leroueil et al. 1996).

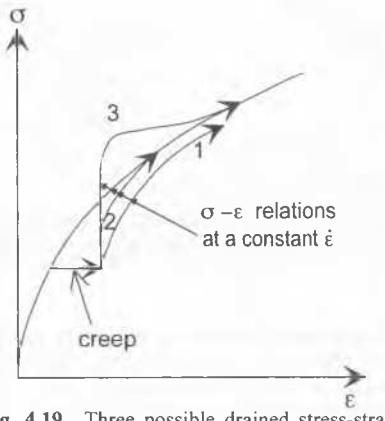

Fig. 4.19 Three possible drained stress-strain relationships upon restart of loading after creep.

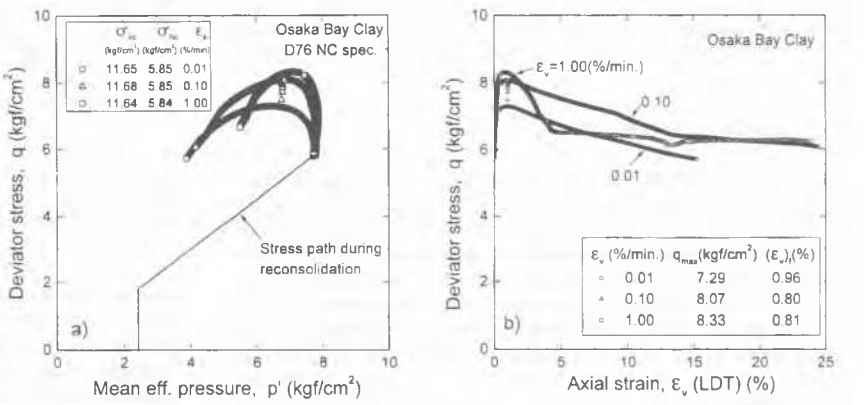

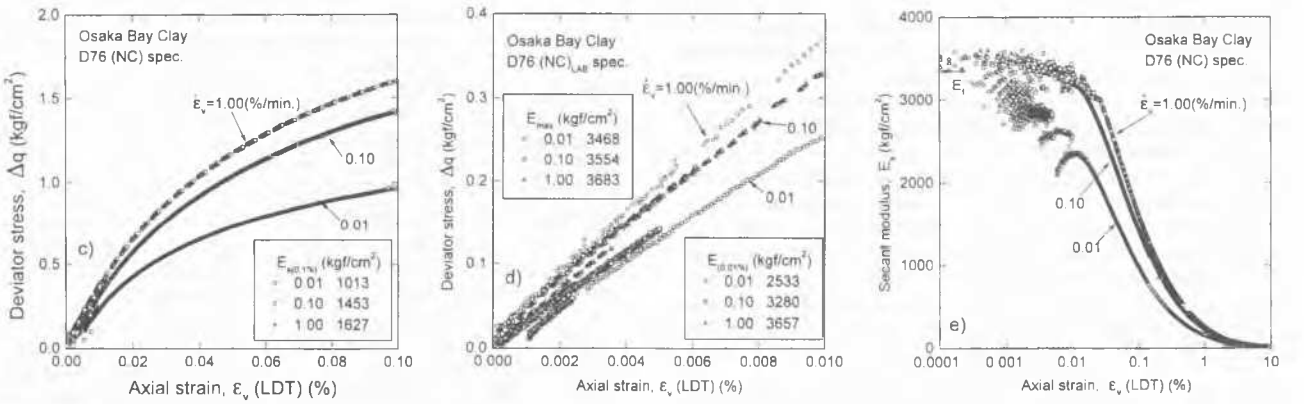

Fig. 4.21 CU TC tests at three strain rates on undisturbed stiff Pleistocene Osaka Bay clay (w_n= 50.8 %; w_p=55.7%; PI= 31): a) effective stress paths, b) q and ε_v relationships for $\varepsilon_v \leqq 2.5\%$, c) $\varepsilon_v \leqq 0.1\%$, d) $\varepsilon_v \leqq 0.01\%$, and e) E_s and ε_v relationships (Mukabi 1995).

(from point **a** to from **b**) become compatible with those developed after yielding (from point **d** to point **e**) when the behaviour is corrected for the creep volume change by a method equivalent to normalization based on the equivalent effective pressure p_e' (from point **d'** to point **e'**).

On the other hand, cyclic experiments on loose Hostun sand presented in **Fig. 4.18** show that moderate cyclic loading at point **1** and **2** makes the tangential stress-strain behaviour progressively more recoverable. Creep deformation without cyclic loading also makes the tangential behaviour more recoverable (see Point **2**). Moderate cyclic loading and creep deformation can lead to similar changes in the Y_1 and Y_2 zones.

Different stress-strain curves may be observed after the restart of loading as illustrated in **Fig. 4.19**. In cases where the effects of damage can be ignored, the stress-strain curve could eventually rejoin the original curve (i.e., the isotach behaviour described by Suklje 1969) following one of three types of path; 1) gradually converging without exhibiting well-defined yielding, as predicted by the three-component rheological model (Fig. 4.13); 2) after clear yielding, as shown in Figs. 4.9, 4.10, 4.11 and 4.17; or 3) after overshooting the curve, indicating the development of a structure that is damaged by subsequent straining, as shown in **Fig. 4.20**. Re-cementation during creep could be one of the reasons for such over-shooting, although overshooting can be observed in TC tests on air-dried Hostun sand (Figs. 4.8) (see also Fig. 2a of Di Benedetto and Tatsuoka 1997).

The detailed stiffness behaviour of geomaterials cannot be explained by most classical elasto-plastic models, and a kinematic hardening model (Fig. 2.3) is required. The Y_1 and Y_2 zones are translated and modified by over-consolidation, but the zones are always far smaller than the 'elastic' regions defined by classical critical state type models; e.g., Jardine (1992) for clays and Tatsuoka et al. (1994) for clean sands. The Y_1, Y_2 and Y_3 zones expand with the perturbing strain rate, while the initial stiffness is kept rather constant, as typically seen from **Fig. 4.21**, and shown by CU TC tests on reconstituted and natural clays (Tatsuoka and Shibuya 1992) (see also Fig. 4.5). For cohesionless soils, the Y_1 and Y_2 zones increase in size dramatically when cyclic prestraining (CP) is applied at strain levels exceeding the current Y_2 zone (Hoque and Tatsuoka 1997).

4.4 Anisotropy in quasi-elastic properties

The quasi-elastic deformation characteristics of geomaterials show two types of anisotropy; 1) inherent anisotropy due to an anisotropic macro or micro fabric, which persists even when stress state changes, which leads to anisotropic stiffnesses at isotropic stress states (Jamiolkowski et al. 1991), and 2) anisotropy induced by an anisotropic current stress state, which may be modified easily by stress changes. However, stress changes that cause large strains can in turn alter the soil fabric, and hence modify its inherent anisotropy; so the two aspects can be difficult to separate.

Inherent anisotropy: Only limited laboratory tests studies have been performed on undisturbed samples to evaluate inherent anisotropy. A well cemented sedimentary soft mudstone from Sagamihara was found to exhibit only slight inherent strength and stiffness anisotropy in TC tests (Tatsuoka et al. 1997; Hayano et al. 1997), while King et al. (1994) showed that isotropically reconsolidated core samples of Whitchester mudstone exhibited an average ratio of E_h/E_v= 1.5 by the seismic method. Multi-direction oedometer BE tests by Jamiolkowski et al. (1995) (see Fig. 3.7a) showed that undisturbed samples of relatively soft Italian clays exhibited significant inherent anisotropy with G_{hh}/G_{vh}= 1.5. More data are needed to obtain general conclusions for natural soils and in the following sections, only reconstituted cohesionless soils are discussed.

TC and plane strain compression (PSC) tests on isotropically consolidated sand or gravel specimens prepared by pluviation

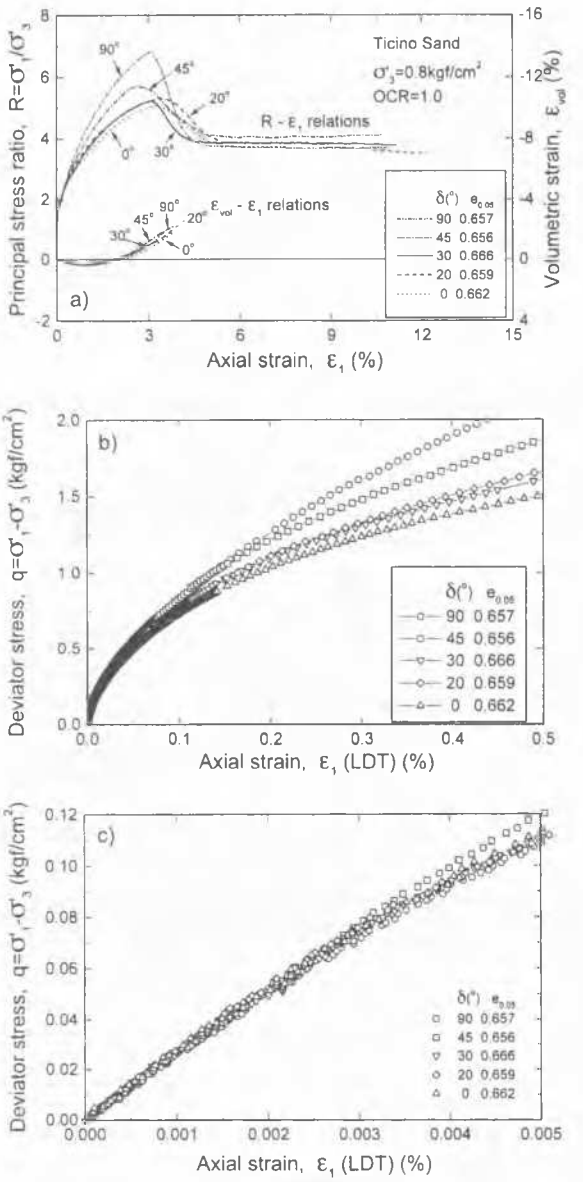

Fig. 4.22 Anisotropy in PSC tests on air-dried air-pluviated Ticino sand; δ is the angle of σ_1 with respect to bedding plane: stress-strain relationships a) $\varepsilon_v \leqq 12\%$, b) $\varepsilon_v \leqq 0.5\%$ and c) $\varepsilon_v \leqq 0.005\%$ (Park 1993).

(through air or water) or vertical compaction show their stiffest and strongest behaviour when the σ_1' direction is normal to the bedding plane: see Oda (1972, 1981), Arthur and Menzies (1972), Tatsuoka et al. (1986), Symes et al. (1984) and Park and Tatsuoka (1994) for sands, Oda (1981) for glass beads and Dong and Nakamura (1997) for gravels. As shown in **Fig. 4.22**, the effect of inherent anisotropy increases with strain level pre-peak, decreases in the post-peak regime and disappears at the residual state. Inherent anisotropy of the initial stiffness is not noticeable in Fig. 4.22c, although it may have been modified during a sequence of freezing and thawing and isotropic consolidation employed for preparing the specimens. **Fig. 4.23a** shows ratios of drained Young's moduli $E_v = \partial \sigma_v' / \partial \varepsilon_v$ to $E_h = \partial \sigma_h' / \partial \varepsilon_h$ (determined by changing σ_h' in one horizontal direction), obtained by applying very small increments of stress to 23 cm-square-prismatic triaxial specimens of air-pluviated poorly-graded sands and vertically compacted well-graded gravels. With these untilted specimens, at isotropic stress states, E_v is generally larger than E_h. This observation is consistent with the micro-scopic observation that pluviation and vertical compaction leads to far more numerous normals to interparticle contact in the vertical direction than in the horizontal direction (Oda, 1972). On the other hand, as shown in **Fig. 4.23b,** air-

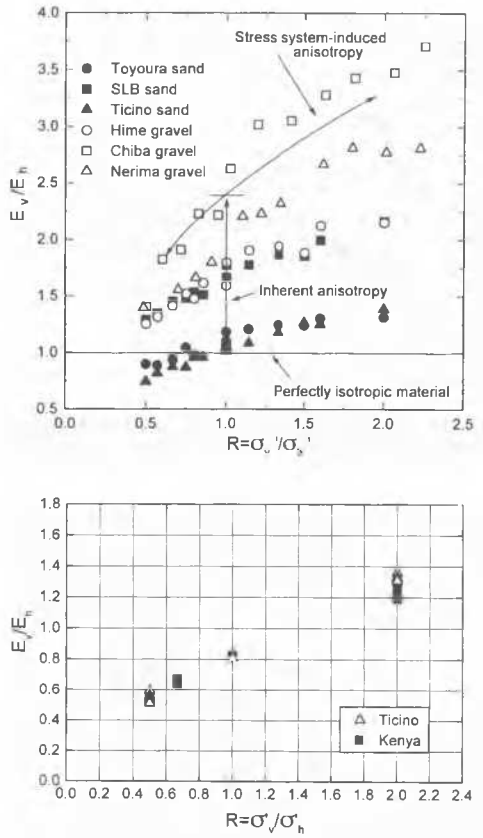

Fig. 4.23 E_v/E_h plotted against stress ratio σ_v'/σ_h'; a) very small cyclic tests on sands and gravels (Kohata et al. 1997) and b) wave velocity measurements in air-pluviated sands in a large calibration chamber (after Bellotti et al. 1996; Fioravante et al. 1997).

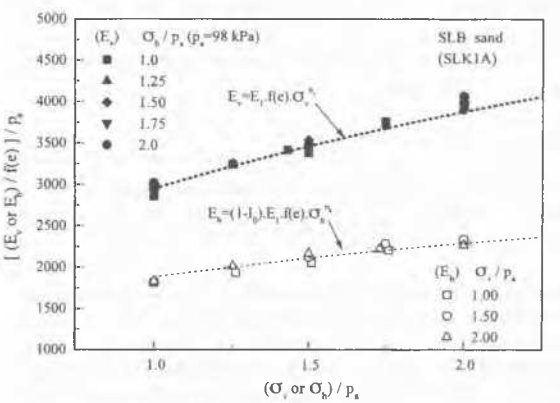

Fig. 4.24 Typical E_v and σ_v' relationships with variable σ_h', and E_h and σ_h' relationships with variable σ_v', under triaxial stress conditions with the two lateral principal stresses held equal (Hoque and Tatsuoka 1997).

pluviated sands exhibited $E_h > E_v$ at isotropic stress states in wave propagation measurements (see also Stokoe et al. 1991), suggesting that wave propagation tests may not be good indicators of inherent anisotropy in static deformation and strength parameters. This inconsistency between the static and seismic methods has not yet been explained fully.

Current stress state-induced anisotropy: Hardin (1978) suggested that for cohesionless soils, the initial quasi-elastic Young's modulus $E_x = \partial \sigma_x' / \partial \varepsilon_x$ in any particular direction is a unique function of the relevant normal stress σ_x'. Hardin's proposal has been supported by body wave measurements in sands (Stokoe et al. 1991; Jamiolkowski et al. 1991; Bellotti et al. 1996; Fioravante et al. 1997) and static tests on sands (**Fig. 4.24** and Lo Presti et al. 1995b) and gravels (Jiang et al. 1997). **Fig.**

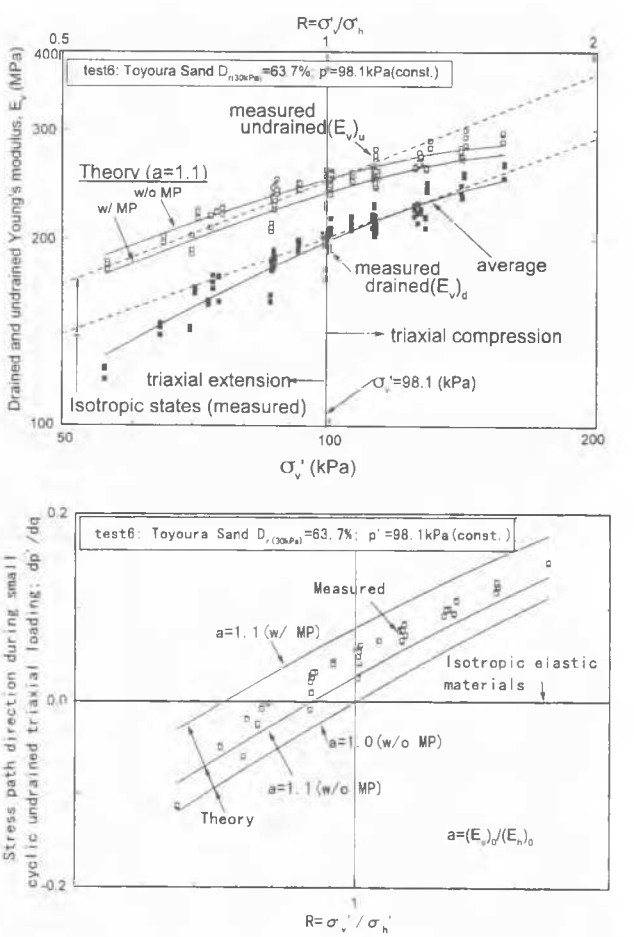

Fig. 4.25 a) Drained and undrained Young's moduli $(E_v)_d$ and $(E_v)_u$ at a constant p′ (=98kPa) (data points) and isotropic stress state (broken curves), plotted against axial stress σ_v', and b) dp′/dq during small undrained cyclic loading at a constant p′ (= 98 kPa); from very small cyclic TC proving tests (ε_v = 0.012 %/min.) on saturated air-pluviated Toyoura sand (e= 0.735) (Hamaya et al. 1997).

4.25a shows drained and undrained moduli, $(E_v)_d$ and $(E_v)_u$, (defined at axial strains $\varepsilon_v \cong 10^{-5}$) for saturated air-pluviated Toyoura sand, plotted against the current axial stress σ_v', for a specimen consolidated along isotropic and constant p′ stress paths under triaxial stress conditions. At constant p′, the drained modulus $(E_v)_d$ is strongly affected by σ_v'; the undrained modulus $(E_v)_u$ will be discussed later. **Fig. 4.26a** shows that $(E_v)_d$ values (estimated from measured undrained moduli based on Eq. 4.9 described later) also correlate well with the axial stress σ_v' for a sedimentary soft sandstone. These data were obtained from very small unload/reload cycles applied at isotropic stress states and during large amplitude drained cyclic triaxial tests at a constant σ_h' (= σ_{v0}') (**Fig. 4.26b**). **Fig. 4.27** shows similar results for a stiff Pleistocene clay; $(E_v)_d$ and $(E_v)_u$ correlate with σ_v', rather than p′.

If we combine the Hardin's power law expression for the drained quasi-elastic Young's modulus of an inherently cross-anisotropic material, then, if the anisotropy is symmetrical about the vertical axis, we obtain for triaxial stress conditions:

$$(E_v)_d = \partial \sigma_v' / \partial \varepsilon_v = (E_v)_0 \cdot (\sigma_v' / \sigma_0')^{nv} \cdot F(e)/F(e_0) \qquad (4.1a)$$

$$(E_h)_d = \partial \sigma_h' / \partial \varepsilon_h = (E_h)_0 \cdot (\sigma_h' / \sigma_0')^{nh} \cdot F(e)/F(e_0) \qquad (4.1b)$$

where $(E_h)_d$ is defined for changes of σ_h' in one lateral direction, $(E_v)_0$ and $(E_h)_0$ are the values of $(E_v)_d$ and $(E_h)_d$ when σ_v' and σ_h' are equal to the reference pressure σ_0', F(e) is the void ratio function with e_0 being the void ratio when σ_v' and σ_h' are equal to σ_0'. The ratio $a=(E_v)_0/(E_h)_0$ quantifies the inherent anisotropy at $p' = \sigma_0'$. As shown in **Fig. 4.28**, soft rocks

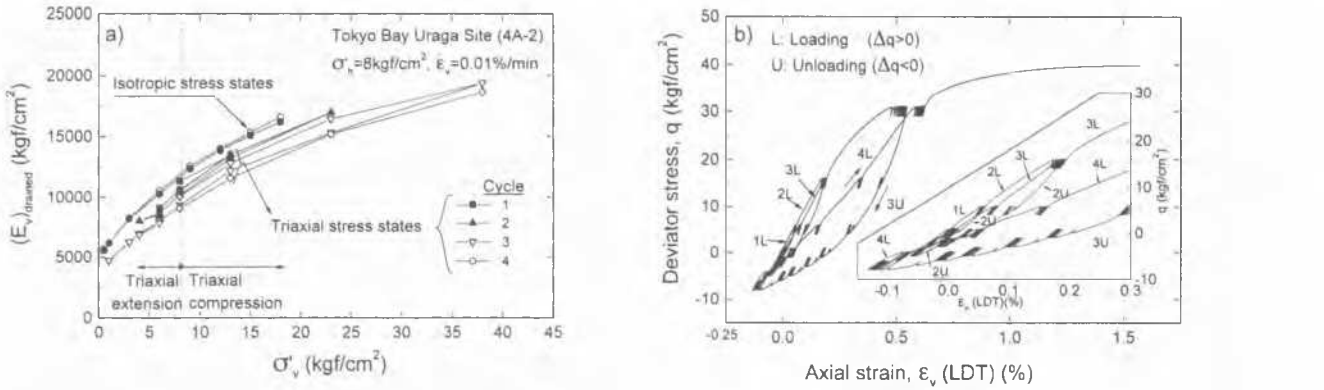

Fig. 4.26 Cyclic triaxial tests on a RCT sample of Uraga sedimentary soft sandstone (approx. 1.5M years old); a) relationships between $(E_v)_d$ and σ_v' during isotropic compression and large amplitude drained cyclic triaxial tests (σ_h' = 8 kgf/cm^2), and b) stress-strain relationships during large cyclic loading (Hayano et al. 1997)

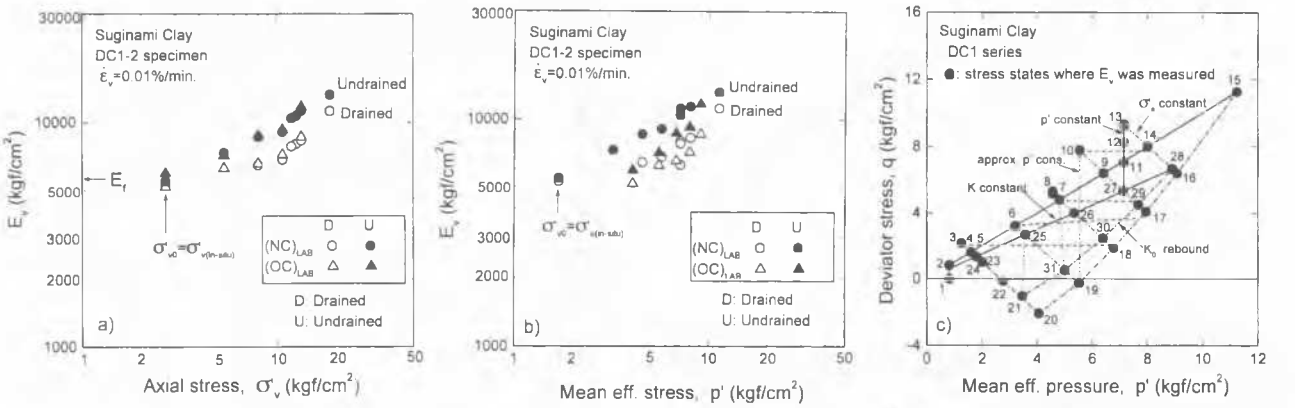

Fig. 4.27 Drained and undrained moduli $(E_v)_d$ and $(E_v)_u$, defined for $\varepsilon_v \leqq 10^{-5}$, plotted against; a) σ_v' and b) p′; from very small TC probing tests on block samples of undisturbed Pleistocene clay at Suginami (w_n= 38 %; w_p=23%; PI= 25 averaged for the sub-layer), and c) effective stress paths and stress points for E_v measurements (Mukabi 1995); E_f: the field seismic Young's modulus

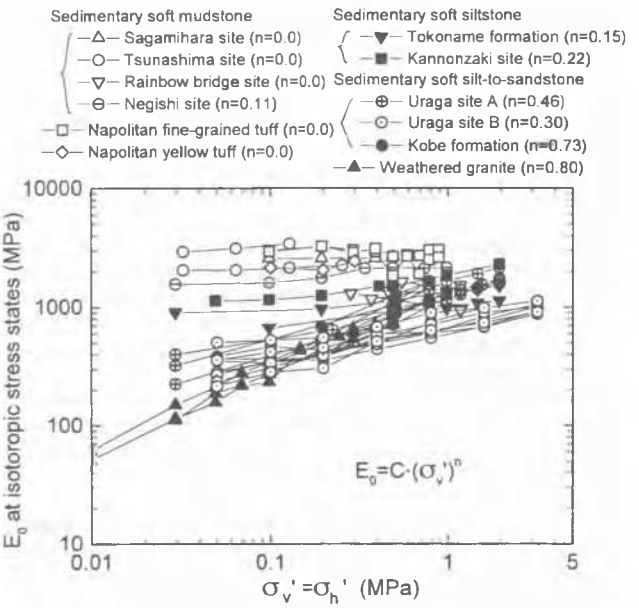

Fig. 4.28 Relationship between E_0 and isotropic confining pressure for sedimentary soft rocks (except for one weathered granite) (Tatsuoka et al. 1995c; Kohata et al. 1997).

become more stress-dependent (over the engineering pressure range) as the intrinsic grain size of the original soil becomes larger. We note also that Eq. 4.1 becomes less applicable to cemented materials as σ_v' or σ_h' approaches zero. Note that the change in void ratio during each test is negligible for the data shown in Fig. 4.28. When the powers nv and nh are the same and equal to n, we obtain;

$$(E_v)_d/(E_h)_d = (E_v)_0/(E_h)_0 \cdot (\sigma_v'/\sigma_h')^n \qquad (4.2)$$

With uncemented materials n≅0.5, and the ratio $(E_v)_d/(E_h)_d$ increases in a non-linear fashion with the stress ratio R= σ_v'/σ_h', and vice versa, as shown in Fig. 4.23.

Measurements of shear wave velocity $(V_s)_{xy}$ indicate that the shear modulus $G_{xy}=\partial\tau_{xy}/\partial\gamma_{xy}$ depends on the two orthogonal normal stresses σ_x' and σ_y' acting in the plane of shear deformation (Roesler 1979). More specifically, it is a function of $(\sigma_x')^{n/2}(\sigma_y')^{n/2}$, where the power n is the same as that in Eq. 4.2 (Stokoe et al. 1991, 1995). However, Porovic and Jardine (1994) showed from torsional shear and RC shear tests on water-pluviated Ham River sand under a wide range of triaxial stress conditions that the small strain shear modulus G_{vh} correlates closely with the mean stress p′. Samtamarina and Cascante (1996) found from similar torsional RC tests on an air-pluviated silica sand that G_{vh} was a function of s′=(axial stress σ_v' + lateral stress σ_h')/2. Tatsuoka and Kohata (1995) argued that G_{vh} is linked to the Young's modulus E_{45} as $G_{vh}=E_{45}/\{2(1+\nu_0)\}$, where E_{45} is the Young's modulus defined for major elastic strain increments developed in the direction inclined at 45 degrees to the vertical. Then, E_{45} is a function of the normal stress s′ in that direction. ν_0 is the relevant quasi-elastic Poisson's ratio which is independent of the ratio σ_v'/σ_h'. Then, G_{vh} becomes a function of s′.

4.5 Elastic compliance matrix

The simplest anisotropic model is cross-anisotropic elasticity, possessing a vertical axis of symmetry. Even for this model,

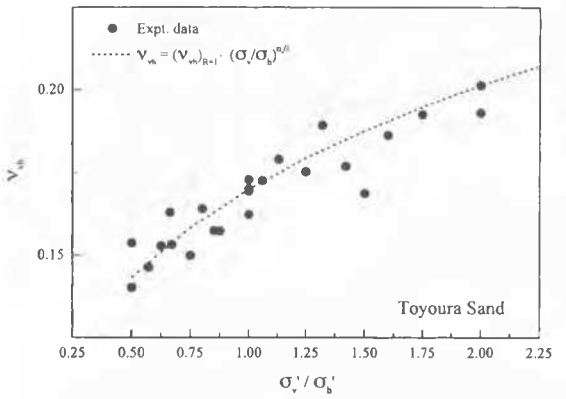

Fig. 4.29 Poisson's ratio for elastic strain increments $\nu_{vh} = -d\varepsilon_h^e/d\varepsilon_v^e$ for air-pluviated Toyoura sand (Hoque and Tatsuoka 1997).

only limited experimental data are available for the full compliance matrix $[(C_1)_{ijkl}^e]$ defined in Eq. 2.3. We note also that the inherent cross-anisotropy developed by vertical soil deposition on a flat plane may be lost through, for example, rotation of the σ_1 axis away from the inherent axis of symmetry.

It is seen from **Fig. 4.29** that the Poisson's ratios for quasi-elastic strain increments (in triaxial compression $\nu_{vh} = -\partial \varepsilon_h / \partial \varepsilon_v$) for normally consolidated Toyoura sand increases with the stress ratio $R = \sigma_v' / \sigma_h'$, approximately following:

$$\nu_{vh} = (\nu_{vh})_{R=1} \cdot R^{n/2} \quad (R=\sigma_v'/\sigma_h') \tag{4.3}$$

where $(\nu_{vh})_{R=1}$ is the value of ν_{vh} when R= 1. According to Eq. 4.3, ν_{vh} exceeds 0.5 at large R values for materials having high peak R values (Jiang et al. 1997). Such dilatant behaviour during cyclic loading is important practically in pavement design (Boyce 1980; Brown 1996). Due to the lack of experimental data regarding the cross-coupling compliance terms such as $\nu_{hv} = -\partial \varepsilon_v / \partial \varepsilon_h$, the compliance matrix is often assumed to be symmetrical. In that case, we obtain:

$$\nu_{vh} / (E_v)_d = \nu_{hv} / (E_h)_d \tag{4.4}$$

Eqs. 4.2, 4.3 and 4.4 then imply:

$$\nu_{vh} = \nu_0 \cdot \sqrt{a} \cdot R^{n/2} \tag{4.5a}$$

$$\nu_{hv} = \nu_0 \cdot (1/\sqrt{a}) \cdot (1/R)^{n/2} \tag{4.5b}$$

where $a = (E_v)_0/(E_h)_0$, which is $(E_v)_d/(E_h)_d$ at R= 1, and ν_0 is the value of $\nu_{vh} = \nu_{hv}$ when $R = a^{-1/n}$ (Tatsuoka and Kohata 1995).

The ratio of undrained and drained Young's moduli $(E_v)_u/(E_v)_d$ at isotropic stress states is generally larger than 1.0 as shown for air-pluviated sands by Tatsuoka and Kohata (1995) and for gravels by Hicher (1996). It may be seen from Fig. 4.25a, however, that the ratio $(E_v)_u/(E_v)_d$ decreases with the increase in R. This trend can be explained as follows. The elastic principal strain increments in an undrained triaxial test are:

$$d\varepsilon_v^e = \{1/(E_v)_d\} \cdot d\sigma_v' - \{2\nu_{hv}/(E_h)_d\} \cdot d\sigma_h' \tag{4.6a}$$

$$d\varepsilon_h^e = \{(1-\nu_{hh})/(E_h)_d\} \cdot d\sigma_h' - \{\nu_{vh}/(E_v)_d\} \cdot d\sigma_v' \tag{4.6b}$$

The undrained condition: $d\varepsilon_v^e + 2d\varepsilon_h^e = 0$ together with Eqs. 4.1, 4.5 and 4.6 gives;

$$dp'/dq = (1-2x)/\{(3 \cdot (1+x))\};$$
$$x = -d\sigma_h'/d\sigma_v' = (1-2 \cdot a^{0.5} \cdot R^{n/2} \cdot \nu_0)/\{2 \cdot a \cdot R^n \cdot (1-\nu_0 - \nu_0 \cdot a^{-0.5} \cdot R^{-n/2})\} \tag{4.7}$$

The ratio dp'/dq is always zero for isotropic elastic materials. The theoretical relationships based on Eq. 4.7 using n=0.503, ν_0 =0.15 and $\nu_{hh} = \nu_0$ are shown in **Fig. 4.25b**; the code MP signifies that the effects of membrane penetration were accounted for. In Fig. 4.25a, the following theoretical relationship between $(E_v)_u$ and σ_v' is shown:

$$(E_v)_u = d\sigma_v / d\varepsilon_v^e = (E_v)_d \cdot G(R);$$
$$G(R) = (1+x)/(1+2\nu_0 \cdot a^{0.5} \cdot R^{n/2} \cdot x) \tag{4.8}$$

where $d\sigma_v$ is the total axial stress increment. In so doing, the averaged $(E_v)_d$ and σ_v' relationship for the constant p′ stress path, which is shown by the thin solid curve in Fig. 4.25a, was used. It may be seen from Figs. 4.25a and b that the theoretical relationships fit well the measured ones, implying that the assumption of a symmetrical compliance matrix does not lead to large errors in this interpretation.

The compliance matrix for quasi-elastic strain increments (also for total or plastic strain increments) developed under ordinary triaxial conditions is often represented by using stress and strain increment invariants, while ignoring the third invariants of stress and strain increments (e.g., Atkinson and Sällfors 1991; Boyce, 1980) as:

$$\begin{bmatrix} d\varepsilon_{vol} \\ de_s \end{bmatrix} = \begin{bmatrix} C_{vp} & C_{vq} \\ C_{sp} & C_{sq} \end{bmatrix} \cdot \begin{bmatrix} dp' \\ dq \end{bmatrix} \tag{4.9}$$

where $p' = (\sigma_1' + \sigma_2' + \sigma_3')/3$ and $q = (1/\sqrt{2})\{(\sigma_1' - \sigma_2')^2 + (\sigma_2' - \sigma_3')^2 + (\sigma_3' - \sigma_1')^2\}^{1/2}$ and $d\varepsilon_{vol}$ and de_s are the corresponding strain increment invariants. If the more general compliance matrix $[(C_1)_{ijkl}^e]$ defined in Eq. 2.3 is symmetrical, then so is the compliance matrix in the form of Eq. 4.9. The shear and bulk moduli for quasi-elastic strain increments depend on effective stress path direction, except when the media are isotropic and therefore the coupling terms C_{vq} and C_{sp} are zero. For example, for cross-anisotropic media with the vertical axis of symmetry under triaxial stress conditions, the shear modulus for quasi-elastic strains $G_0 = dq/3de_s = (d\sigma_v' - d\sigma_h')/\{2(d\varepsilon_v^e - d\varepsilon_h^e)\}$ is a function of the effective stress path direction $\tan\theta = dp'/dq$ as:

$$G_0 = 3/(6A \cdot \tan\theta + 2B) \tag{4.10}$$
$$A = C - D \text{ and } B = 2C + D:$$
$$C = (1 + \nu_{vh})/(E_v)_d \text{ and } D = (1 - \nu_{hh} + 2\nu_{hv})/(E_h)_d$$

For this reason and as dp'/dq is not unique in undrained tests, the ratio $(G_0)_{undrained}/(G_0)_{drained}$ is not unique. On the other hand, the same combination of p′ and q can be obtained for different 3D stress combinations for which the compliance matrix in Eq. 4.9 becomes different when following Eqs. 4.1 and 4.5, and therefore the compliance matrix is unable to describe the stress state-induced anisotropy. The introduction of the third invariant is not sufficient, but the reference of stress coordinates to the axis of the material's inherent fabric appears to be necessary as in Eqs. 4.1 and 4.5. More modification is necessary when dealing with continuous rotation of the principal stress directions. When dealing with only triaxial compression and extension stress states, the use of σ_v' and σ_h', instead of σ_1' and σ_3', with $q = \sigma_v' - \sigma_h'$ can alleviate the problems described above.

4.6 Effects of structuration and destructuration on quasi-elastic modulus

Structuration; Soil structure (or micro-structure) significantly affects the stress-strain properties of geomaterials (e.g., Vaughan and Kwan 1985; Leroueil and Vaughan 1990; Burland 1990; Hight et al. 1992; Burland et al. 1996). Quasi-elastic stiffnesses increase as structure develops through ageing in the early stage of the diagenesis (e.g., Anderson and Stokoe 1978). In Fig. 4.20, for example, the quasi-elastic shear modulus G_0 measured by the oedometer BE test increased during ageing, moving from point **b** to point **c**. As seen in **Fig. 4.30,** the dimensionless parameter N_G indicating the rate of increase in G_0 per log cycle of time increases with the secondary compression index $C\alpha e$.

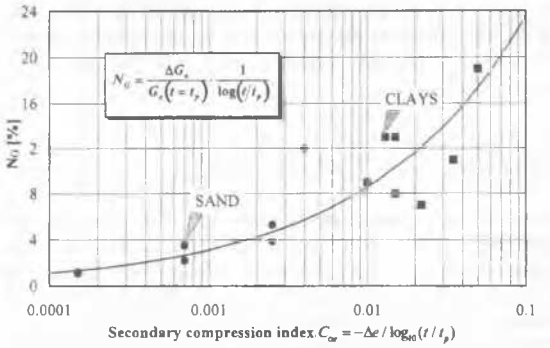

Fig. 4.30 Relationship between the parameter N_G and the secondary compression index $C\alpha e$; t_p= time at EOP (Lo Presti et al. 1996).

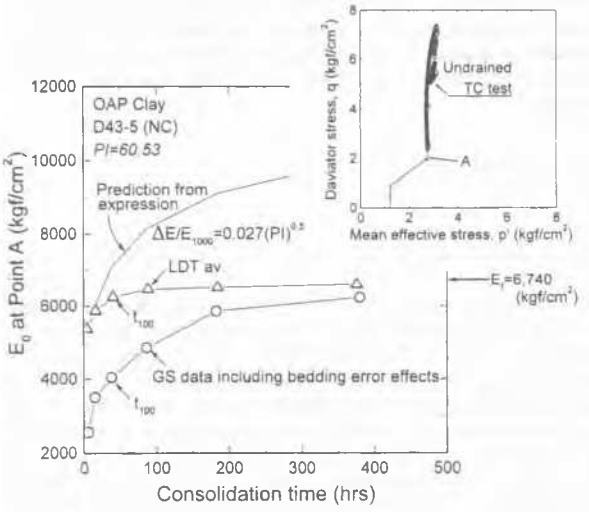

Fig. 4.31 Time history of E_0 during secondary reconsolidation at the field stress state **A** in a triaxial test and effective stress paths of undisturbed OAP Pleistocene clay (w_n= 47 %; w_p=35%; PI= 61 averaged for sub-layer) (Mukabi et al. 1994).

Considering a geomaterial mass in the field at an equilibrium condition after long in-situ ageing, a least disturbed sample would exhibit both small $C\alpha e$ and N_G values in laboratory tests, while the opposite is true for "disturbed samples". In the case shown in **Fig. 4.31**, the increase in E_0 after the end of primary consolidation (EOP) is relatively minor when based on the reliable data from local axial strain measurements (denoted as LDT_{av}). Note also that the final E_0 value is close to the E_f value deduced from the field down-hole seismic shear velocity, indicating high quality of the sample. In this case, the increase in E_0 after EOP is largely over-estimated when based on the empirical rule: $\Delta E/E_{100}= 0.027(PI)^{0.5}$ (ΔE is the increase in E_0 per log cycle of time and E_{100} is E_0 at EOP), obtained for soft clay samples obtained by thin-wall sampling (Kokusho et al. 1982).

Destructuration (or damage): Two opposing factors may affect the stiffness of natural soils when subjected to large strains in, for example, an oedometer test; 1) stiffening due to densification and 2) softening due to destructuration. In Fig. 4.20, the G_0 value developed in an aged clay after the restart of loading did not follow the $G_0 \sim e$ relationship, moving from point **a** to point **b**. Similar normally consolidated behaviour has been found in RC tests on clays by Anderson and Woods (1975) . In **Fig. 2.2e,** the $(E_v)_d$ value (defined for $\Delta\varepsilon_v= 10^{-5}$) from small unload/reload cycles of a drained crushed sandstone gravel initially increases with σ_v' in accordance with Eq. 4.1a. As the peak state is approached, however, the $(E_v)_d$ value starts decreasing, and this trend becomes more obvious post peak (from point **e** to point **f**), while the $(E_v)_d$ values during global unloading and reloading are smaller than those during the primary loading; such reductions

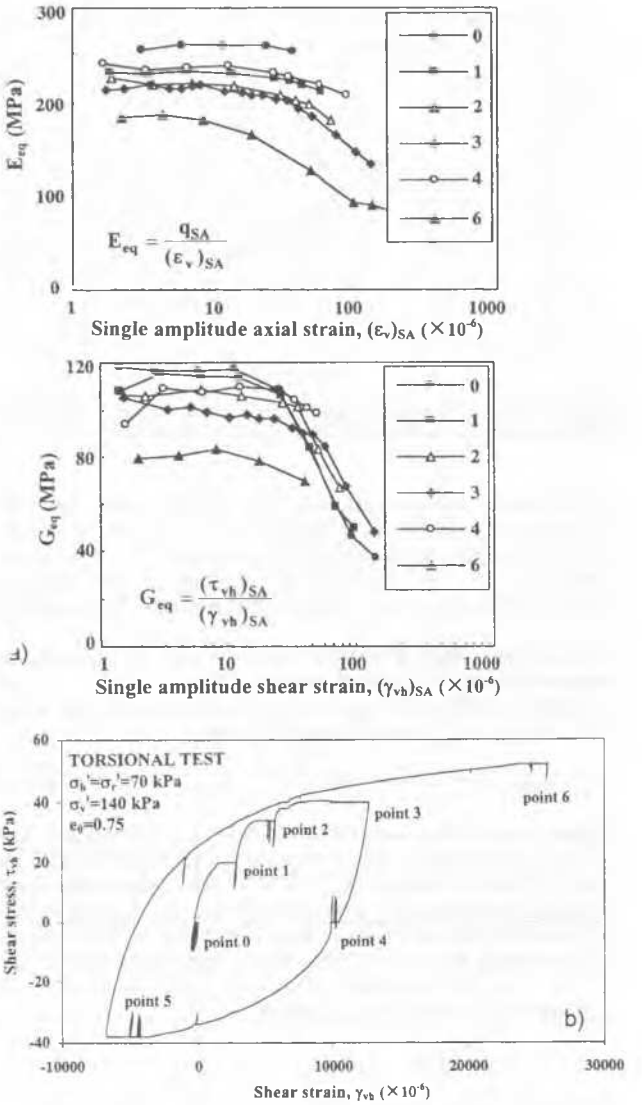

Fig. 4.32 a) Relationships between E_{eq} and G_{eq} and strain amplitude obtained from drained cyclic tests performed during torsional shearing at constant normal effective stresses, and b) overall shear stress and shear strain relationships during torsional shear; air-dried air-pluviated Hostun sand (Cazacliu 1996; Di Benedetto et al. 1994).

cannot be explained by dilation, and are attributed to destructuration by straining. **Fig. 4.32a** shows the values of E_{eq} and G_{eq} of Hostun sand obtained by applying very small to moderate cyclic changes in the axial stress σ_v' or torsional shear stress τ_{vh}. The cycles were applied with increasing strain amplitudes at several τ_{vh} values while keeping σ_v' and σ_h' constant (see **Fig. 4.32b**). The values of E_{eq} and G_{eq} at point **4** are smaller than those at nearly the same stress state (point **0**), suggesting the effects of destructuration. It is also seen that, despite the constant σ_v' and σ_h' values at points **1** to **6**, the E_{eq} and G_{eq} values at a given strain amplitude decreased with the increase in the shear stress τ_{vh}. Similar data for London clay are shown in Fig. 3.9 (i.e., a decrease in G_0(RC) with the increase in γ), confirming that structural changes (or damage) increase with the applied shear stress or strain level (Yu and Richart 1984). Also for the data shown in Fig. 4.25a, the values of $(E_v)_d$ measured under triaxial extension conditions deviate from the relationship established at isotropic stress states (shown by the broken line) to a larger extent as the stress ratio σ_v'/σ_h' decreases. The greater sensitivity of the soil structure in triaxial extension (compared with triaxial compression) has also been observed in tests on gravel (Flora et al. 1994) and sand (Hoque and Tatsuoka 1997).

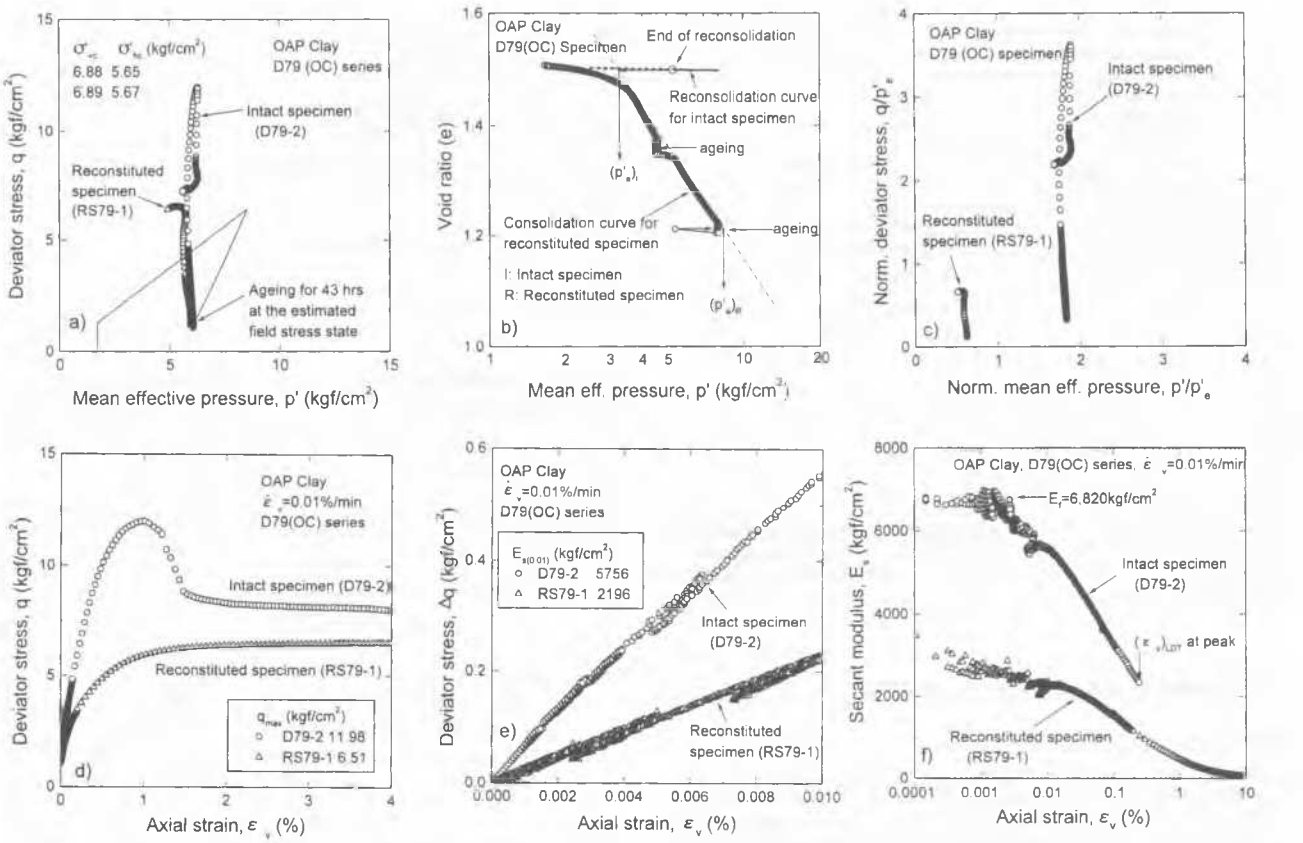

Fig. 4.33 CU TC tests on undisturbed specimen of Pleistocene OAP clay (w_n= 45 %; w_p=36%; PI= 56 averaged for the layer) and reconstituted one from slurry with w = 2 x w_L = 184.5%; a) effective stress paths, b) p′ and e relationships during consolidation, c) overall undrained stress paths normalized by the equivalent pressure p_e', d) overall stress-strain curves, e) stress-strain behaviour at small strains and f) E_{sec} and log ε_v relationships (Mukabi 1995).

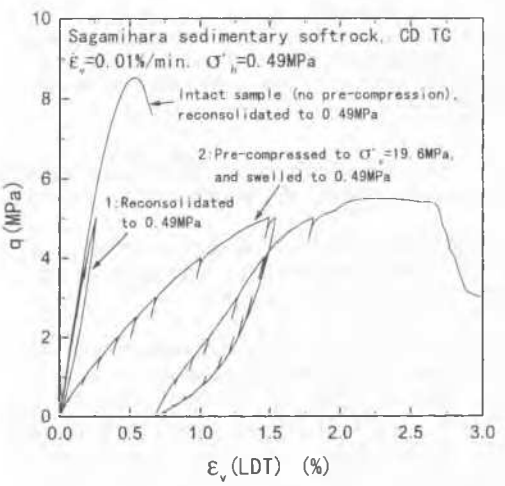

Fig. 4.34 Stress-strain behaviour of Sagamihara sedimentary soft mudstone from drained TC tests at $\sigma_h' = \sigma_{v0}'$ =0.49kPa, before and after isotropic compression to a pressure of p′=19.6MPa (Wang 1996).

The effects of structure are most often assessed by comparing the behaviours of undisturbed and reconstituted samples. For the case shown in **Fig. 4.33**, a reconstituted sample of a stiff Pleistocene clay was consolidated one-dimensionally to σ_v' =6.9 kgf/cm^2 from slurry at a water content of 184.5% (two times the liquid limit) in a small oedometer chamber. Then, the reconstituted sample was reset in a triaxial cell to follow the consolidation stress path shown in Fig. 4.33a. The undisturbed sample exhibited very small strains during reconsolidation and a E_0 value similar to the field value E_f, suggesting little sample disturbance. Despite a smaller consolidated void ratio, the reconstituted specimen exhibited much smaller values of initial stiffness, overall pre-peak stiffness and peak strength than the undisturbed sample. The q/p_e' and p'/p_e' normalized effective stress plot (Fig. 4.33c) compares behaviour for the same void ratio, showing similar trends to Bothkennar clay (Smith et al. 1992; Allman and Atkinson 1992). Some other apparently less cemented clay deposits have shown a lower sensitivity of stiffness at moderate strain levels (Jardine et al. 1991; Smith 1992; Jardine 1995).

The effects of destructuring due to straining are particularly important for well cemented materials, as can be seen from the reduction in $(E_v)_d$ with TC loading (Fig. 3.2) and by large amplitude cyclic loading (Fig. 4.26). In the latter case, with large cyclic loading, the E_{tan} value at the same stress state, decreased gradually in the similar way with the $(E_v)_d$ value (the data is not shown). **Fig. 4.34** compared stress-strain relationships from CD TC tests on two sedimentary soft mudstone samples, both isotropically reconsolidated to the field vertical stress level σ_{v0}'. CD TC tests were performed by using one specimen before and after isotropic compression to a pressure of 200 kgf/cm^2, which exceeds the Y_3 yield pressure. In the second TC loading, the specimen was brought to failure. For reference, another TC test was performed to failure using a fresh specimen isotropically reconsolidated directly to σ_{v0}'. Although the dry density increased from 1.29 g/cm^3 to 1.72 g/cm^3 through the isotropic compression to 200 kgf/cm^2, the overall pre-peak stiffness and peak strength decreased largely due to the damage to the cemented structure by the isotropic compression. This result indicates that this type of sedimentary softrock is not merely a heavily over-consolidated material, but its stiffness and strength originate largely from real cementation. Hight and Jardine (1993) argued that the same is true for the well-known London Tertiary clays.

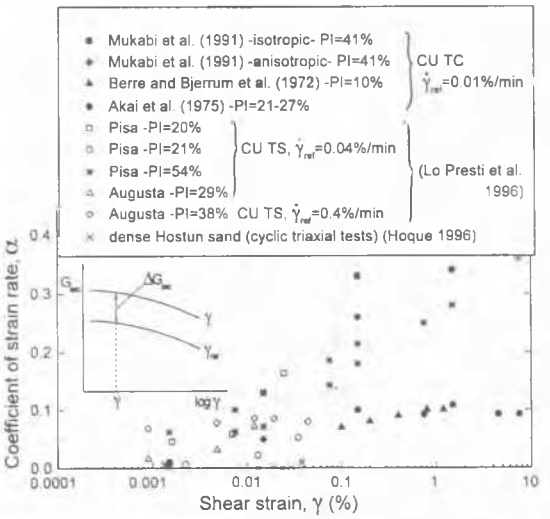

Fig. 5.1 Relationship between the coefficient of strain rate effect α for G_{sec} and γ from TC and TS tests on a variety of geomaterials (after Lo Presti et al. 1996 and 1997) and drained CL triaxial tests on Hostun sand (Hoque 1996).

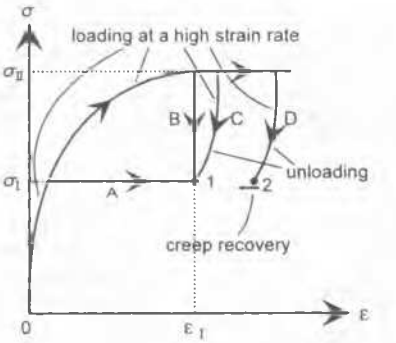

Fig. 5.2 Potential problems of isochronous models applied to behaviour after unloading.

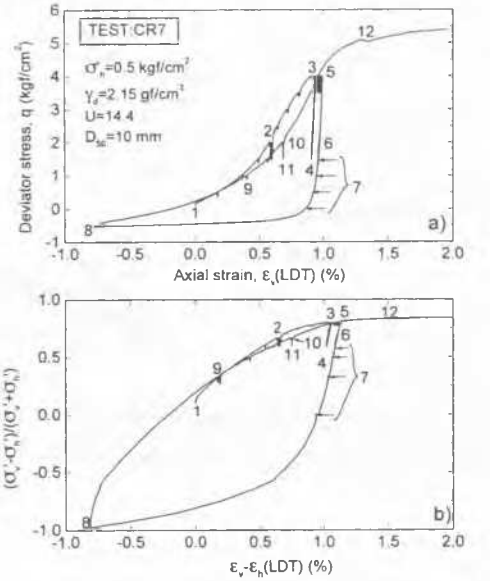

Fig. 5.3 Cyclic triaxial test on very dense well graded Kyushu gravel: a) q and ε_v relationships and b) $(\sigma_v' - \sigma'_h)/(\sigma_v' + \sigma'_h) \sim \varepsilon_v - \varepsilon_h$ relationships; creep tests at stages 2 and 5 and creep recovery tests at stage 7 (Uchimura 1996b).

5 INTERMEDIATE STRAIN BEHAVIOUR

5.1 General

The non-linear and irreversible deformation characteristics developed at intermediate strains are very important in evaluating ground movement, but are more difficult to characterize than the quasi-elastic properties. Approaches for deriving suitable design parameters include:

1. Combining quasi-elastic stiffness from field shear wave velocity measurements with larger strain data from field loading tests;
2. Non-linear analyses of results from pressuremeter or plate loading tests; or
3. Laboratory stress-strain measurements over the operational strain range in the field (say from about 10^{-5} to about 10^{-2}) involving the highest possible quality samples and relevant testing stress paths.

These three approaches are complementary to each other as limitations are inherent in each. For example, sample disturbance affects laboratory test results, while only limited stress and strain states can be developed in field tests.

5.2 Viscous effects

The effects of strain rate on relatively small strain behaviour are less understood than those on the yielding and strength characteristics (Leroueil and Marques 1996). **Fig. 5.1** shows the relationship between the coefficient of strain rate effect $\alpha(\gamma)$ for the secant shear modulus $G_{sec}(\gamma) = \tau/\gamma$, defined below, and strain level γ obtained from ML TC and TS tests on a variety of geomaterials:

$$\alpha(\gamma) = \{\Delta G_{sec}(\gamma) / G_{sec}(\gamma, \dot{\gamma}_{ref})\} / \Delta(\log \dot{\gamma}) \qquad (5.1)$$

where $\Delta G_{sec}(\gamma)$ is the difference between G_{sec} values at shear strain rates $\dot{\gamma}$ and $\dot{\gamma}_{ref}$, and $\Delta \log \dot{\gamma}$ is the difference between $\log \dot{\gamma}$ and $\log \dot{\gamma}_{ref}$. In this figure, data from cyclic triaxial tests on Hostun sand are also included, for which the peak-to-peak secant modulus and the single amplitude strain were used for G_{sec} and γ. The following trends of behaviour may be noted:

1. For all the geomaterials, the value of $\alpha(\gamma)$ increases with γ, while as strains approach 10^{-5}, the values become very small (i.e., quasi-elastic). This is a reconfirmation of the classical work (Figs. 8.7 and 8.8 of Ishihara 1996).
2. The value of $\alpha(\gamma)$ is small for the dense Hostun sand, while at larger strains, the value of $\alpha(\gamma)$ increases with plasticity index.

These data presented in Fig. 5.1 were obtained for a limited range of strain rate. For a wider range of strain rate, $\alpha(\gamma)$ may vary more considerably with strain rate: see Fig. 4.6.

Under typical field conditions, the creep rate is small prior to any construction activity and the soil has aged under its in-situ stress conditions. The effects of strain rate on initial behaviour at small strains (in the Y_1 and Y_2 zones) upon loading would probably be small (as indicated for point **c** in Fig. 4.12). The behaviour at larger strains, after engaging the Y_2 yield surface, is more strain rate-dependent.

Creep deformation and stress relaxation after unloading is often encountered in the field. Suppose that in **Fig. 5.2**, specimens **A** and **B** have reached point **1** through, respectively, rapid loading followed by creep deformation at the lower stress σ_{I} and relaxation at the strain ε_{I}, both developing over the same period of time. Another specimen **C** could reach the same point (**1**) by rapid loading and unloading without any creep period being allowed. Isochronous models, in which the relationship among stress, strain and time is unique irrespective of stress-strain-time history, cannot explain such behaviour. Note also that the isotach behaviour (Fig. 4.19) cannot be modelled by an isochronous model. Specimens, such as **D** at point **2**, are

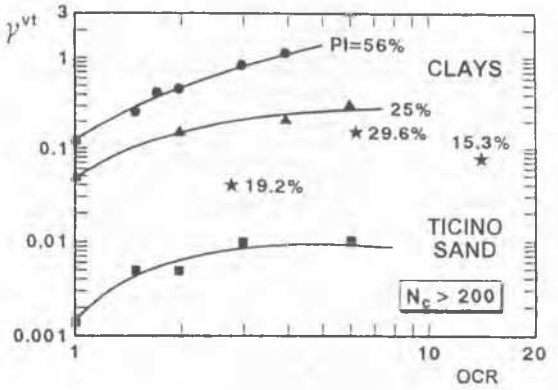

Fig. 5.4 Effects of PI and OCR on the volumetric threshold shear strain from resonant-column (RC) tests (Lo Presti 1989).

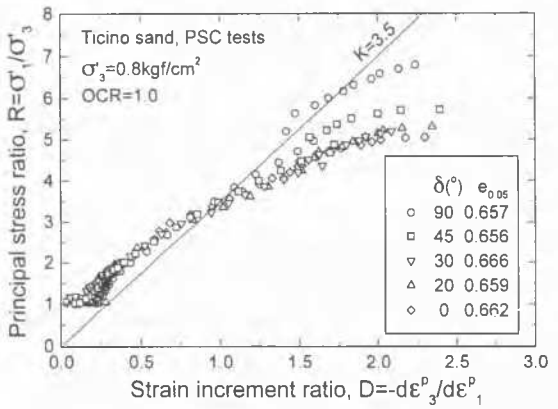

Fig. 5.5 Stress-dilatancy relationships from PSC tests on Ticino sand (see Fig. 4.22; Park 1995).

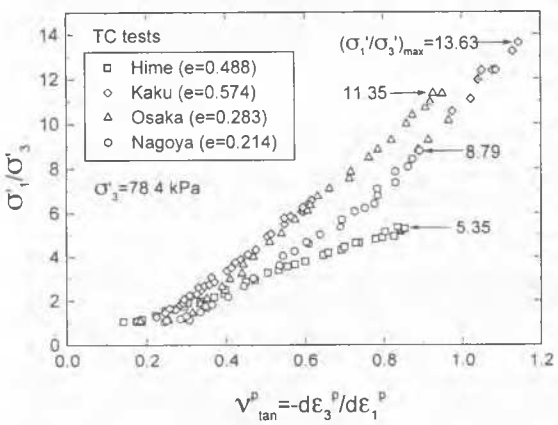

Fig. 5.6 Stress-dilatancy relationships from TC tests on slightly wet dense gravels (Dong et al. 1994).

likely to show marked creep recovery (i.e., decrease in ε with time) when sufficient creep deformation has been allowed to occur at the stress level $\sigma_{\square}$, as seen in Figs. 4.8, 4.10a, 4.11 and 5.3. Creep recovery can be explained, at least partly, by the three-component model (Fig. 4.13). However, it is well known that with soft soils, positive creep straining may restart after some creep recovery (Yoshikuni et al. 1993). To model such behaviour, another viscous component should be added in line to the three component model (i.e., the Burger model).

5.3 Strain coupling, or dilatancy

Stress increments and plastic strain increments are not interrelated by the elastic equations. However, within FEM and other numerical methods of analysis, it is convenient to define an incremental compliance matrix whose form mirrors that of an elastic material:

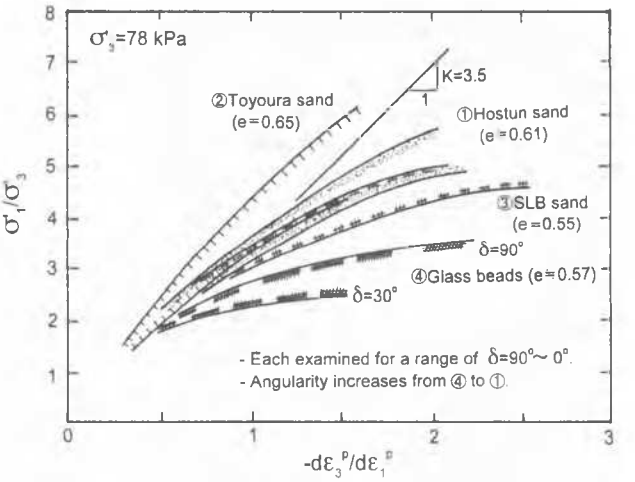

Fig. 5.7 Stress-dilatancy relationships from PSC tests on granular materials having different particle shapes (Park 1993).

$$[d\varepsilon_{ij}^p] = [C_{ijkl}^p] \cdot [d\sigma_{kl}] \qquad (5.2)$$

The matrix $[C_{ijkl}^p]$ can vary continuously and may contain coupling components, through which plastic volumetric strain increments can be caused by plastic shear strain increments, while normal strains may be provoked by shear stresses and vice versa. While behaviour under general stress conditions is poorly understood, Zdravkovic and Jardine (1997) showed that for a dense quartzitic silt, the matrix is not symmetric and can change with the perturbing stress path once the yield locus Y_2 is exceeded (at strains of 10^{-4} or less). The size of the Y_2 zone for monotonic loading could be different from the size of the steady state Y_2 zone developed during cyclic loading. For a given level of p′, the latter may grow as PI and OCR increase (see **Fig. 5.4**).

For cohesionless soils, Rowe (1962) proposed that plastic straining was governed by "the stress-dilatancy relationship (SD relationship)":

$$R = K \cdot D \quad (K = \text{a constant}) \qquad (5.3)$$

where $R = \sigma_1'/\sigma_3'$, $D = -2d\varepsilon_3^p/d\varepsilon_1^p$ (triaxial compression; TC), $-d\varepsilon_3^p/2d\varepsilon_1^p$ (triaxial extension; TE) and $-d\varepsilon_3^p/d\varepsilon_1^p$ (plane strain; PS). Comparisons with plane strain and triaxial test data lead to the following remarks:

1. Eq. 5.3 provides a reasonable approximation to the plane strain behaviour of granular media although the relationships are slightly curved (**Figs. 5.5 to 5.7**).
2. Tests on tilted samples show that inherent anisotropy has some effects on the SD relationship, particularly at high R values (Figs. 5.5 and 5.7).
3. The equivalent 'plastic' Poisson's ratio ν_{tan}^p (which is a half of D under triaxial compression) becomes very large at large R values for dense gravels having a very large peak stress ratio at low pressure (Fig. 5.6).
4. Eq. 5.3 also appears to provide reasonable predictions for cyclic loading although care is required as the directions of the major principal stress σ_1' and the major plastic principal strain increment $d\varepsilon_1^p$ are orthogonal to each other during unloading from peak (Pradhan et al. 1989).
5. The coefficient K increases as the particles become more angular (Fig. 5.7).
6. The flow rule during creep deformation is controlled by the current stress ratio following the SD relationship, as seen from continuous relationships between volumetric and axial strains shown in Fig. 4.9 for sand and between axial and lateral strains shown in Fig. 4.10b for gravel.

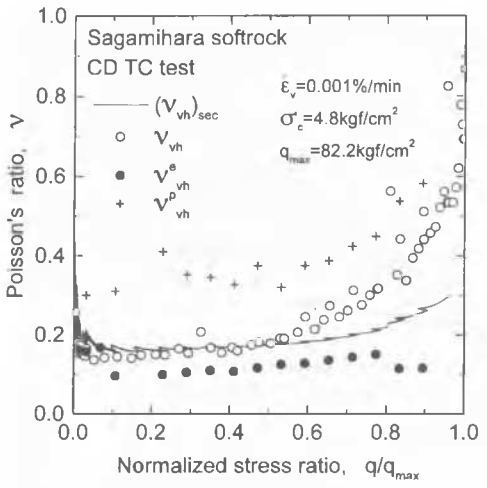

Fig. 5.8 Poisson's ratios of Sagamihara sedimentary soft mudstone from a drained TC test (Hayano and Tatsuoka 1997).

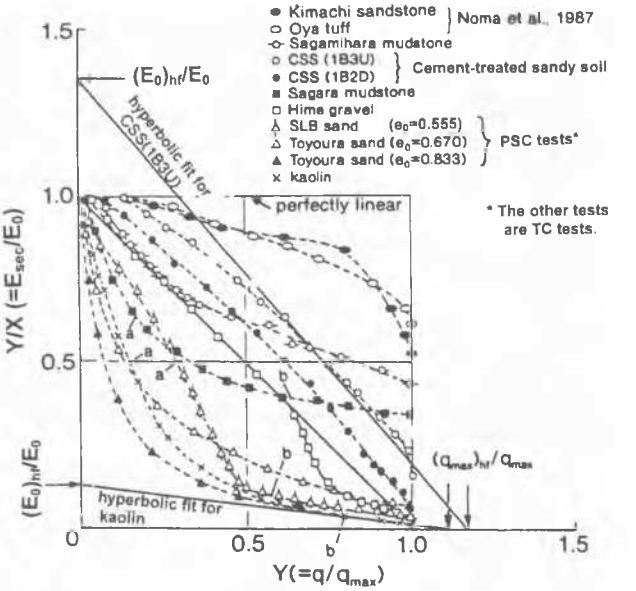

Fig. 5.9 E_{sec}/E_0 and q/q_{max} relationships from PSC and TC tests on various geomaterials; $(E_0)_{hf}$ and $(q_{max})_{ft}$ = the values of E_0 and q_{max} in hyperbolic fit (Tatsuoka and Shibuya 1992).

Little is known concerning the strain coupling characteristics of cemented soils, since making multiple measurements of small plastic strains under drained conditions is very difficult. The data shown in **Fig. 5.8** were obtained by locally measuring both axial and lateral strains in a CD TC test using a square-prismatic specimen of sedimentary soft mudstone. The Poisson's ratio for elastic strain increments $\nu_{vh}{}^e = -d\varepsilon_h{}^e/d\varepsilon_v{}^e$ remains between 0.1 and 0.2 throughout, while $\nu_{vh}{}^p = -d\varepsilon_h{}^p/d\varepsilon_v{}^p$ exceeds $\nu_{vh}{}^e$ by an amount that increases with q/q_{max}, reaching 0.6 prior to failure. The tangential Poisson's ratio for total strain increments $\nu_{vh} = -d\varepsilon_h/d\varepsilon_v$ increases with q/q_{max} from values close to $\nu_{vh}{}^e$ to the values of $\nu_{vh}{}^p$.

5.4 Non-linear stress-strain relationships

Uncemented and highly cemented geomaterials and unstructured and structured soils show a wide range of non-linear deformation characteristics as seen from **Fig. 5.9**. Generally, well cemented geomaterials exhibit more linear deformation characteristics. Representing the full range of behaviour by a single model is difficult. On the other hand, Biarez and Hicher (1994) argued that reconstituted clays, sands and gravels can show similar non-linear stiffness and peak strength characteristics at comparable densities and pressure levels, and proposed a classification of behaviour and a correlation among parameters. They introduced normally and over-consolidated behaviours for apparently different types of geomaterials consisting of "elastic particles without bond". The following two classes of parameters were considered;

1) Parameters that are independent of particle arrangements (i.e., particle material property, particle geometric description, aspects of the mechanical behaviour that are independent of stress-strain history):- the parameters are grouped for the constitutive laws and standard mechanical tests; and
2) Parameters that depend on geometric arrangements of particles, being affected by stress-strain history and so on.

Realistic non-linear models need to take into account the effects of, at least; a) initial shear stress level (or the degree of proximity to the Y_3 and failure envelopes), b) the effective pressure level, c) the recent stress-time histories (positive and negative effects, including those of OCR and structuration occurring at the current state), d) the perturbing stress-strain-time conditions, including those of the sharpness of change in stress path direction between virgin- or re-consolidation stress path and perturbing stress path and cyclic loading, and e) the anisotropy (as seen from Fig. 4.22). Anisotropic non-linear stiffness under more general stress conditions requires special tests such as hollow cylinder experiments (e.g., Symes et al. 1984) or a combination of TC, PSC and TE tests (Lam and Tatsuoka 1988) in which the direction σ_1' can be changed relative to the structure axis .

However, for practical purposes, stiffness non-linearity is often modelled in terms of greatly simplified relationships between;

a) E_{sec}/E_0 (or E_{tan}/E_0) and ν_{sec} (or ν_{tan}) and ε_v (or y= q/q_{max}) ; or
b) G_{sec}/G_0 (or G_{tan}/G_0) and γ (or y = τ/τ_{max}), and K_{sec}/K_0 (or K_{tan}/K_0) and ε_{vol} (or p').

Stress and strain are often normalized by using the peak strength and initial stiffness for the model to be applied to general cases (e.g., the hyperbolic relation; Hardin and Drnevich 1972). For a drained triaxial test at a constant lateral stress σ_h', for example, the popular normalization is;

$$y = q/q_{max}; \quad x = \varepsilon_v / (\varepsilon_v)_r \qquad (5.4)$$

where q is the deviator stress $\sigma_v' - \sigma_h'$ and $(\varepsilon_v)_r$ is the reference strain equal to "the peak strength q_{max}"/ "the initial Young's modulus E_0". The normalized tangent stiffness $\partial y/\partial x$ is equal to E_{tan}/E_0.

When using fixed values of q_{max} and E_0, however, normalized y and x relationships cannot take into account effects of pressure change and damage during shearing, as demonstrated in Figs. 2.2, 4.26 and 5.3. In those cases, the quasi-elastic Young's moduli E_v appearing in the quasi-elastic Y_1 region increase with the axial stress σ_v', and this trend is reflected in the current E_{tan} values. On the other hand, at a constant σ_v', the E_v and E_{tan} values decrease due to destructuration by large-scale cyclic loading. Thus, in the case of Fig. 4.26, the stress-strain curve of the fourth loading (4L) is concave upwards with a different shape to those of the first, second and third loading. In the case of the Fig. 5.3, the stress-strain curve from point **9** is located below the first loading curve. Similar behaviour has been observed for other types of gravel (Flora et al. 1994; Jiang et al. 1997). When the effects of both σ_v' and damage on E_v and E_{tan} are important and the q_{max} value is insensitive to damage, it can be considered that changes in the ratio E_{tan}/E_v with shearing represent non-linearity due to shear straining. In that case, the relationship between E_{tan}/E_v and y= q/q_{max} is equivalent to the relationship between $\partial y/\partial x = E_{tan}/E_0$ and y for the cases where E_v is kept constant and equal to the initial value E_0 throughout shear straining. **Fig. 5.10a** shows the $\partial y/\partial x$ (=E_{tan}/E_v) and y(=q/q_{max}) relationships obtained from the results shown in Fig. 4.26. The normalized stress and strain (y and x) relationships obtained by integrating

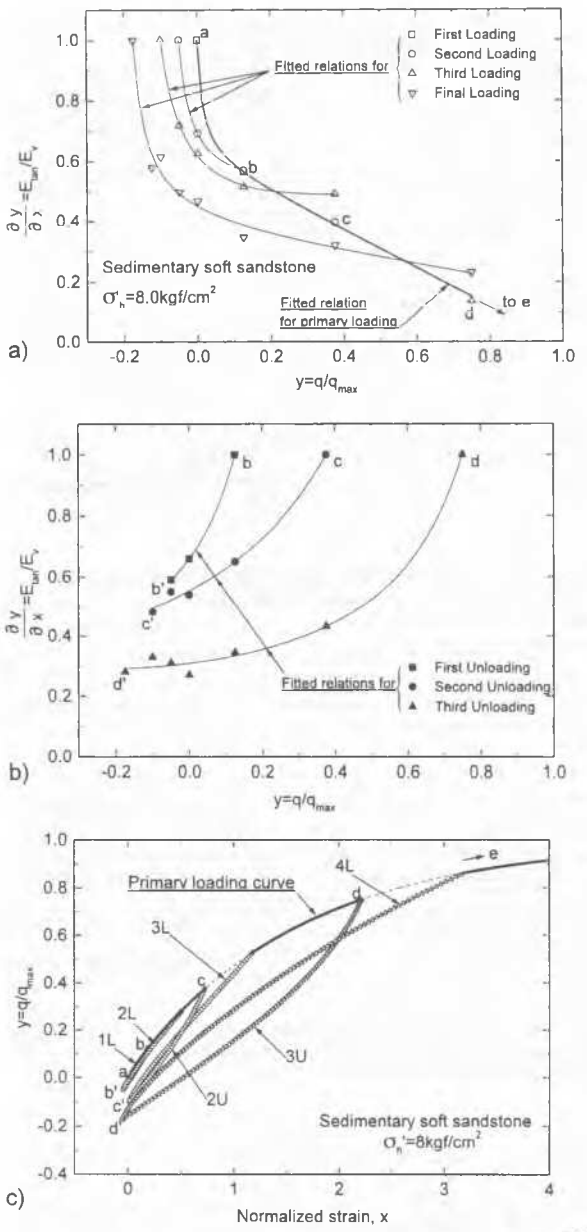

Fig. 5.10 Relationships between $\partial y/\partial x$ (=E_{tan}/E_v) and y (= $q/(q_{max}$ in TC)) during a1) loading and a2)unloading and b) integrated y and x relationships; from the experiment for a sedimentary soft sandstone shown in Fig. 4.26.

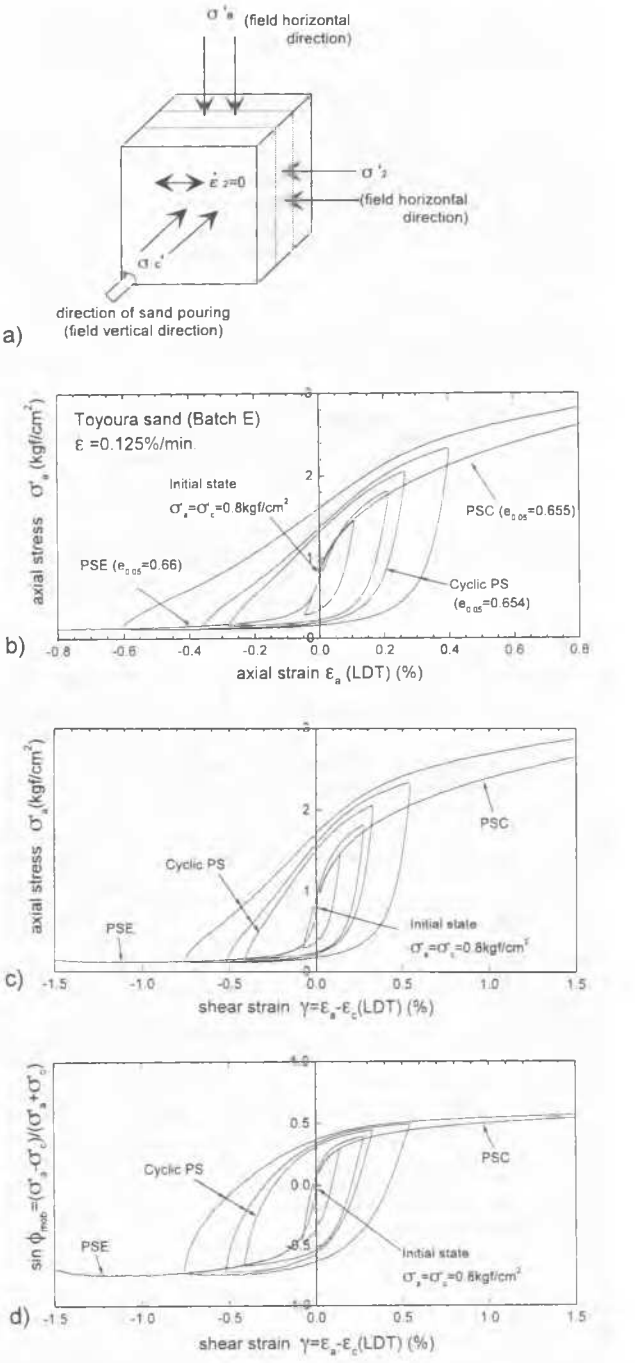

Fig. 5.11 Monotonic and cyclic plane strain tests on saturated air-pluviated Toyoura sand; a) specimen configuration, b) σ_a' and ε_a relationships, c) σ_a' and ε_a - ε_r relationships and d) $(\sigma_a' - \sigma_c')/(\sigma_a' + \sigma_c')$ and ε_a - ε_c relationships (Yamada et al. 1996).

the curves are shown in **Fig. 5.10b**. These y and x relationships are considered not to include the effects of pressure change and damage occurring during shear straining, thus having more general features than the original q and ε_v relationships. The E_{tan} value at a given strain $\varepsilon_v = x\cdot(q_{max}/E_v)$, which is to be used for numerical analysis, is obtained as "$(\partial y/\partial x)$ at $x''\cdot E_v$, where E_v is a function of σ_v', damage and other factors.

When modelling the shear deformation of uncemented soils, it is generally necessary to account for the mobilized friction angle. **Fig. 5.11**, for example, shows results from a pair of plane strain compression and extension tests and one cyclic plane strain test, which modelled active and passive earth pressure conditions for dense Toyoura sand. In these tests, the directions of the axial stress σ_a' and the intermediate principal stress σ_2' were parallel to the sample's bedding planes, while the direction of the confining pressure σ_c' acted normally to the bedding (**Fig. 5.11a**); σ_a' and σ_c' were equivalent to the in-situ horizontal and vertical stresses σ_h' and σ_v'. Special measures were taken so that σ_2' could become smaller than σ_c' (constant) under extension conditions. The axial and lateral strains ε_a and ε_c were measured locally. The σ_a' and ε_a relationships (**Fig. 5.11b**) are clearly non-symmetrical and resemble the classical curves expected for passive and active earth pressures. The relationships between σ_a' and shear strain $\gamma = \varepsilon_a - \varepsilon_c$ (**Fig. 5.11c**) is also non-symmetric about the q= 0 axis. However, a smooth and nearly symmetrical relationship is obtained between $\sin\phi_{mob} = (\sigma_a' - \sigma_c')/(\sigma_a' + \sigma_c')$ and γ (**Fig. 5.11d**). The same result can be seen in Fig. 5.3b and for other gravelly soils (Flora et al. 1994; Jiang et al. 1997).

Modelling behaviour during cyclic loading (CL) is important for surprisingly many static loading problems. Unload and reload stress-strain relationships are often obtained from the skeleton relationship $\tau = f(\gamma)$ starting from $\tau = 0$. When following the proportional rule (**Fig. 5.12**), we obtain, noting that $f(-\gamma) = -f(\gamma)$;

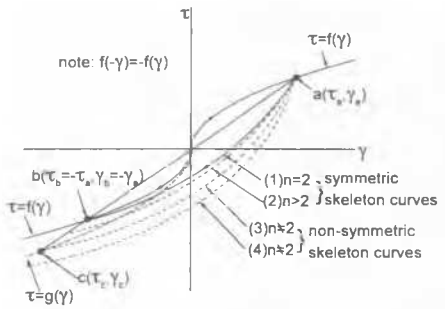

Fig. 5.12 Proportional rule for cyclic loading.

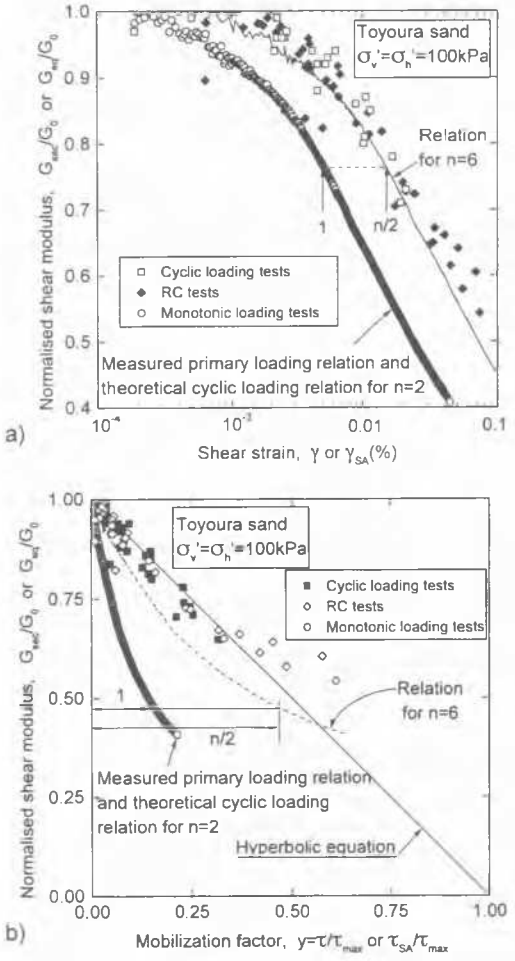

Fig. 5.13 Comparison between a) G_{sec}/G_o - γ and G_{eq}/G_o - γ_{SA} curves and b) G_{sec}/G_o - $y = \tau/\tau_{max}$ and G_{eq}/G_o - $y = \tau_{SA}/\tau_{max}$ curves; from ML and CL torsional shear tests and torsional RC tests on Toyoura sand; K_c= 1.0 (Lo Presti et al. 1997): n is the factor used in Eq. (5.5).

$$(\tau - \tau_a)/n = f\{(\gamma - \gamma_a)/n\} \qquad (5.5)$$

where (τ_a, γ_a) is the coordinate of point **a** where the loading direction is reversed. The Masing's second rule states n= 2, and the stress-strain relationships for the opposite loading directions are symmetric about the origin and the unloading curve rejoins the primary curve at the symmetric point **b** with $\tau_b = -\tau_a$ (case **1** in Fig. 5.12). However, many experiments involving pairs of drained ML and CL torsional shear tests on sand (which give symmetrical primary loading curves) have shown that when the primary loading relation is used as the skeleton function, the operational value of n used in Eq. 5.5 is larger than two, reaching about 6 for the case shown in **Fig. 5.13**. The meaning of the

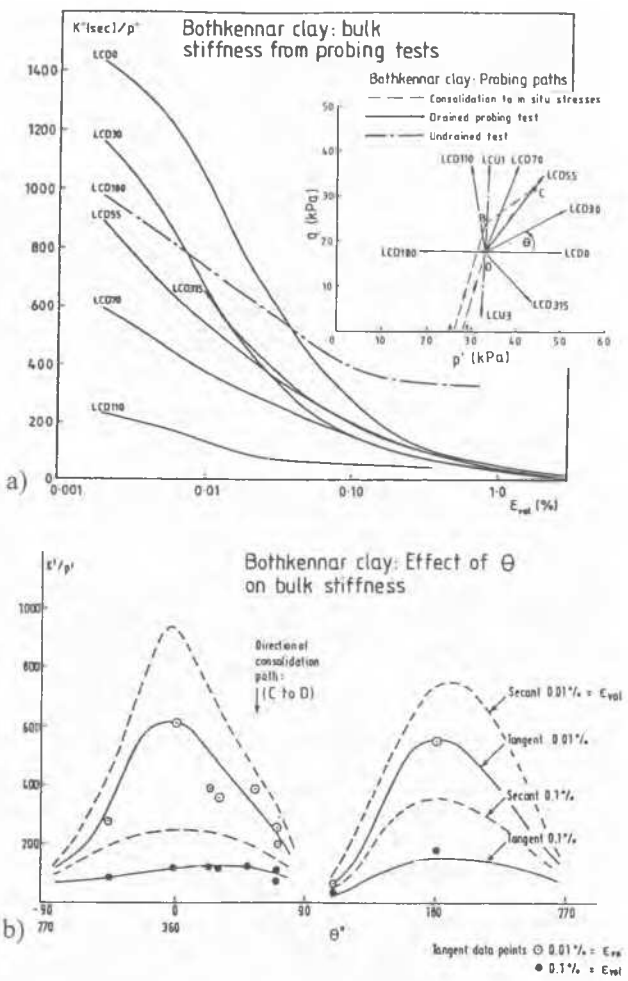

Fig. 5.14 Drained TC probing tests on Bothkennar clay: a) K_{sec}= $(\Delta p' / \Delta\varepsilon_{vol})$ / p' and $\Delta\varepsilon_{vol}$ relationships and b) variation of K' with stress path direction θ (Smith et al. 1992).

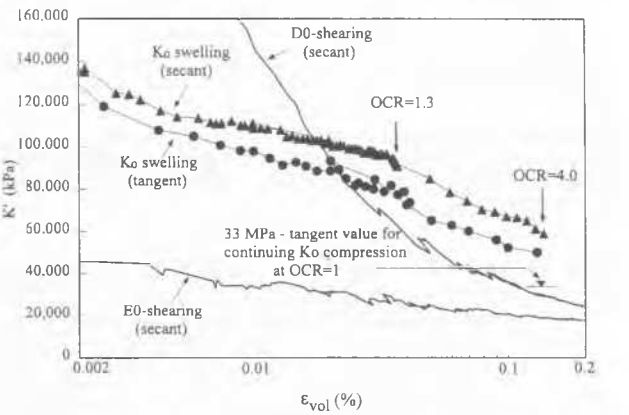

Fig. 5.15 K_{sec} and K_{tan} and $\Delta\varepsilon_{vol}$ relationships for an artificial quartzitic silt; K_0 swelling from p' = 200 kPa (OCR= 1.0) to OCR= 4.0, TC loading with a constant σ_h' (D0) and circumferential loading with a constant σ_v' (E0) (Zdravkovic and Jardine 1997).

factor n in Eq. 5.5 are shown in Fig. 5.13. When the primary loading curves for positive and negative values of $\tau = f(\gamma)$ and $\tau = g(\gamma)$, respectively, are not symmetrical about the origin, as under most practical conditions, point **c** (the intersection of the primary curve $\tau = g(\gamma)$ and the straight line passing through point **a** and the origin) is given by $(\tau - \tau_a)/n = g\{(\gamma - \gamma_a)/n\}$ with $n = -(\tau_a - \tau_c)/\tau_c$, which is usually different from two (case **3** in Fig. 5.12). A similar model was proposed by Bardet (1996).

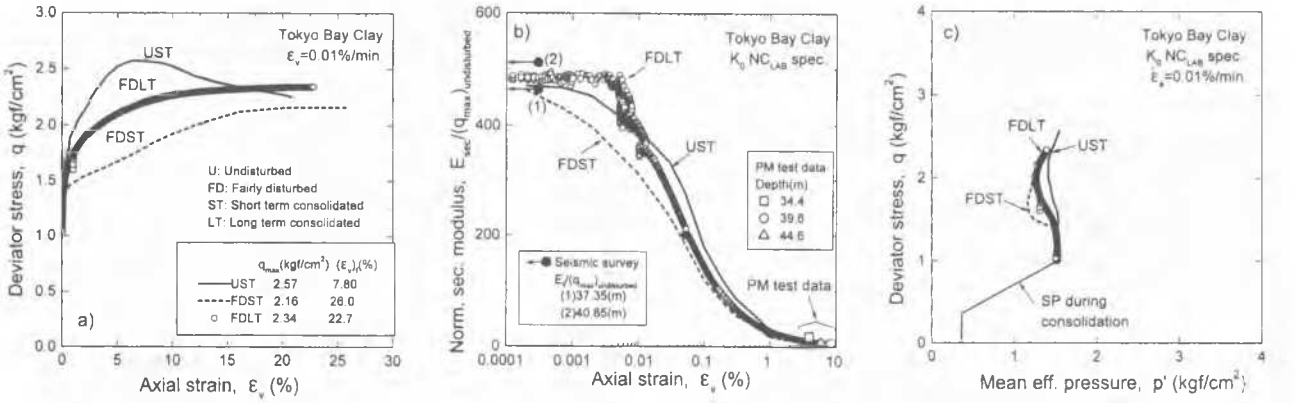

Fig. 6.1 CU TC tests on three samples showing different degrees of disturbance from a Pleistocene clay deposit in Tokyo Bay (w_n= 44.8 %; w_p=30%; PI= 20 averaged for the sub-layer), re-consolidated to the field stress state: a) q and ε_v relationships, b) $E_{sec}/(q_{max})_{undisturbed}$ - ε_v curves, and c) effective stress paths (Mukabi 1995)

Furthermore, the value of n may not be constant during cyclic loading; for uncemented unstructured geomaterials subject to drained cyclic loading which does not reach failure, reloading curves do not generally rejoin the primary curve, but locate outside the primary loading curve (see Fig. 5.11). In the same way, either the cyclic stress amplitude developed at a constant strain amplitude increases or the cyclic strain amplitude seen at a constant stress amplitude decreases. In such cases an ultimate stationary condition is approached through cyclic strain hardening or shake down. Under unstable cyclic conditions, the opposite may occur due to damage by straining, as is often observed with cemented or structural geomaterials (see Fig. 5.3). In addition, creep deformation displaces the unload/reload curves at high shear stress levels (e.g., England 1994). Additional rules are required to model these features and account for behaviour under more general stress conditions. Note also that the cyclic stress and strain relationships of all geomaterials may be subjected to rate effects. For example, data from RC tests on saturated clay are biased to indicate a more extensive linear region than static tests and to give more non-linear relationships at large strain due to the generation of excess cyclic pore water pressure.

Non-linear analyses require information on how the non-linear bulk moduli or Poisson's ratios vary with strain and stress states. The behaviour of soils from small to large strains has been modelled in many successful FE simulations of practical problems by combining non-linear, effective stress-dependent functions for G and bulk modulus K′ with classical elasto-plastic soil models (Jardine et al. 1991; Hight and Higgins 1995). **Figs. 5.14** and **5.15** show the non-linear relationships between K_{sec}= $\Delta p'/\Delta\varepsilon_{vol}$ and K_{tan}= $\partial p'/\partial\varepsilon_{vol}$ and volumetric strain ε_{vol}, obtained from drained TC probing tests on clay and silt. To obtain such data for clay is very time consuming and technically difficult. The use of non-linear models of G and K (or E and v) which are independent of stress path direction is equivalent to assuming that the coupling terms in the compliance matrix relating (dp′, dq) and ($d\varepsilon_{vol}$, $d\varepsilon_s$) are negligible. However, the cross-coupling terms are in fact important (Jardine 1992b). Note from Fig. 5.14 that for stress paths close to the p′ constant path (where θ=90° or 270°), significant positive $\Delta\varepsilon_{vol}$ strains are caused by shear strain increments leading to low values of K′ with the contractive Bothkennar clay, while the reverse is true the for stress path D0 for a dilative silt (Fig. 5.15). The effect of anisotropy is another factor to be considered. Jardine et al. (1991), Jardine (1995) and Hight and Higgins (1995) recommend that when using such a simplified non-linear model, the input parameters should be selected from tests that mimic the in-situ stress path conditions as closely as possible, and the kinematic aspects are taken account of soil stiffness behaviour. Models which address these issues more explicitly are described by Simpson (1992), Stallebrass and Taylor (1997) and others.

6 SAMPLE DISTURBANCE AND RE-CONCOLIDATION METHODS

6.1 Sample disturbance

The classical problem of sample disturbance has become important again in the light of recent small strain measurements. Its effects on tangential stiffness may not be uniform at all strains; the effects on peak strength could be different from those at small strain stiffness. For example, **Fig. 6.1** compares the deformation properties seen in CU TC tests on three samples of Pleistocene clay retrieved by the fixed piston thin wall sampling with coring at the sample bottom end (i.e., the Denison sampler). Some of these deep offshore samples of low plasticity clay were apparently disturbed. One of the less disturbed specimens (UST) was re-consolidated directly to the field stress state and aged for about one day. Two other, more disturbed specimens, FDST and FDLT, were re-consolidated to the same field stress state as specimen UST, but specimen FDLT was re-aged for eleven days. Three overall stress-strain relationships are very different due to the variable influences of sample disturbance and re-ageing. Specimen UST showed the highest strength and greatest brittleness, while the ageing of FDLT led to some strength recovery. Note that in Fig. 6.1b, the values of the secant Young's modulus E_{sec} of the three specimens have been divided by the peak strength of the specimen UST. The linear quasi-elastic axial strain limit for specimen UST was larger than that for the more disturbed one FDST, but smaller than that for the more aged specimen FDLT. The initial undrained Young's moduli E_0 of the three specimens are similar, falling close to those inferred moduli E_f from the down hole shear wave measurements despite the possible influence of anisotropy. This result suggests that a good agreement of V_S or G_0 (or E_0) between laboratory and field tests may not indicate negligible effects of sample disturbance on the full deformation and strength characteristics (Hight 1996). This comparison would also be devalued if the effects of anisotropy and/or heterogeneity in the field are significant but not considered in the comparison.

However, comparisons between laboratory and field measurements of quasi-elastic stiffness are still useful when assessing specimen disturbance. Detailed studies of the soft lightly cemented Bothkennar clay indicated that laboratory G_0 values from samples retrieved by large diameter block and thin walled sharp tube sampling (the Sherbrooke and Laval samplers) were very similar to the field seismic cone moduli G_f (**Fig. 6.2a**), whereas samples obtained by the standard UK push-in piston sampling technique exhibited smaller G_0 values (**Fig. 6.2b**). It is likely that the consistent trend reported by Richart (1977) for G_0 values from RC tests on reconsolidated 'undisturbed' clay samples to fall below the respective field values (G_f) would be, at least partly, due to the large effects of sample disturbance. On the other hand, Tanaka et al. (1995) claimed that for soft clays,

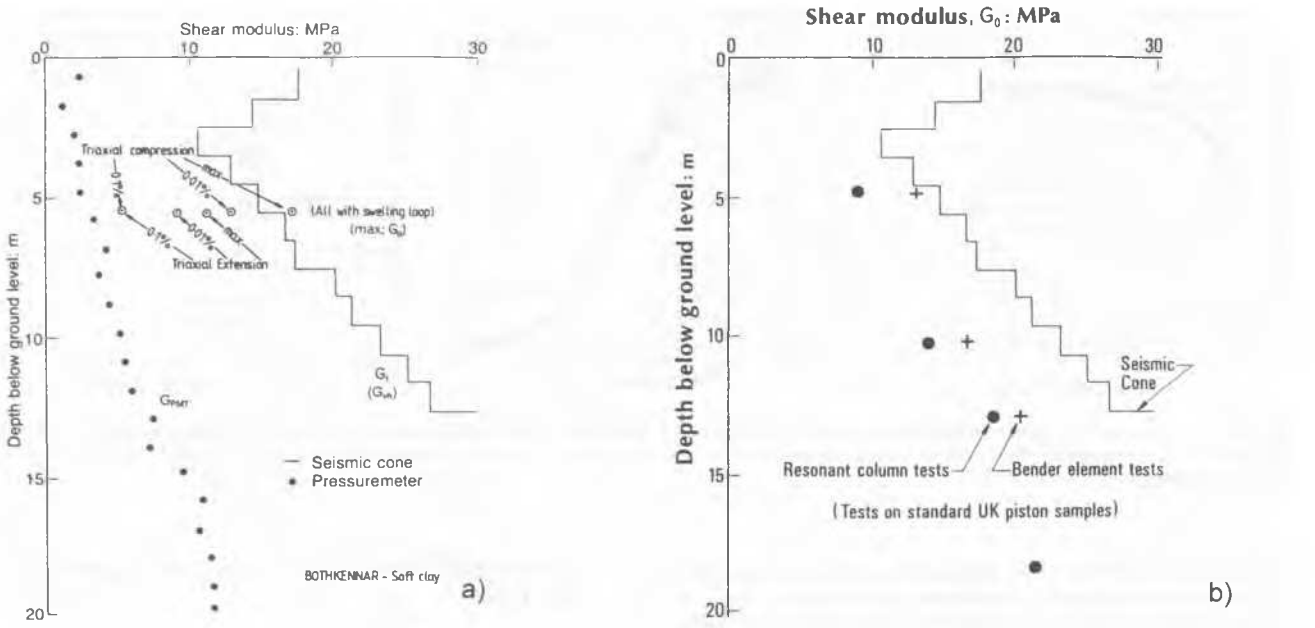

Fig. 6.2 a) Field pressuremeter (G_{PMT}) and seismic (G_f) values compared with data from CU triaxial tests on high-quality samples of Bothkennar clay reconsolidated to in-situ stresses; and b) G_f values compared with data from RC and BE samples obtained by the standard UK piston sampling (after Hight 1995; Hight et al. 1992; Jardine 1995).

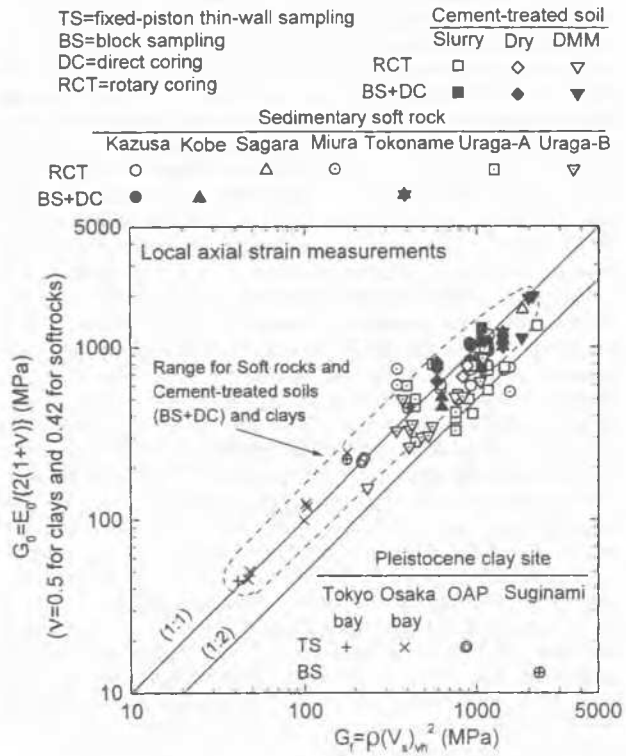

Fig. 6.3 G_0 values from CU TC tests on undisturbed samples of several Pleistocene clays, sedimentary soft rocks and cement-treated soils (re-consolidated to in-situ stresses), compared with respective field seismic values G_f (Tatsuoka et al. 1995b; Kohata et al. 1997)

the fixed piston thin wall tube sampler which is conventionally used in Japan causes less disturbance than push-in or displacement type tube sampling. Fixed piston thin wall sampling with rotary coring at the bottom end of the sampling tube is usually suitable for obtaining good quality samples of stiff plastic clay. It may be seen from **Fig. 6.3** that the G_0 values from CU TC tests on undisturbed samples of several Japanese Pleistocene clays obtained by this method and reconsolidated to the field stress state compare very well with the respective field values G_f (the possible effects of anisotropy are not considered in this comparison). Laboratory tests on thin wall pushed samples of UK stiff clays have shown reasonable agreement with field geophysical stiffness measurements (e.g., Jardine et al. 1985), while careful rotary coring yields better results (Hight and Jardines 1993; Hight et al. 1997). For these materials, peak strength may be more affected by disturbance than small strain stiffness.

The in-situ freezing method is most suitable for obtaining undisturbed samples of sands and gravels (Yoshimi et al. 1989). Yet, for gravels, comparisons between laboratory and field measurements could be masked by the possible interaction between wave length and particle size: Tanaka et al. (1995) showed that G_0 values from cyclic triaxial tests on frozen undisturbed gravel samples containing particles larger than 1.0 mm were consistently lower than the respective G_f value with the minimum of G_0/G_f equal to around 0.35. Hight and Georgiannou (1995) showed that for loose clayey sands having low failure strains, large undrained brittleness in triaxial compression and low undrained strength in triaxial extension, the field properties can be completely modified by damage during the undrained shearing in the tube sampling process and subsequent reconsolidation. The rotary core tube (RCT) sampling can easily disturb very dense uncemented structured sand, while reasonable samples can be obtained by careful block sampling (Tatsuoka et al. 1997).

For softrocks, the conventional RCT sampling may seriously disturb samples, perhaps due to the rocking and twisting motions of the sampling tube and a coring diameter which is larger than the sample diameter (Tatsuoka et al. 1995a). In **Fig. 6.4**, E_0 values from CU TC tests on samples reconsolidated to σ_{v0}' are compared with respective field down- or up-hole E_f values at Sagamihara test site. The samples were obtained by; 1) RCT sampling (three series), 2) block sampling (BS) and subsequent coring by using a well-fixed diamond core barrel in the laboratory, and 3) hand-operated direct coring (DC) using a 5 cm-diameter core barrel which is not mechanically fixed. We note:

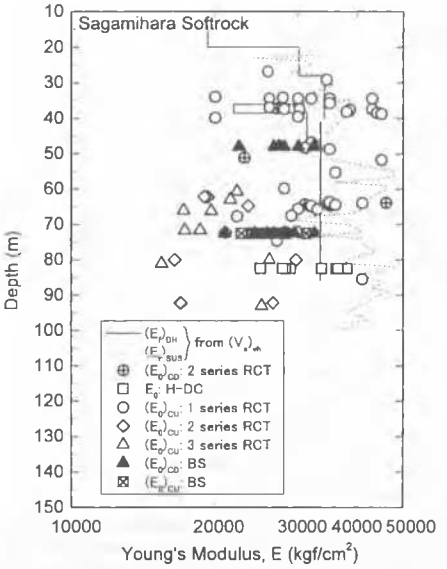

Fig. 6.4 Comparison of E_0 values from CU TC tests on "undisturbed" soft mudstone samples with respective field seismic E_f values at Sagamihara site; DH; down-hole PS logging and SUS; suspension method (Tatsuoka et al. 1997); E_f values converted from G_f assuming ν =0.42.

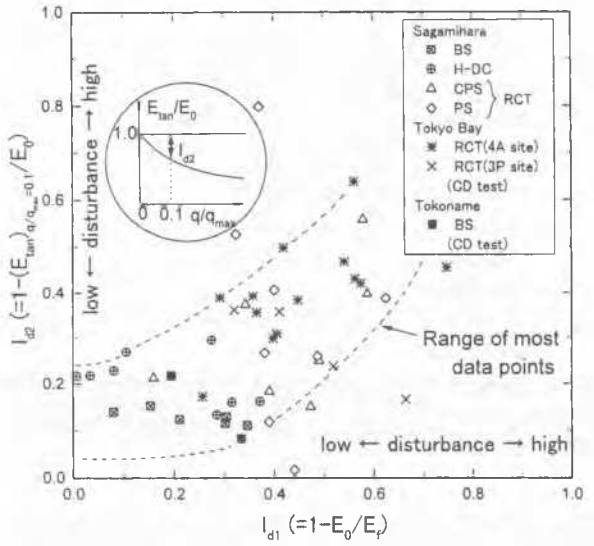

Fig. 6.5 Relationships between disturbance indexes I_{d1}= 1.0 - E_0/E_f and I_{d2}= 1.0 - "(E_{tan}/E_0) at q/q_{max}= 0.1" for Japanese sedimentary softrocks; E_0 and I_{d2} from TC test data of samples reconsolidated to σ_{v0}' and E_f from field seismic $(V_s)_{vh}$ (Matsushita et al. 1997).

1. While a good agreement was seen between the E_0 and E_f values for the first series of RCT samples, the two subsequent series of RCT exhibited generally lower G_0 values. Small differences in technique may have significant effects.
2. Even though the quality of BS and DC samples is consistently better than the last two series of RCT samples (see also Fig. 6.3), they may have been disturbed to some extent by the site excavation; and
3. The ratio E_0/E_f generally decreases with depth, perhaps due to stress relief effects.

With sedimentary softrocks, sampling disturbance leads to a reduction in the initial modulus E_0 and more pronounced non-linearity at small strains. Stiffness at very small strains is recovered by ageing during reconsolidation, while that at larger strains is not. Two indexes, I_{d1} and I_{d2}, which reflect these

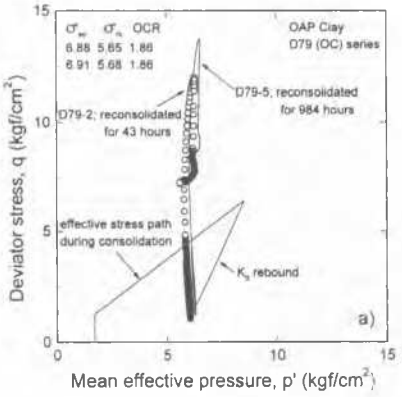

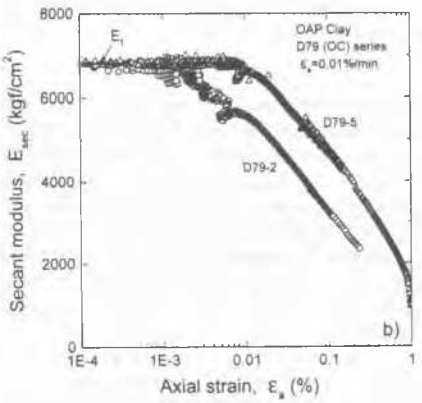

Fig. 6.6 Ageing effects in two CU triaxial compression tests on undisturbed samples of Pleistocene OAP clay (w_n= 45 %; w_p=36%; PI= 56, averaged for the sub-layer); a) effective stress paths and b) undrained stiffness curves (Mukabi 1995).

features (for isotropically consolidated samples) are plotted in **Fig. 6.5**, showing a general trend to rise together. I_{d2} reflects also the intrinsic strain and pressure non-linearity, and is usually non-zero even when I_{d1}= 0.0. The effects of sample disturbance on the peak strength from CU TC tests are usually much less clear than with clay (Tatsuoka et al. 1995a). The unconfined compressive strength q_u of softrocks is usually an unreliable measure of the strength due to the large and combined effects of sample disturbance and lack of confinement (Tatsuoka and Kohata 1995).

6.2 Reconsolidation methods

To simulate field behaviour, a specimen should be re-consolidated to the field stress state, which is usually anisotropic. Due to the kinematic nature of the Y_1 and Y_2 zones, the behaviour becomes less linear as the equilibrium stress state approaches the Y_3 locus. On the other hand, the stress-time history during reconsolidation, including swelling and ageing, can have noticeable effects on the behaviour upon loading especially for disturbed, or normally consolidated, samples. The effects can be important also for least disturbed samples. **Fig. 6.6** shows results from two CU TC tests on undisturbed Pleistocene clay, re-aged for, respectively, 43 hours and 984 hours at the final reconsolidation stress state. The more aged specimen D79-5 has a far larger linear zone (see also Fig. 2.23 of Tatsuoka and Kohata 1995). **Fig. 6.7** shows the effects of reconsolidation paths on high quality samples of Bothkennar clay; path ABCD leads to far greater stiffness than path ED, while the G_0 value for path ABCD is closer to the field value G_f (Fig. 6.2). Similar effects of reconsolidation stress path on non-linear behaviour were observed for Japanese Pleistocene clays (see Figs. 2.12, 2.22 and 2.23 of Tatsuoka and Kohata, 1995); in that case, however, the effects on G_0 were very small (see Fig.

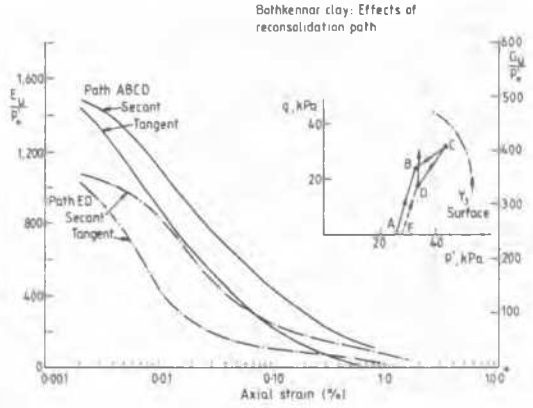

Fig. 6.7 Effects of reconsolidation procedure on undrained TC stiffness of Bothkennar clay (Smith et al. 1992).

2.13 of Tatsuoka and Kohata 1995; see also Fig. 6.6b). It is the standard practice at the Imperial College that specimens are aged until the creep rate becomes 1% of the strain rate to be applied in the subsequent shear tests. As long re-ageing is not always practical, a swelling method as path ABCD shown in Fig. 6.7 could be conveniently used to alleviate some of the effects of sample disturbance. However, there is not a widely accepted standard swelling method, and the full recovery of field behaviour by reconsolidation and reageing may be impossible with many disturbed samples.

With structured and/or cemented geomaterials, the reconsolidation procedure should keep the effective stress path well within the Y_3 locus before swelling back to the field stress state, if damage to the structure and/or bonding is to be avoided (e.g., Fig. 4.34). Although it is often overlooked, proper reconsolidation and ageing procedures are important also for softrocks, particular for less cemented materials (see Fig. 4.28).

7 SOME RECENT ADVANCES IN FIELD TESTS AND CORRELATION WITH LABORATORY TESTS

7.1 Field wave velocity measurements

Unlike other geophysical site investigation methods (resistivity, gravimetric and electromagnetic), the seismic method can give direct values of the field elastic stiffness. This method first became popular for Soil Dynamics purposes. In Japan, the seismic method was first used in the 1970's to estimate ground movement associated with ground excavation and subsequent construction of high-rise buildings in, and on, stiff soils (Tatsuoka and Shibuya 1992; Majima et al. 1997). Later uses include predicting the settlements of major bridge foundations and the deformation of large or deep shafts in sedimentary softrocks (Tatsuoka and Kohata 1995; Tatsuoka et al. 1995, 1997). **Fig. 7.1** shows a typical profile of $G_f = \rho \cdot (V_s)_{vh}^2$ at the Rainbow Bridge site from a local up-hole method, called the suspension method (Kitsunezaki 1985), which is becoming popular in Japan. The seismic method is now being used to assess both dynamic and static problems in many countries. However, some basic issues are still not well understood.

Differences among different seismic methods: Only very small strains are involved in ordinary body wave velocity measurements. Therefore, if deposits are homogeneous continua which are not locally structured or layered, the velocities $(V_s)_{vh}$ of horizontally polarized shear waves propagating vertically (as obtained from the down- or up-hole methods) should be the same as those propagating in the horizontal direction $(V_s)_{hv}$ of vertically polarized shear waves (as obtained from the cross-hole method), independently of the deposit's anisotropy. Such features were confirmed in tests on

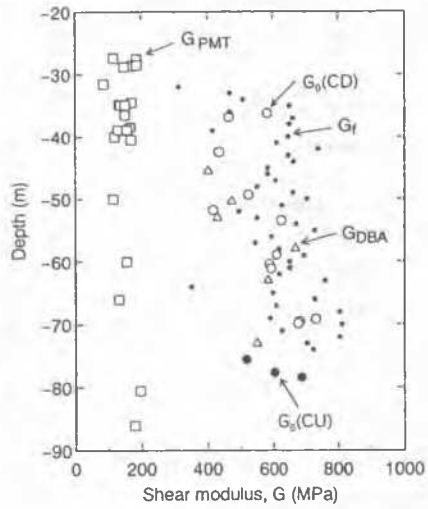

Fig. 7.1 Back-calculated equivalent linear shear stiffness G_{DBA} from field full-scale behaviour at Rainbow Bridge site on an about 1.5 million years old sedimentary soft mudstone deposit compared with G_f from field shear wave velocity, G_0 from TC tests and G_{PMT} (Izumi et al. 1997).

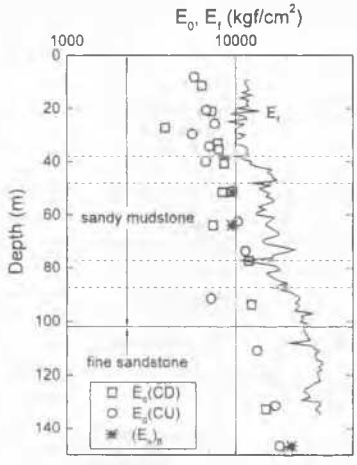

Fig. 7.2 Comparison between seismic E_f by the suspension method (assuming $\nu = 0.43$) and E_0 from TC tests for a sedimentary softrock at Tokyo Bay Entrance Bridge site (by the courtesy of Ministry of Construction, Japan).

homogeneous air-pluviated Ticino and Kenya sands in a large calibration chamber (Bellotti et al. 1996; Fioravante et al. 1997).

However, some field measurements in Tertiary sand deposits (Hight et al. 1997), structured clays (Butcher and Powell 1995) and NC clays (Sully and Campanella 1995) show noticeable differences between $(V_s)_{vh}$ and $(V_s)_{hv}$. One possible reason is that in a deposit consisting of alternative softer and stiffer layers, $(V_s)_{hv}$ tends to reflect the velocity of the stiffer thin layers to a larger extent than $(V_s)_{vh}$, which represents the average over the relevant depth interval. For this reason, the cross-hole method may over-estimate the stiffness of a thin softer layer, particularly when the source-receiver borehole spacing and/or in-hole station spacings are too large (Butler and Curro 1981). On the other hand, the $(V_s)_{vh}$ values by the suspension method can clearly detect detailed local layering (see Figs. 6.4, 7.1 and **7.2**). The average for some depth interval of $(V_s)_{vh}$ from the suspension method usually agrees with the value from the down hole PS logging.

In addition, inherent or/and stress state-induced anisotropy could cause $(V_s)_{hh}$ to be different from $(V_s)_{vh}$ and $(V_s)_{hv}$ (e.g., Ng et al. 1995; Jamiolkowski and Manassero 1995; Hight et al. 1997).

Table 7.1 List of site characteristics for comparison between laboratory and field seismic G_0 and G_f values (Lo Presti 1997).

Site	Geological age	Sedimentation	PI [%]	LL [%]	CaCO3 [%]	Void ratio	CF [%]	OCR	$\left(\frac{V_s(Lab)}{V_s(Field)}\right)_{AV}$	SD
Fucino +	Pleistocene	lacustrine	45-75	90-120	10-30 (*) 50-75 (**)	1.6-3.0	25-30	1.1-1.8	0.98	0.08
Avezzano +	Pleistocene	lacustrine	10-30	30-57	50-75 (*) 75-100 (**)	1.0-1.8	8-15	2.8-8.2	0.82	0.11
Garigliano +	Holocene	alluvial	10-40	25-60	18-32	0.9-1.2	18-40	1.2-1.4	0.99	0.12
Pisa +	Pleistocene	estuarine	23-46	35-77	5-12	0.8-1.8	30-70	1.5-2.0	0.90	0.12
Montalto di Castro +	Pleistocene	marine	15-34	40-57	14-34	0.6-0.8	30-45	1.8-2.5	0.82	0.12
Location B (Brignoli et al. 1995)	Holocene	marine	NA	NA	25	NA	$\cong 0$	$\cong 1$	0.84	0.09
Location C (Brignoli et al. 1995)	Holocene	marine	NA	NA	NA	NA	NA	2.0-6.0	0.88	0.10
Augusta (Maugeri 1997)	Pliocene to Pleistocene	marine	30-45	52-68	18-42	0.7-1.0	45-65	2.0-6.0	0.90	0.05

(*) depth above 25 m
(**) depth below 25 m

+ Jamiolkowski et al. (1995)

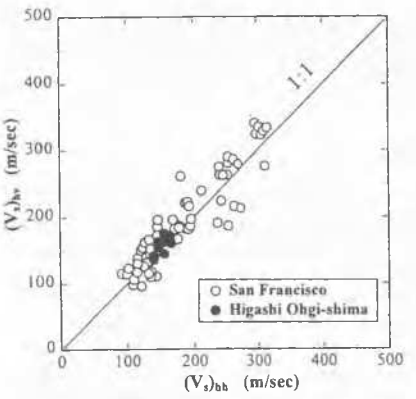

Fig. 7.3 Comparison between $(V_s)_{hv}$ and $(V_s)_{hh}$ from cross-hole BE tests in reclaimed sand deposits (Nishio 1995).

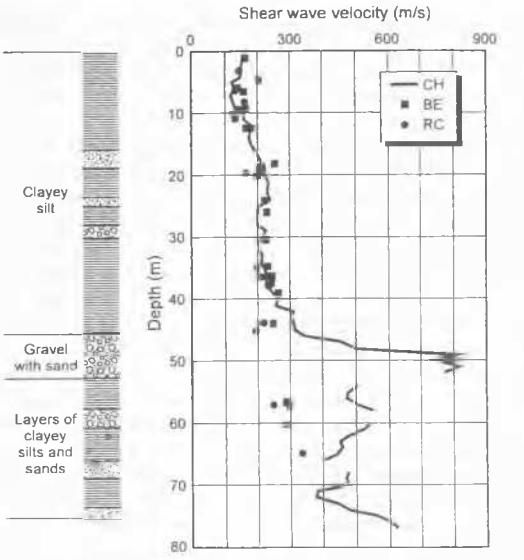

Fig. 7.4 Comparison between laboratory and field cross-hole measurements of $(V_s)_{vh}$ and $(V_s)_{hv}$ at Garigliano site, Italy (Jamiolkowski et al. 1995).

Such effects were clearly detected by body wave velocity measurements in different directions in large reconstituted homogeneous sand specimens at isotropic and anisotropic stress states (Stokoe et al. 1995; Bellotti et al. 1996; Fioravante et al. 1997). In the field, however, the separation of the effects of local layering and anisotropy would be difficult. Yet, in structured Pleistocene clay deposits in Italy, $(V_s)_{hh}$ is generally slightly larger than $(V_s)_{vh}$ (Jamiolkowski et al. 1995). Older Eocene and Cretaceous UK clay deposits with high OCRs (i.e., London clay and older clay deposits) are more anisotropic with $(V_s)_{hh}$ being noticeably larger than $(V_s)_{vh}$ (Butcher and Powell 1995; Hight et al. 1997). On the other hand, Nishio and Katsura (1994) showed that anisotropic effects are not significant in two reclaimed sand deposits, based on the cross-hole BE method (**Fig. 7.3**): rather $(V_s)_{hv}$ is slightly larger than $(V_s)_{hh}$.

Finally, the various wave velocity measurement methods employ different wave frequencies depending on the natural frequency of the deposit and the frequency of forced vibration. Different results might be obtained if the wave velocity depends significantly on the wave frequency. The existing data suggest that this effect may not be significant for homogeneous deposits.

Correlation between laboratory tests and field wave velocity measurements: Many studies have shown that for homogeneous uncemented and cemented deposits, G_0 values from laboratory tests (static and dynamic loading tests and wave propagation measurements) on high-quality undisturbed samples are close to those from field values $G_f = \rho \cdot V_s^2$;

1) for sands; Yoshimi et al. (1989) and Hight et al. (1997);
2) for gravels; Yasuda et al. (1996);
3) for stiff clays; Figs. 4.21, 4.27, 4.33, 6.1, 6.3 and 6.6, Hight and Jardine (1993), Mukabi et al. (1994), Tatsuoka and Kohata (1995), Tatsuoka et al. (1995) and Hight et al. (1997);
4) for sedimentary soft rocks and cement-treated soils; Figs. 6.3, 6.4a and 7.1, Tatsuoka and Shibuya (1992), Tatsuoka and Kohata (1995), Tatsuoka et al. (1995a, b, 1997), Hight et al. (1997) and King (1996); and
5) for soft clays; Fig. 6.2, Hight et al. (1995), Shibuya et al. (1995) and Shibuya and Tanaka (1996).

As typically shown in **Fig. 7.4**, experience in Italy is that laboratory values (G_0) from RC and BE tests are generally similar to field values (G_f) from the cross-hole seismic method, particularly for cohesive soils. For the cases of the clay deposits summarized in **Table 7.1**, the ratio of G_0/G_f is 0.67 to 0.98. The ratios of G_0/G_f for cohesionless soils are generally smaller, perhaps due to greater effects of sample disturbance.

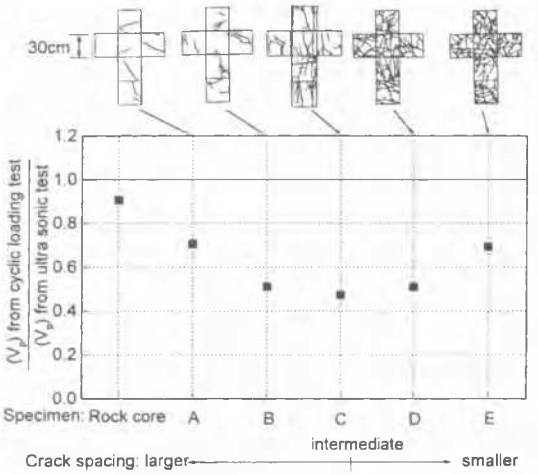

Fig. 7.5 Ratio of "V_p from static cyclic loading tests" to "V_p from ultra-sonic wave velocity (f= 54 kHz)" plotted against the crack spacing apparent in test specimens of hard rock and sketches of crack patterns (Sato et al. 1997a and b).

In a number of cases where the agreement is very poor, sample disturbance is the first factor to be considered, followed by a sensitivity to testing stress state and path, caused by inherent and/or stress-system induced anisotropy. The underestimation of the field K_0 value could also be an important factor for heavily OC soils as could heterogeneity in a geomaterial where the G_f values vary locally (e.g., Figs. 7.1 and 7.2). In the latter case, the average G_f value obtained over a depth interval should be compared with several G_0 lab measurements made over the same interval. Finally, the effects of wave length relative to discontinuity length (such as particle diameter or distance between adjacent cracks) on body wave velocities could be very important. When the wave length is similar to the discontinuity size, as in the case of laboratory ultra-sonic wave velocities measurements on softrocks having micro-defects (Nishi et al. 1989) or BE tests on large diameter cohesionless soils (Souto et al. 1994; Tanaka et al. 1995), the measured velocities may over-reflect the properties of the stiffer parts within the mass. This problem is well-known for hard rock masses including discontinuities. On the other hand, in the case of most field seismic surveys in uncemented soils, it is likely that the wave length is much larger than the discontinuity size, and the wave velocity reflects the average properties of the ground mass. The same would be true for undisturbed rock masses which contain few discontinuities, where the wave length is much smaller than the discontinuity size. In accordance with the above, **Fig. 7.5** shows the ratio of "primary wave velocity V_p converted from the E_0 value seen in static cyclic loading tests" to "V_p from ultra-sonic tests" for air-dried hard rock cores. The ratio has a minimum when the crack spacing is intermediate, while the ratio approaches unity as crack spacing becomes larger (as for intact rock cores) and smaller (as for uncemented soils). Note that the dominant P wave velocity V_p reflects the stiffness of pore water for the case of water-saturated uncemented soils under normal pressure levels. Interestingly, at the four sites from which these hard rock cores were obtained, the $(V_s)_{vh}$ values from the field down-hole and suspension seismic surveys were consistent with the values back-calculated from the predominant vibrations in the field full-scale behaviour during earthquakes. This agreement is likely to be due to similar wave lengths. It is also reported that as the discontinuity spacing in a rock mass decreases, V_s values from laboratory ultra-sonic wave velocity measurements on core samples trend to exceed those from field seismic surveys and those back-calculated from field full-scale seismic behaviour (Sato et al. 1997a). Ultra-sonic wave measurements may not be adequate to evaluate the average stiffness of a highly discontinuous geomaterial.

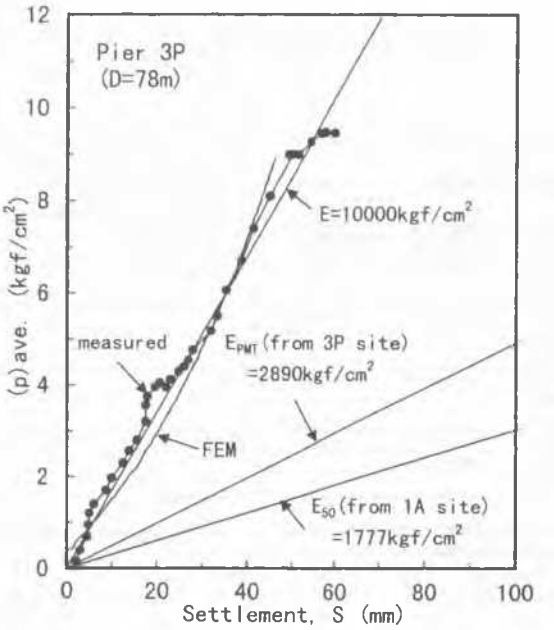

Fig. 7.6 Relationship between average applied pressure $(p)_{ave}$ and centre-line settlement of pier foundation 3P of Akashi Kaikyo Bridge on sedimentary sandstone and its numerical simulation (Siddiquee et al. 1995; Tatsuoka et al. 1996b).

7.2 Field loading tests

***Pressuremeter tests*:** Field loading tests are often preferred in cases where sample disturbance may have a serious impact on laboratory test results. Principally, three approaches exist for the application of their results (Tani 1995).

1. Index properties may be obtained from the tests, which lead to design parameters through empirical relationships.
2. Average stiffnesses are deduced by linear analysis, which is associated with a characteristic ground strain ε, defined as the cavity strain at the bore hole wall for pressuremeter tests (PMTs) or a settlement/diameter ratio S/D_{PLT} for plate loading tests (PLTs).
3. A non-linear stress-strain relationship is interpreted by non-linear analysis of the test results.

The Menard Pressuremeter measures a relatively large strain stiffness parameter, called the "equivalent (elastic) modulus", which is usually much smaller than the quasi-elastic modulus. In practice, this modulus has been interpreted by using locally established empirical rules to give specific parameters which have been used successfully, particularly in foundation design in France (e.g., Gambin 1995). This empirical approach may not work with unprecedented structures, such as the very large foundations of the Akashi Kaikyo Bridge. In **Fig. 7.6**, the measured settlement of that bridge's pier 3P (constructed on a sedimentary soft rock of the Kobe Formation) is compared with that predicted by a linear solution using the average E_{PMT} value for a depth restricted to the footing diameter (by following approach 2). The E_{PMT} values were obtained by linear analysis of pressure-cavity expansion relations from conventional primary loading PMTs. It is seen that the E_{PMT} value is too small: the same was true with many other structures including: the bridge's anchor 1A (on the same softrock deposit) and Pier 2P (on a stiff uncemented gravel); the foundations for Rainbow Bridge on sedimentary soft mudstone (Fig. 7.1); many high-rise buildings and deep and/or wide excavations in sedimentary soft rocks (Tatsuoka and Kohata 1995; Tatsuoka et al. 1995c). Based on such experiences, in engineering practice, E_{PMT} values are often converted by using empirical correlations into larger equivalent E values comparable to the Plate Loading Test (PLT) E_{PLT} value obtained from unload/reload cycles (Tatsuoka and Kohata 1995). However, there is no sound rationale for this conversion.

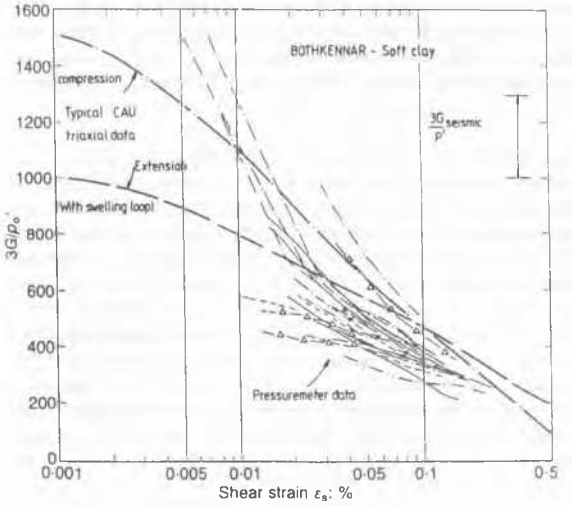

Fig. 7.7 Non-linear undrained stiffness from self-boring PMTs in Bothkennar clay, compared with data from CU TC and TE test and seismic tests (Jardine 1992a).

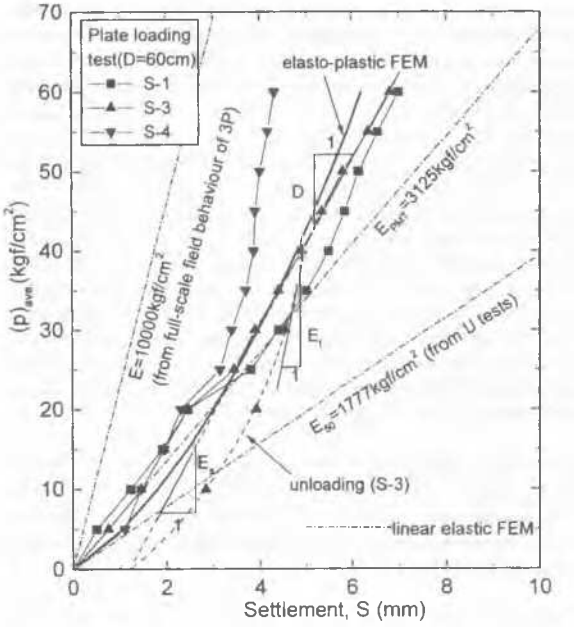

Fig. 7.8 PLTs on sedimentary sandstone performed at the bottom level of Anchor foundation 1A of Akashi Kaikyo Bridge and their numerical simulations; the unload curve is shown only for PLT S-3 (Siddiquee et al. 1995; Tatsuoka et al. 1996b).

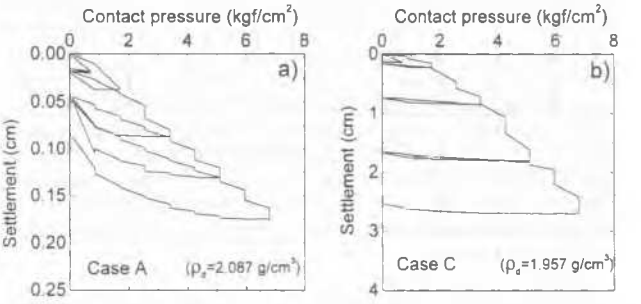

Fig. 7.9 Typical results of PLTs on a) very dense and b) loose Chiba gravel; triaxial test results on the same type of gravel are shown in Fig. 2.2 (by the courtesy of Japan Railway Technical Research Institute).

A further difficulty with PMTs is the dependency of the stiffness on many factors: the equipment type; measurement accuracy and the test procedures (pre-bored or self-bored, different stress-time histories, with or without unload-reload cycles, or different load levels at which stiffness is measured); and the analysis method adopted (different preconceived geomaterial models; linear or specific non-linear model, or different drained conditions assumed) (see Clarke 1995). In non-linear analysis of drained PMT tests (approach 3), it is often assumed that the non-linear stress-strain relation of a given geomaterial is controlled by p′ and the p′ value remains constant, as implied by linear elastic analyses of cavity expansion. Perhaps for these reasons, only strain non-linearity is usually considered. For real geomaterials under drained conditions, however, p′ increases upon loading, and the stiffness is not simply a function of p′, as discussed in **4.4**. Therefore, when stress state changes are relatively large, as in PMTs in drained stiff materials such as dense gravels, the pressure-dependency of stiffness should be taken into account. Partial drainage, unloading/reloading (or cyclic loading) and creep effects (and tensile failure in softrock) are other important factors. Non-linear analysis taking into account the above factors is feasible only by rigorous numerical methods (e.g., FEM) (e.g., Tsubouchi et al. 1994). In such non-linear analysis, the stress-strain models and flow rules are necessarily preconceived, and the sophisticated analysis required to derive the matching soil parameters is usually very difficult (Tani 1995).

With careful undrained tests involving negligible disturbance in saturated clay deposits, the no-volume change condition can be used to simplify the analysis, and PMTs can provide useful information on how stiffness varies with strain without using FEM (Jardine 1992a). **Fig. 7.7** shows such results obtained from unload curves of self-boring PMTs with care being taken to isolate creep effects, which may mask the initial small strain behaviour when unloaded from a certain shear stress level.

Even under ideal conditions in advanced PMTs, the smallest reliable cavity wall strain measurements would currently be of the order of 10^{-4} (0.01%). Small strain stiffness measurements by field seismic survey and laboratory stress-strain tests are, therefore, complementary to the PMTs and vice versa (see Figs. 7.1 and 7.7).

Plate loading tests: The conventional plate loading test procedure (PLT) using a rigid plate often results in an erroneously soft initial relationship between the average plate contact pressure $(p)_{ave}$ and the plate settlement **S**. Such a response could be due to a) effects of bedding errors at the interface between the plate and the ground surface and b) the presence of a thin disturbed surface layer produced by excavating and trimming. Marsland and Eason (1973) and Tatsuoka et al. (1997) demonstrated that for London clay and a sedimentary soft mudstone, respectively, there is no initial soft response in the relationship between $(p)_{ave}$ and center-line axial strains measured in the ground. In-situ axial strain measurements are recommended whenever feasible, since they are not very costly compared with the total PLT cost. Another reason for the appearance of S-shaped load-settlement curves is the dependency of drained stiffness on pressure, as seen in the results of PLTs on a sedimentary soft sandstone shown in **Fig. 7.8**. The vertical tangent stiffness in the ground largely reflects the tangent Young's modulus E_{tan} applying to vertical strains in the ground immediately below the plate. If the increase in E_{tan} with σ_v' overwhelms the decrease due to strain non-linearity, the tangent $\partial (p)_{ave} / \partial S$ can increase with $(p)_{ave}$ before, at larger loads, the tangent starts to decrease due to yielding of the ground. The same feature was seen in PLTs on a very dense gravel (**Fig. 7.9a**).

The average stiffness obtained by approach 2 is used directly in ordinary Rock Mechanics practice. However, noting that the stiffness from the initial primary loading curve is too small, the design stiffness is often obtained from the tangent modulus (D) of the apparently linear part of the curve at pressure levels exceeding those involved in full-scale behaviour, or from the secant or tangent moduli (E_s or E_t) associated with unload/reload curves (see Fig. 7.8). To estimate the settlement of high-rise

buildings on Bouldery clay in Singapore, Wong et al. (1996) recommended the use of stiffnesses determined after at least two unloading and reloading cycles in PLTs (and PMTs), even though the buildings apply positive net pressure to the ground. In these methods, the effects of either cyclic loading or the large pressure at which the PLT stiffness is evaluated may compensate, at least partly, for the bedding errors and relatively large strains involved in PLTs. The value of E_s as shown in Fig. 7.8 was used at the design stage of the foundations for the Akashi Kaikyo Bridge. The Young's modulus back-calculated from the full-scale behaviour of pier P3 is about 10,000 kgf/cm^2 (Fig. 7.6), which is a value marginally greater than the E_s value and the tangent modulus D developed on the primary PLT loading curve at $(p)_{ave}$ exceeding 25 kgf/cm^2 (Fig. 7.8). However, the values of E_s and D in fact depend too greatly on the arbitrary effects of bedding errors, pressure levels, strains, manner of cyclic loading and so on for these to be reliable design parameters.

Another routine approach is to calculate an equivalent vertical sub-grade reaction k_v from the PLT $(p)_{ave}$-S curve. After applying a scale factor, the k_v value is used to estimate full-scale behaviour (as in ordinary Soil Mechanics practice). The scale effects are expressed as;

$$k_v = (k_v)_{PLT} \cdot (D/D_{PLT})^n \quad (7.1)$$

where k_v and $(k_v)_{PLT}$ are, respectively, the coefficient of vertical sub-grade reaction for a prototype structure with a diameter D and the value from a PLT with a plate diameter of D_{PLT}. The scale effect has been discussed extensively elsewhere (e.g., Burland and Burbridge 1985), and a power n= -3/4 is often used in practice, while a simple elastic treatment (i.e., the direct use of D, E_s or E_t) is equivalent to assuming n= -1.0. For the case shown in Figs. 7.6 and 7.8, D/D_{PLT} is equal to 78 m/0.6 m (= 180), and when $(k_v)_{PLT}$ for $(p)_{ave}$ less than 25 kgf/cm^2 is used, a power n= -0.69 is back-calculated, which is only marginally different from -3/4. However, a small error in the n value leads to a large error when applying to such a very large structure as above (Izumi et al. 1997). Basically, the value of n may be explained by strain and pressure non-linearity of stiffness(Hettler and Gudehus 1985).

A realistic FEM analysis would automatically take into account the scale effect (Figs. 7.6 and 7.8). When in-situ axial strain measurements are made, it is possible to make a non-linear interpretation of the true in-situ stress strain behaviour by making reasonable assumptions regarding the stress changes imposed by the PLT (Jardine et al. 1985; Burland 1989; Tatsuoka et al. 1997). Good agreement has been found with undrained clays and a sedimentary softrock between such curves and other high quality stiffness measurements. A non-linear interpretation may also be made when drained pressure-dependent conditions apply. Figs. 7.5 and 7.8 show the results from such FEM analysis, in which the small strain stiffness G_0 was determined from the field shear wave velocities, and strain and pressure non-linearities were evaluated by CD TC tests on undisturbed samples. The FEM analyses simulate the observed behaviour very well in both cases. FEM analysis in which secant stiffnesses vary as functions of strain and pressure and are compatible with those developed at each point in the ground offer only an approximate approach, but may be useful in practice.

In Figs. 7.6 and 7.8, predictions based on the E_{50} values from conventional unconfined compression tests on block-sampled cores (measuring axial strains externally) are compared with the measured relationships. These predictions are utterly unreliable.

8 SUPPORTING CASE HISTORIES

The importance of taking into account non-linearity for predicting ground deformation and structural displacements at working loads has been demonstrated for a number of case histories. Jardine et al. (1991) found that a non-linear FEM approach based on locally instrumented stress path tests gave good predictions in several case histories involving loading and unloading in North Sea sediments, London Tertiary deposits and other natural soils. Some further general comments are given below.

Loading problems: Experience with spread foundations on sedimentary softrock for the Akashi Kaikyo and Rainbow Bridges showed that settlement predictions developed from seismic shear moduli worked well when strain and pressure non-linearity effects were account for. Case histories involving high-rise buildings on relatively stiff uncemented soils in Japan support the same conclusion (Tatsuoka and Shibuya 1992; Majima et al. 1997). However, the behaviour of the foundations for a large suspension bridge, the Tatara Oh-hashi Bridge, constructed on weathered granite, showed that inherent discontinuities in the rock mass and construction disturbance can have very large effects and that the direct use of the seismic stiffness method can lead to serious underestimates of the settlements (Tatsuoka et al. 1996b).

Unloading problems: The field monitoring of excavation in sedimentary softrock at Sagamihara and Negishi, and in sands and clays for high-rise buildings, shows that the seismic stiffness method should take into account the effects of disturbance (or damage) caused by excavation works in addition to strain and pressure non-linearity effects. These features become larger when low pressure zones prevail in the ground. The accurate prediction of in-situ initial lateral stress is also important when predicting the outward movements: smaller "field" stiffnesses are back-calculated when lower initial lateral stresses are assumed.

Principal stress axis rotation: The effects of rotating the principal stress directions during construction may be important in many problems (Jardine 1995). However, its modelling and numerical analysis is very complicated.

9 SUMMARY AND CONCLUSIONS

Recent developments have shown new light on the pre-failure behaviour of geomaterials, showing their properties be more complex than had been anticipated. A better understanding of geomaterial stress-strain behaviour at small and intermediate strains is vital for both improving the predictions of ground deformation and structural displacements and developing a more consistent framework for geomaterial modelling. Important factors discussed in this report include:

1) for the intrinsic properties of geomaterials; kinematic hardening, anisotropy, rheological aspects, natural structure, structuration and destructuration, and stiffness dependency on recent stress-time history, current stress-state and perturbing stress-strain conditions;
2) non-linearity and its modelling; and
3) for laboratory and field tests; errors in strain measurements, measurable and controllable ranges of stress and strain and effects of disturbance of samples and test ground.

It is demonstrated that quantifying the quasi-elastic behaviour shown by geomaterials at very small strains is useful in practice, especially for small strain problems involving relatively linear materials. Field shear wave velocity measurements, therefore, have a practical role to play except for materials having a large amount of discontinuities (fissures, cracks etc), very heterogeneous deposits and those with very large particles. Carefully instrumented field loading tests and/or laboratory stress-strain tests are essential to supplement the above (or vice versa) particularly for largely strain-non-linear and pressure-dependent materials. The quasi-elastic properties may also be used to normalize pre-peak stress-strain behaviour to take into account the effects of pressure changes and structuration and destructuration.

Non-linear FEM approaches developed from field and laboratory stress-strain measurements have been highly successful in

predicting full-scale load-displacement behaviour in a wide range of civil engineering applications. New families of soil models are now being developed. But it should be finally re-emphasized that predicting ground movements is a multi-faceted problem; modelling the ground's stress-strain behaviour is only one of the key aspects as listed in Tables 1.2.

Acknowledgments: The authors are grateful to their previous and current colleagues at Univ. of Tokyo, Imperial College, ENTPE and Politecnico di Torino for their cooperation in research and their help in preparing this paper.

REFERENCES

Abbreviations;

ASIP; Advances in Site Investigation Practice, Proc. ICE Conf., London, 1994 (Craig eds), Thomas Telford
CGJ; Canadian Geotechnical Journal
GTJ; Geotechnical Testing Journal, ASTM
ICE; Institution of Civil Engineers, UK
IS Hokkaido '94; Pre-Failure Deformation of Geomaterials, Proc. Fist Int. Conf., IS Hokkaido '94 (Shibuya et al. eds), Balkema
IS Tokyo '95; Earthquake Geotech. Eng., Proc. First Int. Conf., IS Tokyo '96 (Ishihara eds), Balkema
JGS; Japanese Geotechnical Society
JNCGE; Japan National Conference on Geotechnical Engineering, JGS
JSCE; Japanese Society of Civil Engineers
S&F; Soils and Foundations, Journal of JGS

Akai,K., Adachi,T. and Ando,N. (1975): Existence of a unique stress-strain-time relation of clays, S&F **15-1**, 1-16.
Amaya,M. (1997): Internal report, IIS, Univ. of Tokyo.
Ampadu,S.I.K. and Tatsuoka,F.(1989): An automated stress path control triaxial system, GTJ **12-3**, 238-243.
Anderson,D.G. and Woods,R.D. (1975): Time-dependent increase in shear modulus of clay, J. GE Div., ASCE, 102-GT5, 525-537.
Anderson,D.G. and Stokoe,K.H.II, (1978): Shear modulus: a time-dependent soil properties, Dynamic Geotech. Testing, ASTM STP **654**, 66-90.
Arthur,R.F. and Menzies,B.K. (1972): Inherent anisotropy in a sand, Géotechnique **22-1**, 115-128.
Atkinson,J.H., Richardson,D. and Stallebrass,S.E. (1990): Effect of stress history on the stiffness of over-consolidated soil, Géotechnique **40-4**, 531-540.
Atkinson,J.H. and Sällfors,G. (1991): Experimental determination of soil properties, Proc. 10th EC on SMFE, Firenze **3**, 915-956.
Bardet,J.P. (1996): Scaled memory model for cyclic behavior of soils, J. Geotech. Engrg., ASCE, **121-11**, 765-775.
Berre,T. and Bjerrum,L. (1972): Shear strength of normally consolidated clays, Proc. 8th ICSMFE, Moscow, **1**, 39-49.
Bellotti,R., Jamiolkowski,M., Lo Presti,D.C.F. and O'Neill,D.A. (1996): Anisotropy of small strain stiffness in Ticino sand, Géotechnique **46-1**, 115-131.
Biarez,J. and Hicher,P.Y. (1994): Elementary mechanics of soil behaviour, Balkema.
Boyce,H.R. (1980): A non-linear model for the elastic behaviour of granular materials under repeated loading, Proc. Int. Sym. on Soils under Cyclic and Transient Loading, Swansea, Balkema, 285-294.
Brignoli,E.G.M., Gotti,M. and Piccoli,S. (1995): In situ and laboratory shear wave velocities of different natural soil deposit, Proc. First Int. Conf. on Earthquake Geotechnical Engineering, IS Tokyo '95, **1**, 327-332.
Brignoli,E.G.M., Gotti,M. and Stokoe,K.H.II. (1996): Measurement of shear waves in laboratory specimens by means of piezoelectric transducers, GTJ **19-4**, 384-397.
Brown,S.F. (1996): Soil mechanics in pavement engineering, 36th Rankine Lecture, Géotechnique **46-3**, 383-426.
Bulter,D.K. and Curro,J.R.Jr. (1981): Crosshole seismic testing - Procedures and pitfalls, Geophysics **46-1**, 23-29.
Burland,J.B. (1989): Small is beautiful -the stiffness of soils at small strains, CGJ **26**, 499-516.
Burland,J.B. and Burbridge,M.C. (1985): Settlement of foundations on sand and gravel, Proc. ICE, Part 1; Design and Construction **78**, 1325-81.
Burland,J.B. (1990): On the compressibility and shear strength of natural clays, 30th Rankine Lecture, Géotechnique **41-3**, 329-378.
Burland,J.B., Rampello,S., Georgiannou,V.N. and Calabresi,G. (1996): A laboratory study of the strength of four stiff clays, Géotechnique **46-3**, 491-514.
Butcher,A.P. and Powell,J.M. (1995): Practical considerations for field geophysical techniques used to assess ground stiffness, ASIP, 701-714.
Cazacliu,B. (1996): Comportement des sable en petites et moyennes déformations; Prototype d'essai de torsion compression confinement sur cylindre creux, Thése de Doctorat, ECP-ENTPE.
Clarke,B.G. (1995): Moderator's report on Session 4(b): pressuremeter, permeability and plate tests, ASIP, 623-641.
Clayton,B.G. and Hope,V.S. (1995): Moderator's report on Session 5: geophysical testing, ASIP, 774-788.
Cuccovillo,T. and Coop,M.R. (1996). The measurement of local axial strains in triaxial testing using LVDTs, Géotechnique **45-1**, 167-171.
Dobry,R., Ladd,R.S., Yokel,F.Y., Chung,R.M. and Powell,D. (1982): Prediction of pore pressure buildup and liquefaction of sand during earthquakes by cyclic strain method, National Bureau of Standards Building Science **138**, Washington DC.
Di Benedetto,H. and Hameury,O. (1991): Constitutive law for granular skeleton materials: description of the anisotropic and viscous effects; Comp. Met. and Ad. In Geomec. (Beer et al., eds), Balkema, 599-603.
Di Benedetto,H., Hameury,O. and Cazacliu,B. (1992): Incremental constitutive law for sand: anisotropic and cyclic effects; Proc. 10th WCEE, Balkema, 2555-60.
Di Benedetto,H., Hameury,O. Cazacliu,B., Cambou,B. and Dubujet,Ph.(1995): Behaviour of sand under stress paths with axis rotation, IS Tokyo '95, **1**, 289-294.
Di Benedetto,H., Cazacliu,B., Boutin,C., Doanh,T. and Touret,J.P. (1997): Compertement des sables avec rotation d'axes: nouvel appareil couvrant quatre décades de déformation, Proc. 14th ICSMFE, Hamburg, **1**, 279-282.
Di Benedetto,H. and Ibraim,E. (1996): Internal Report, Département Génie Civil et Bâtiment, ENTPE.
Di Benedetto,H. and Tatsuoka,F. (1997): Small strain behaviour of geomaterials: modelling of strain effects, S&F **37-2**, 127-138.
Dong,J., Nakamura,K., Tatsuoka,F. and Kohata,Y. (1994): Deformation characteristics of gravels in triaxial compression tests and cyclic triaxial tests, IS Hokkaido '94, **2**, 17-23.
Dong,J. and Nakamura,K.(1997): Anisotropic deformation characteristics of gravels in large-scale plane strain and triaxial compression tests, Pro. 14th ICSMFE, Hamburg, **1**, 81-84.
Dyvik,R. and Madshus,S. (1985): Laboratory measurements of G_{max} using bender elements, Proc. ASCE Convention, Detroit, 186-196.
England,G.L. (1994): The performance and behaviour of biological filter walls as affected by cyclical temperature changes, Serviceability of Earth Retaining Structures, ASCE Geotech. Special Publication **42**, 57-76.
Fioravante,V. (1996): Personal communication.
Fioravante,V., Fretti,C., Froio,F., Jamiolkowski,M., Lo Presti,D.C.F. and Pedroni,S. (1997): Anisotropy of elastic stiffness in Kenya sand, Géotechnique (submitted).
Flora,A., Jiang,G.L., Kohata,Y. and Tatsuoka,F. (1994): Small strain behaviour of a gravel along some triaxial stress paths, IS-Hokkaido '94, **2**, 279-285.
Gambin,M. 1995; Reasons for the success of Menard Pressuremeter, Proc. of Fourth Int. Sym. on Pressuremeter, May, Sherbrooke, Canada.
Goto,S., Tatsuoka,F., Shibuya,S., Kim,Y.S. and Sato,T. (1991): A simple gauge for local small strain measurements in the laboratory, S&F **31-1**,169-180.
Graham,J. and Houlsby,G.T. (1983): Elastic anisotropy of a natural clay, Géotechnique **32-2**,165-180.
Hamaya,S., Koseki,J., Maeshiro,T. and Tatsuoka,F. (1997): Elastic deformation characteristics of Toyoura sand in drained triaxial test, Proc. 32th JNCGE, Kumamoto, **1**, 685-686 (in Japanese).
Hameury,O. (1995): Quelques aspects du comportement des sables avec ou sans rotation des axes principaux des petites aux grandes déformations, Thése de Doctorat, ECP-ENTPE.
Hardin,B.O. and Richart,F.E.Jr. (1963): Elastic wave velocities in granular soils, J. ASCE 89-SM1, 33-65.
Hardin,B.O. and Black,W.L. (1968): Vibration modulus of normally consolidated clay, J. SMF Div., ASCE 95-SM6, 1531-1537.
Hardin,B.O. and Drnevich,V.P. (1972): Shear modulus and damping in soils: design equations and curves, Jour. of SMF Div., ASCE, 98-SM7, 667-692.
Hardin,B.O. (1978): The nature of stress-strain behavior for soils, Proc. Geotech. Div. Specialty Conf. on Earthquake Eng. and Soil Dynamics, ASCE, Pasadena, **I**, 3-90.

Hardin,B.O. and Bladford,G.E. (1989): Elasticity of articulate materials, J. of Geotech. Engrg., ASCE, **115-6**, 788-805.
Hayano,K., Sato,T. and Tatsuoka,F. (1997): Deformation characteristics of a sedimentary softrock from triaxial compression tests rectangular prism specimens, Géotechnique **47-3**, 439-449.
Hayano,K., Tatsuoka,F., Kawakami,S. and Yoshiizumi,N. (1997): Stress state-dependency of elastic modulus of sedimentary softrock, Proc. 32th JNCGE, Kumamoto, **1**, 1221-1222 (in Japanese).
Hettler,A. and Gudehus,G. (1985): A pressure dependent correction for displacement results form 1g models tests with sand, Géotechnique **35-4**, 497-510.
Hicher,P.Y. (1996): Elastic properties of soils, J. of Geotech. Engrg., ASCE, **122-8**, 641-648.
Hight,D.W., Gens,A. and Symes,M.J. (1983): The development of a new hollow cylinder apparatus for investigating the effects of principal stress rotation in soils, Géotechnique **33-4**, 355-384.
Hight,D.W. (1992): A review of sampling effects in clays and sands, Offshore Site Investigation and Foundation Behaviour, Proc. SUT Int. Conf., Kluwer, Dordrecht, 115-146.
Hight,D.W., Bond,A.J. and Legge,J.D. (1992): Characterization of the Bothkennar clay: an overview, Géotechnique **42-2**, 303-347.
Hight,D.W. and Jardine,R.J. (1993): Small strain stiffness and strength characteristics of hard London Tertiary clays, Geotech. Engrg. of Hard Soils-Soft Rocks, Proc. Int. Conf., Athens (Agnostopoulos et al., eds), Balkema, **1**, 533-552.
Hight,D.W. and Higgins,K.G. (1995): An approach to the prediction of ground movements in engineering practice: Background and application, IS Hokkaido '94, **2**, 909-945.
Hight,D.W. and Georgiannou,V.N. (1995): Effect of sampling on the undrained behaviour of clayey sands, Géotechnique **45-2**, 237-247.
Hight,D.W. (1996): Moderator's report on Session 3: drilling, boring, sampling and description, ASIP, 337-360.
Hight,D.W., Bennell,J.B., Chana,B., Davis,P.D., Jardine,R.J. and Porovic,E. (1997): Wave velocity and stiffness measurements of the Crag and Lower London Tertiaries and Sizewell, Gèotechnique **47-3**, 451-474.
Hoque,E. (1996): Elastic deformation of sands in triaxial tests, Dr. Engineering thesis, Univ. of Tokyo.
Hoque,E. and Tatsuoka,F. (1998): Anisotropy in the elastic deformation of granular materials, S&F **38-1** (in press).
Isenhower,W.M. and Stokoe,K.H.II (1981): Strain rate-dependent shear modulus of San Francisco Bay mud, Proc. Int. Conf. on Recent Advances in Geotech. Earthquake Engrg. and Soil Dynamics, St. Louis (Prakash eds), **II**, 597-602.
Ishihara,K. (1996): Soil behaviour in Earthquake Goetechnics, Oxford Science Publications.
Izumi,K., Ogihara,M. and Kameya,H. (1997): Displacements of bridge foundations on sedimentary softrock; a case study on small strain stiffness, Gèotechnique **47-3**, 619-632.
Jamiolkowski,M., Leroueil,S., and Lo Presti,D.C.F. (1991): Design parameters from theory to practice, Theme Lecture, Proc. Geo-Coast '91, Yokohama, **2**, 877-917.
Jamiolkowski,M., Lancellotta,R., Lo Presti,D.C.F. and Pallara,O. (1995): Stiffness of Toyoura sand at small and intermediate strain, Proc. 13th ICSMFE, New Delhi, **1**, 169-172.
Jamiolkowski,M., Lancellotta,R. and Lo Presti,D.C.F. (1995): Remarks on the stiffness at small strains of six Italian clays, IS Hokkaido '94, **2**, 817-836.
Jamiolkowski,M. and Manassero (1995): Closing address, ASIP, 929-951.
Jardine,R.J. (1985): Investigations of pile-soil behaviour with special reference to the foundations of offshore structures, PhD thesis, Univ. of London.
Jardine,R.J., Fourie,A.B., Maswoswse,J. and Burland,J.B. (1985): Field and laboratory measurements of soil stiffness, Proc. 11th ICSMFE, San Francisco, **2**, 511-514.
Jardine,R.J., St.John,H.D., Hight,D.W. and Potts,D.M. (1991): Some practical applications of a non-linear ground model, Proc. 10th ECSMFE, Firenze, **1**, 223-228.
Jardine,R.J. (1992a): Non-linear stiffness parameters from undrained pressure meter tests, CGJ **29**, 436-447.
Jardine,R.J.(1992b): Some observations on the kinematic nature of soil stiffness, S&F **32-2**, 111-124.
Jardine,R.J. (1995): One perspective of the pre-failure deformation characteristics of some geomaterials, IS Hokkaido '94, **2**, 855-885.
Jardine (1995): Moderator's report on Session 6: laboratory test, ASIP, 900-915.
Jiang,G.L., Tatsuoka,F., Flora,A. and Koseki,J. (1997): Inherent and stress state-induced anisotropy in very small strain stiffness of a sandy gravel, Géotechnique **47-3**, 509-521.
Jiang,G.L. and Kohata,Y. (1996): Personal communication.
Kim,Y.-S., Tatsuoka,F. and Ochi,K. (1994): Deformation characteristics at small strains of sedimentary soft rocks by triaxial compression tests, Géotechnique **44-3**,461-478
Kim,D.-S. and Stokoe,K.H.II (1994): Torsional motion monitoring system for small-strain (10^{-5} % to 10^{-3} %) soil testing, GTJ. **17-1**,17-26.
Kim,D.-S. and Stokoe,K.H.II (1995): Deformation characteristics of soils at small to medium strains, IS Hokkaido '94, **1**, 89-94.
King,M.S., Andrea,M. and Shams Khanshir,M. (1994): Velocity anisotropy in Carboniferous mudstones, Int. J. Rock Mech. Min. Sci. & Geomech. Abstr **31-3**, 261-263.
King,M.S. (1996): Personal comminucation.
Kitsunezaki,C. (1985): Some basic problems of shear wave logging by means of the suspension-type sonde, Jour. of Mining College, Akita Univ.
Kohata,Y. Tatsuoka,F., Dong J., Teachavorasinskun,S. and Mizumoto,K. (1994): Stress-state affecting elastic deformation moduli of geomaterials, IS-Hokkaido '94, **1**, 3-9.
Kohata,Y., Tatsuoka,F., Wang,L., Jiang,G.L., Hoque,E. and Kodaka,T. (1997): Modelling the non-linear deformation properties of stiff geomaterials, Géotechnique **47-3**, 563-580.
Kokusho,T., Yoshida,Y. and Esashi,Y. (1982): Dynamic properties of soft clay for a wide strain range, S&F **22-4**,1-29.
Kuwano,R. (1997): Personal communication (at Imperial College).
Lam,W-K. and Tatsuoka,F. (1988): Effect of initial anisotropic fabric and σ_2 on strength and deformation characteristics of sand, S&F **28-1**, 89-106.
Lanier,J., Di Prisco,C. and Nova,R. (1991): Etude expérimentale et analyse théorique de l'anisotropie induite du sable d'Hostun, Revue française géotechnique **49**, 67-76.
Leroueil,S. and Vaughan,P.R. (1990): The general and congruent effects of structure in natural soils and weak rocks, Géotechnique **50-2**, 467-488.
Leroueil,S. and Marques,M.E.S. (1996): Importance of strain rate and temperature effects in geotechnical engineering, Measuring and Modeling Time Dependent Soil Behavior, ASCE Geotech. Special Publication **61**, 1-60.
Leroueil,S., Perret,D. and Locat,J. (1996): Strain rate and structuring effects on the compressibility of a young clay, Measuring and Modeling Time Dependent Soil Behavior, ASCE Geotech. Special Publication **61**, 137-150.
Lo Presti,D.C.F. (1989): Proprietà Dinamiche dei Terreni, XIV Conferenza Geotechnica di Torino, Dipartimento di Ingegneria Strutturale, Poltecnico di Torino, 62.
Lo Presti,D.C.F., Pallara,O., Lancellotta,R., Armandi,M. and Maniscalco,R. (1993): Monotonic and cyclic loading behaviour of two sands at small strains, GTJ **16-4**, 409-424.
Lo Presti,D.C.F., Pallara,O., Costanzo,D. and Impavido,M. (1994): Small strain measurements during triaxial tests: many problems, some solutions, IS Hokkaido'94, **1**, 11-16.
Lo Presti,D.C.F. (1995): General Report on "Measurement of shear deformation of geomaterials in the laboratory", IS Hokkaido '94, **2**, 1067-1088.
Lo Presti,D.C.F., Jamiolkowski,M. and Pallara,O. (1995a): Pisa clay stiffness from static and dynamic laboratory tests, IS Tokyo '95, **1**, 113-119.
Lo Presti,D., Jamiolkowski,M., Pallara,O. Pisciotta,V. and Ture,S. (1995b): Stress dependence of sand stiffness, Proc. IC. on Recent Advances in Geotech. Earthquake Engng and Soil Dynamics. St Louis. (Prakash eds), **1**, 71-76.
Lo Presti,D.C.F., Jamiolkowski,M., Pallara,O. and Cavallaro,A. (1996): Rate and creep effect on the stiffness of soils, Measuring and Modeling Time Dependent Soil Behavior, ASCE Geotech. Special Publication **61**, 166-180.
Lo Presti,D.C.F., Jamiolkowski,M., Pallara,O., Cavallaro,A. and Pedroni,S. (1997): Shear modulus and damping of soils, Géotechnique **47-3**, 603-617.
Lo Presti,D.C.F., Maugeri,M., Cavallaro,A. and Pallara,O. (1998): Shear molulus and damping of a stiff marine clay from in situ and laboratory tests, ISC **98**, Atlanta (submitted).
Mair,R.J. (1993): Developments in geotechnical engineering research: application to tunnel and deep excavation; Unwin Memorial Lecture 1992, Proc. ICE **93**, 27-41.
Majima,M., Tamaoki,K., Akino,N. and Aoki,M. (1997): Behaviour of ground due to building construction, Tsuchi-to-kiso, Jour. JGS **45-11** and **12** (in press; in Japanese).
Marsland,A. and Eason,B.J. (1973): Measurements of displacements in the ground below loaded plates in deep boreholes, Proc. BGS symposium on Field Investigation, London.

Matsumoto,M., Sato,T. and Tatsuoka,F. (1997): Effects of creep history and strain rate on deformation characteristics of sedimentary soft mudstone, Proc. 32th JNCGE, Kumamoto, **1**, 1227-1228 (in Japanese).

Matsushita,M.,Hayano,K., Matsumoto,M., Kodaka,T. and Tatsuoka,F. (1997): Evaluation of sample disturbance effects for sedimentary soft rocks, Proc. 52th Annual Conf. of JSCE III-A, 548-549 (in Japanese).

Momoya,Y. (1997): Internal report (Geotech. Lab., Univ. of Tokyo).

Mroz,Z. (1967). On the description of anisotropic work hardening, J. Mech. Phys. Solids **15**, 163-175.

Muir-Wood,D. (1990): Strain-dependent moduli and pressuremeter tests, Géotechnique **40-3**, 509-512.

Mukabi,J.N., Tatsuoka,F., Kohata,Y., Tsuchida,T. and Akino,A. (1994): Small strain stiffness of Pleistocene clays in triaxial compression, IS Hokkaido '94, **1**, 189-195.

Mukabi,J.N. (1995): Deformation characteristics at small strains of clays in triaxial tests, Dr. Engng Thesis, Univ. of Tokyo.

Murayama,S., Michihiro,K. and Sakagami,T. (1984): Creep characteristics of sands, S&F **24-2**, 1-15.

Oda,M. (1972): Initial fabrics and their relation to mechanical properties of granular material, S&F **12-1**, 17-36.

Oda,M. (1981): Anisotropic strength of cohesionless sands, J. of GE Div., ASCE, 107-GT9, 1219-1231.

d'Onofrio,A., Silvestri,F. and Vinale,F. (1997): A new torsional device, GTJ (submitted).

Ng,C., Bolton,M. and Dasari,G. (1995): The small strain stiffness of a carbonate stiff clay, S&F **35-4**, 109-114.

Nishio,S. and Katsura,Y. (1994): Shear wave anisotropy in Edogawa Pleistocene deposit, IS Hokkaido '94, **1**, 169-174.

Nishi,K., Ishiguro,T. and Kudo,K. (1989): Dynamic properties of weathered sedimentary soft rocks, S&F **29-3**, 67-8.

Park,C.-S. (1993): Deformation and strength characteristics of a variety of sands by plane strain compression tests, Dr. of Engng Thesis, Univ. of Tokyo (in Japanese).

Park,C.-S. and Tatsuoka,F. (1994): Anisotropic strength and deformation of sands in plane strain compression, Proc. 13th ICSMFE, New Delhi, **1**, 1-6.

Porovic,E. and Jardine,R.J. (1994): Some observations on the static and dynamic shear stiffness of Ham river sand, IS Hokkaido '94, **1**, 25-30.

Porovic,E. (1995): Investigations of soil behaviour using a resonant column torsional shear hollow cylinder apparatus, PhD Thesis, Univ. of London.

Pradhan,T.B.S., Tatsuoka,F. and Soto,Y. (1989): Experimental stress-dilatancy relations of sand subjected to cyclic loading, S&F **29-1**, 45-64.

Rampello,S. and Silvestri,F. (1993): The stress-strain behaviour of natural and reconstituted samples of two over-consolidated clays, Geotech. Engrg. of Hard Soils-Soft Rocks, Proc. Int. Conf., Athens (Agnostopoulos et al. eds), Balkema, **1**, 769-778.

Richart,Jr.,F.E. (1977): Dynamic stress-strain relationships for soils, S-O-A Paper, Proc. 9th ICSMFE, Tokyo, **3**, 605-612.

Riemer,M.F., Gookin,W.B., Bray,J.D. and Wartman,J. (1996): Using reflected shear waves to measure small strain dynamic properties, GTJ (submitted).

Roesler,S.K. (1979): Anisotropic shear modulus due to stress anisotropy, Jour. of GE Div., ASCE, 105-GT7, 871-880.

Rowe,P.W. (1962). The stress-dilatancy relation for static equilibrium of an assembly of particles in contact, Proc. Royal Society A **269**, 500-527.

Santamarina,J.C. and Cascante,G. (1996): Stress anisotropy and wave propagation: a micromechanical view, **GTJ** 33, 770-782.

Santucci de Magistris,F. and Hamaya,S. (1996): Internal Report, IIS, Univ. of Tokyo.

Sato,M., Ueda.M, Hasebe,N. and Kondo,H. (1997a): Comparison among wave velocities from seismic observation waves and field tests for hard rock mass, J. of JSCE, Ⅲ-38, 75-87 (in Japanese).

Sato,M., Ueda.M, Hasebe,N. and Umehara,H. (1997b): Dynamic elastic modulus of dam concrete earthquake motion, J. of JSCE, V-35, 43-55.

Scholey,G.K., Frost,J.D., Lo Presti,D.C.F. and Jamiolkowski,M. (1995): A review of instrumentation for measuring small strains during triaxial testing of soil specimens, GTJ **18-2**, 137-156.

Schultheiss,P.J. (1981): Simultaneous measurements of P & S wave velocities during conventional laboratory testing procedures, Marine Geotechnology **4**, 343-367.

Shibuya,S., Tatsuoka,F., Teachavorasinskun,S., Kong,X.-J., Abe,F., Kim,Y.-S., and Park,C.-S. (1992): elastic deformation properties of geomaterials, S&F **32-3**, 26-46.

Shibuya,S., Mitachi,T., Fukuda,F. and Degoshi,T. (1995a): Strain rate effects on shear modulus and damping of normally consolidated clay, Importance of measuring local strains in cyclic triaxial tests on granular materials, GTJ **18-3**,365-375.

Shibuya,S., Mitachi,T., Yamashita,S. and Tanaka,H. (1995b): Effects of sample disturbance on G_{max} of soils- a case study, IS Tokyo '95, **1**, 77-82.

Shibuya,S., Mitachi,T., Hosomi,A. and Hwang,S.-C. (1996): Strain rate effects on stress-strain behaviour of clay as observed in monotonic and cyclic triaxial test, Measuring and Modeling Time Dependent Soil Behavior, ASCE Geotech. Special Publication **61**, 214-227.

Shibuya,S. and Tanaka,H. (1996): Estimate of elastic shear modulus in Holocene soil deposits, S&F **36-4**, 45-56.

Shibuya,S., Hwang,S.C. and Mitachi,T. (1997): Elastic shear modulus of soft clays from shear wave velocity measurements, Géotechnique **47-3**, 593-601.

Siddiquee, M.S.A., Tatsuoka, F., Kohata, Y., Yoshida, O. and Yamamoto,Y. and Tanaka, T. (1995): Settlement of a Pier Foundation for Akashi- Kaikyo Bridge and its numerical analysis, Rock Foundation of Large-Scale Structures, Proc. Int. Workshop, Tokyo, Balkema, 413-420.

Simpson,B. (1992): Retaining structures: displacement and design, Thirty second Rankine Lecture, Géotechnique **42-4**, 541-576.

Smith,P.R. (1992): Properties of high compressibility clays with reference to construction of soft ground, PhD Thesis, Univ. of London.

Souto,A., Hartikainen,J. And Ozudogru,K. (1994): Measurement of dynamic parameters of road pavement materials by the bender element and resonant column tests, Géotechnique **44-3**, 519-526.

Stallebrass,S.E. and Taylor,R.N.(1997): The development and evaluation of a constitutive model for the prediction of ground movements in overconsolidated clay. Géotechnique **47-2**, 235-253.

Stokoe,K.H.II, Lee,J.N.-K. and Lee, S.-H. (1991): Characterization of soil in calibration chambers with seismic waves, Calibration Chamber Testing (Huang eds), Elsevier, 363-376.

Stokoe,K.H.II, Hwang,S.K. and Lee,J.N.-K. (1995): Effect of various parameters on the stiffness and damping of soils at small strains, IS Hokkaido '94, **2**, 785-816.

Sugo,K., Sato,Y., Tatsuoka,F., Yoshimine,M. and Ohnaka,H. (1997): Effects of curing method on deformation and strength characteristics of cement-mixed sand, Proc. 32th JNCGE, Kumamoto, **2**, 2397-2398 (in Japanese).

Suklje,L. (1969): Rheological aspects of soil mechanics, Wiley-Interscience, London.

Sully.J.P. and Campanella,R.G. (1995): Evaluation of in situ anisotropy from crosshole and downhole shear wave velocity measurements, Géotechnique **45-2**, 267-282.

Symes,M.J.P.R., Gens,A. and Hight,D.W. (1984): Undrained anisotropy and principal stress rotation in sand, Géotechnique **34-1**, 11-27.

Takeuchi,T., Tanaka,T., Yamamoto,S. and Inoue,A. (1997): Akashi Kaikyo Bridge-a case history, Tsuchi-to-kiso, Jour. of JGS **45-9**, 43-48 (in Japanese).

Tanaka,Y., Kokusho,T., Okamoto,T. and Kudo,K. (1995): Evaluation of initial shear modulus of gravelly soil by laboratory test and PS-logging, IS Tokyo '95, **1**, 101-106.

Tanaka, H., Sharma, P., Tsuchida, T. and Tanaka, M. (1996): Comparative study on sample quality using several types of samplers, S&F **36-2**, 57-68.

Tani,K. (1995): General report; Measurement of shear deformation of geomaterials - Field tests, IS Hokkaido '94, **2**, 1115-1131.

Tatsuoka,F., Sato,T., Park,C.S., Kim,Y.S., Mukabi,J.N. and Kohata,Y. (1994): Measurements of elastic properties of geomaterials in laboratory compression tests, GTJ **17-1**, 80-94.

Tatsuoka, F. and Shibuya,S. (1992): Deformation characteristics of soils and rocks from field and laboratory tests, Keynote Lecture, Proc. 9th Asian Reg. Conf. on SMFE, Bangkok, 1991, **2**, 101-170.

Tatsuoka,F., Siddiquee,M.S.A., Park,C.-S., Sakamoto,M. and Abe,F. (1993): Modelling stress-strain relations of sand, S&F **33-2**, 60-81.

Tatsuoka,F., Teachavorasinskun,S., Dong,J., Kohata,Y. and Sato,T. (1994a): Importance of measuring local strains in cyclic triaxial tests on granular materials, Dynamic Geotech. Testing II, ASTM STP 1213 (Edelhar et al., eds), 288-302.

Tatsuoka,F., Sato,T., Park,C.S., Kim,Y.S., Mukabi,J.N. and Kohata,Y. (1994b): Measurements of elastic properties of geomaterials in laboratory compression tests, GTJ **17-1**, 80-94.

Tatsuoka,F. (1994): Measurement of static deformation moduli in dynamic tests, Panel Discussion on Deformation of Soils and Displacements of Structures, Proc. 10th EC on SMFE, 1991, **4**, 1219-1226.

Tatsuoka,F., Kohata,Y., Tsubouchi,T., Murata,K., Ochi,K. and Wang,L. (1995a): Disturbance in rotary core tube sampling, ASIP, 281-292.
Tatsuoka, F., Lo Presti, D. & Kohata, Y. (1995b): Deformation characteristic of soils and soft rocks under monotonic and cyclic loads and their relationships, Proc. IC. on Recent Advances in Geotech. Earthquake Engng and Soil Dynamics. St Louis. (Prakash eds), **2**, 851-879.
Tatsuoka,F. and Kohata,Y. (1995): Stiffness of hard soils and soft rocks in engineering applications, Keynote Lecture, IS-Hokkaido '94, **2**, 947-1063.
Tatsuoka,F., Kohata,Y., Ochi,K. and Tsubouchi,T. (1995c): Stiffness of soft rocks in Tokyo Metropolitan area - from laboratory tests to full-scale behaviour-, Proc. Int. Workshop on Rock Foundation of Large-Scaled Structures, Tokyo, Balkema, 3-17.
Tatsuoka,F., Kodaka,T., Nitta,A. and Inoue,A. (1996a): Field loading tests and instantaneous settlement of foundation, Kiso-Ko (Foundation Engrg & Equipment), **1-9**, 2-9 (in Japanese).
Tatsuoka,F., Koseki,J. Kodaka,T. and Inoue,A. (1996b): Report to Honshu-Connection Bridge Authority (in Japanese).
Tatsuoka,F., Ochi,K., Tsubouchi,T., Kohata,Y. and Wang,L. (1997): Sagamihara experimental underground excavations in sedimentary softrock Geotech. Eng., Proc. ICE, **125**, Oct., 206-223.
Teachavorasinskun,S., Tatsuoka,F. and Shibuya,S. (1991): Stiffness of sands in monotonic and cyclic torsional simple shear, Geotech. Eng. Congress 1991, ASCE Geotech. Special Publication **27**, **2**, 863-878.
Teachavorasinskun,S., Tatsuoka,F., and Lo Presti, D.C.F. (1994): Effects of cyclic prestraining on dilatancy characteristics and liquefaction strength of sand, IS-Hokkaido '94, **1**, 75-80.
Tsubouchi,T., Ochi,K. and Tatsuoka,F. (1994): Non-linear FEM analyses of pressuremeter tests in a sedimentary soft rock, IS Hokkaido '94, **1**, 539-544.
Uchimura,T. (1996a): Preloaded prestressed reinforced soil, Master Engng thesis, Univ. of Tokyo (in Japanese).
Uchimura,T. (1996b): Internal report (Geotech. Lab., Univ. of Tokyo).
Vaughan,P.R. and Kwan,C.W. (1985): Weathering, structure and in situ stresses in residual soils, Géotechnique **34-1**, 43-59.
Vaughan,P.R. (1988): Indexing the engineering properties of residual soil, Quarterly Jour. of Engng Geology, London, **21**,69-84.
Viggiani,G. and Atkinson,J.H. (1995a): Interpretation of bender element tests, Géotechnique **45-1**, 149-154.
Viggiani,G. and Atkinson,J.H. (1995): Stiffness of fine-grained soil at very small strains, Géotechnique **45-2**, 249-265.
Wang,L. (1996): Study on field deformation characteristics of sedimentary soft rocks by triaxial tests, Dr. of Engng thesis, Univ. of Tokyo.
Wong,I.H., Ooi,I.K. and Broms,B.B. (1996): Performance of raft foundations for high-rise buildings on the Bouldery Clay in Singapore, CGJ **33**, 219-236.
Yamada,S., Masuda,T., Sato,T., Yamaguchi,I., and Tatsuoka,F. (1996): Sand behaviour in plane strain compression and extension test, Proc. 31th JNCGE, Kitami **1**, 342-343 (in Japanese).
Yasuda,N., Ohta,N. and Nakamura,A. (1996): Dynamic deformation characteristics of undisturbed riverbed gravels, CGJ **33**, 237-249.
Yoshikuni,H., Hirano,T., Nishiumi,H. and Ikegami,S. (1993): The behaviour of swelling and reconsolidation due to unloading, Proc. 48th Annual Conf. of JSCE III, 1010-1011 (in Japanese).
Yoshimi,Y., Tokimatsu,K. and Hosaka,Y. (1989): Evaluation of liquefaction resistance of clean sands based on high quality undisturbed samples, S&F **29-1**, 94-104.
Yu,P. and Richart,F.E.Jr. (1984): Stress ratio effects on shear modulus of dry sands, Jour.. of Geotech. Engrg., ASCE, 110-3, 331-345.
Zdravkovic,L. and Jardine,R.J. (1996): Some anisotropy stiffness characteristics of a silt under general stress conditions, Géotechnique **47-3**, 407-437.

Referred books:

Les Géomatériaux: théories, expérience et modèles (1995), Hermès, Paris, p208.
Mecanique des geomateriaux (1995), Hermès, Paris, p562
Les Géomatériaux: avancées récentes en calcul d'ouvrages (1995), Hermès, Paris, p332